LOCKHEED MARTIN ENERGY RESEARCH LIBRARIES
3 4456 0513262 9

CENTRAL RESEARCH LIBRARY
[redacted] DOCUMENT COLLECTION 2

OAK RIDGE NATIONAL LABORATORY
operated by
UNION CARBIDE CORPORATION
NUCLEAR DIVISION
for the
U.S. ATOMIC ENERGY COMMISSION

ORNL-TM-1720

DECLASSIFIED
CLASSIFICATION CHANGED TO
BY AUTHORITY OF: AECM-2104 a2 06 8/21/74
BY: Bobbie Rudd

FUELS AND MATERIALS DEVELOPMENT PROGRAM QUARTERLY PROGRESS REPORT FOR PERIOD ENDING DECEMBER 31, 1966

CENTRAL RESEARCH LIBRARY
DOCUMENT COLLECTION
LIBRARY LOAN COPY
DO NOT TRANSFER TO ANOTHER PERSON
If you wish someone else to see this document, send in name with document and the library will arrange a loan.

NOTICE This document contains information of a preliminary nature and was prepared primarily for internal use at the Oak Ridge National Laboratory. It is subject to revision or correction and therefore does not represent a final report.

[redacted]

LEGAL NOTICE

This report was prepared as an account of Government sponsored work. Neither the United States, nor the Commission, nor any person acting on behalf of the Commission:

A. Makes any warranty or representation, expressed or implied, with respect to the accuracy, completeness, or usefulness of the information contained in this report, or that the use of any information, apparatus, method, or process disclosed in this report may not infringe privately owned rights; or

B. Assumes any liabilities with respect to the use of, or for damages resulting from the use of any information, apparatus, method, or process disclosed in this report.

As used in the above, "person acting on behalf of the Commission" includes any employee or contractor of the Commission, or employee of such contractor, to the extent that such employee or contractor of the Commission, or employee of such contractor prepares, disseminates, or provides access to, any information pursuant to his employment or contract with the Commission, or his employment with such contractor.

[redacted]

ORNL-TM-1720

Contract No. W-7405-eng-26

FUELS AND MATERIALS DEVELOPMENT PROGRAM QUARTERLY PROGRESS REPORT FOR PERIOD ENDING DECEMBER 31, 1966

Compiled by

P. Patriarca

MARCH 1967

OAK RIDGE NATIONAL LABORATORY
Oak Ridge, Tennessee
operated by
UNION CARBIDE CORPORATION
for the
U.S. ATOMIC ENERGY COMMISSION

[redacted]

LOCKHEED MARTIN ENERGY RESEARCH LIBRARIES

3 4456 0513262 9

[redacted]

[redacted]

[redacted]

FOREWORD

This is the eleventh quarterly progress report describing work performed at the Oak Ridge National Laboratory for the Fuels and Materials Branch, Division of Reactor Development and Technology, U.S. Atomic Energy Commission. The specific programs covered are as follows:

Program Title	Person in Charge	Principal Investigator(s)
Part I. Metals and Ceramics Division		
Controlled Precipitation in Nuclear Materials	W. O. Harms	J. L. Scott J. P. Hammond
Fuel Element Fabrication Development	G. M. Adamson, Jr.	W. R. Martin
Mechanical Properties	C. J. McHargue	J. R. Weir, Jr.
Nondestructive Test Development	W. O. Harms	R. W. McClung
Sintered Aluminum Products	G. M. Adamson, Jr.	E. A. Franco-Ferreira W. R. Martin D. G. Harman
Zirconium Metallurgy	C. J. McHargue	M. L. Picklesimer P. L. Rittenhouse
Weldability of Nickel-Bearing Alloys	G. M. Adamson, Jr.	G. M. Slaughter
Part II. Reactor Chemistry Division		
Fission-Gas Release and Physical Properties of Fuel Materials During Irradiation	O. Sisman	R. M. Carroll J. G. Morgan

[redacted]

[redacted]

[redacted]

[redacted]

CONTENTS

Page

Summary ix

Part I. Metals and Ceramics Division

1. Controlled Precipitation in Nuclear Materials 3
   - Production of Fine Precipitates in Uranium Nitride 3
     - Molybdenum Additions 3
     - Thorium and Oxygen Additions 4
     - Electron Microscopy 10
2. Fuel Element Fabrication Development 13
   - Deposition of Uranium Dioxide by Hydroreduction of Uranium Hexafluoride 13
   - Preparation of Uranium Dioxide by Hydroreduction of Uranium Chlorides 14
   - Preparation of Uranium Compounds by Lithium Vapor Reduction of Uranium Hexafluoride 14
   - Preparation of Plutonium Dioxide Powder from Plutonium Hexafluoride by Thermochemical Reduction 15
   - Deposition of Tungsten-Rhenium Alloys 16
3. Mechanical Properties 20
   - Effect of Helium upon the Mechanical Properties of Type 304 Stainless Steel 20
   - Effect of Helium upon the Mechanical Properties of Titanium-Modified Type 304 Stainless Steel 22
   - Elevated-Temperature Irradiation Embrittlement in the Austenitic Stainless Steels 24
4. Nondestructive Test Development 27
   - Electromagnetic Test Methods 27
     - Analytical Studies 27
     - Phase-Sensitive Eddy-Current Instrument 29
   - Ultrasonic Test Methods 29
     - Fabrication of Reference Notches 29
     - Reference Standards 31
   - Penetrating Radiation Methods 32

[redacted]

[redacted]

5. Sintered Aluminum Products Development 32
Dispersion Preparation 32
Ball Milling 32
Magnetic Separation of SAP Flake 33
Powder Consolidation 34
Evaluation of Product 39
High-Temperature Stability 39
Al_2O_3 Analysis of SAP 41
Evaluation of Commercial Product 42
SAP-UC Compatibility Experiments 48
Nondestructive Test Development 48
Development of Advanced SAP Materials 53
Metal Filings 53
Ribbon Casting 54
6. Zirconium Metallurgy 56
Anisotropy in Zircaloy-2 and Zircaloy-4 56
Multiaxial Testing of Tubing 56
Preferred Orientation in Zircaloy Tubing 57
Yield Loci 59
Studies of Zirconium and Its Alloys in Shear 61
Zircaloy-2 Shear Studies 61
Zirconium Single-Crystal Shear Studies 64
Optical Properties of Zirconium Alloys 66
Properties of High-Purity Zirconium and Its Alloys 70
Anisotropy of Oxidation in Zirconium 70
Inhibition of Oxidation by Anodic Films 72
Effect of Purity on Oxidation 73
Detection of Weld Contamination in Zircaloy-2 by Anodizing 74
7. Weldability of Nickel-Bearing Alloys 80
Special Alloy Fabrication 80
Weldability Studies 82
VARESTRAINT Testing Performed Under Subcontract at Rensselaer Polytechnic Institute 82
Hot-Ductility Testing 86

[redacted]

[redacted]

Influence of Flaws on Properties of Nickel-Bearing Alloys 86

Part II. Reactor Chemistry Division

8. Fission-Gas Release and Physical Properties of Fuel Materials During Irradiation 91

Fission-Gas Release 91

Thermal Conductivity of UO_2 During Irradiation 94

[redacted]

[redacted]

SUMMARY

PART I. METALS AND CERAMICS DIVISION

1. Controlled Precipitation in Nuclear Materials

A uniform distribution of fine oxide precipitates in (U,Th)N was obtained through the use of improved nitride synthesis and powder mixing procedures. The oxide phase is of two types: One resides within the nitride grains and results from the internal oxidation of thorium; the other is essentially UO_2, as originally added, and has the effect of pinning grain boundaries and markedly enhancing densification. We are investigating the role of carbon in both processes.

Procedures and techniques requisite to examination of these UN specimens by electron microscopy are being studied. Replication of fracture surfaces is the method chosen and we are concerned with ways of ensuring that the replicated surface is free of artifacts and with ways of removing the carbon replica in an undamaged condition. Solution of the UN by hot nitric acid has been found to be reasonably successful.

2. Fuel Element Fabrication Development

Submicron-size UO_2 powder has been made using the process of hydroreduction of 2.5% enriched UF_6. This 1-kg lot of material produced is being sintered into high-density pellets to be irradiated and subsequently evaluated. Our work on the preparation of uranium compounds by the lithium vapor reduction of UF_6 has been discontinued and a topical report on the feasibility study has been written.

An apparatus in which PuO_2 can be prepared by the thermochemical reduction of PuF_6 has been built and is currently being evaluated in trial runs using UF_6 as feed material.

The experimental conditions for the deposition of tungsten-rhenium alloys are being examined in order to produce a deposit of uniform composition. We are also studying the phases present in the as-deposited material. We find that the β-tungsten phase is observed at lower rhenium contents when the deposit is formed at 1100°C as compared to 1500°C.

[redacted]

[redacted]

3. Mechanical Properties

It has been established that titanium additions to type 304 stainless steel produce substantial improvement in the postirradiation high-temperature ductility. One aspect of this program concerns the effect of microstructure of titanium-modified stainless steel upon postirradiation properties. The results indicate that, as in standard type 304 stainless steel, the postirradiation ductility of fine-grained titanium-modified stainless steel containing intragranular precipitates is higher than that of the same steel in a coarse-grained condition without the precipitates.

In another approach to the high-temperature embrittlement problem, type 304 stainless steel has been cyclotron bombarded with α-particles to a nearly uniform concentration of 0.1 ppm (atom fraction) of helium to simulate helium generation by fast (n,α) reactions. A severe loss of postbombardment ductility occurred in samples tensile tested from 700 to 900°C. Samples of the same material bombarded by α-particles that passed completely through the samples had the same ductility as unirradiated control samples within the limits of experimental uncertainty.

The ductility of a titanium-modified stainless steel bombarded to contain 0.1 ppm of helium was not altered by the presence of helium.

4. Nondestructive Test Development

We are developing new techniques and equipment for the nondestructive evaluation of materials and components. Major emphasis has been on eddy-current, ultrasonic, and penetrating-radiation methods.

Our analytical work on electromagnetic phenomena has included development of a closed-form solution for the case of a coil positioned above a conducting plane. This approach should be more accurate, but less versatile, than the relaxation method. The latter method has been used to study the effect on the vector potential by placing ferrite cups around the coils. The portable phase-sensitive instrument has been improved to decrease sensitivity to lift-off. Probe coils as small as 0.055 in. in diameter have been fabricated.

[redacted]

We began studies to correlate the response from various shapes of ultrasonic reference discontinuities.

We are conducting quantitative studies on radiographic sensitivity as various conditions such as x-ray energy, specimen thickness, and lead intensifying screens are varied. Special penetrameters for aluminum, steel, and copper are being used.

5. Sintered Aluminum Products Development

We have approached the problem of fabricating aluminum-oxide-strengthened wrought aluminum products by thoroughly characterizing commercially available aluminum powder products and studying means for specific oxide additions. Fabrication and testing of the materials thus developed have shown that in comparison to previously available commercially sintered aluminum materials significant improvement of homogeneity and uniform strength properties may be attained.

Studies aimed at the optimization of ball-milling techniques are continuing. Suitable process parameters have been chosen. A large prototype ball mill has been built and is being put into operation.

Extrusion continues to be the primary means of powder consolidation. Tests are being conducted to arrive at a specific process flowsheet which will result in billets with reproducible and uniform properties. The results of this work have been quite encouraging.

Product evaluation includes numerous techniques such as chemical analysis, x-ray diffraction, electron and light microscopy, mechanical properties, and nondestructive testing. Improved methods of chemical analysis and x-ray diffraction for identification of oxide species have been developed. Mechanical property testing continues to be the primary means of evaluating the extruded SAP product with electron microscopy used as an adjunct in analyzing the results. Excellent progress is being made on the development of a rapid nondestructive test for the determination of the dimensions of SAP flake material.

Studies have been initiated to evaluate the compatibility of SAP material with UC fuel.

[redacted]

Promising work is also being done on the development of advanced SAP materials. It is expected that those studies will result in a SAP product of very low oxide content which achieves properties equal to or better than the 10% oxide material.

6. Zirconium Metallurgy

Preliminary biaxial tests have been run on Zircaloy tubing and the test system is now being modified to allow programming of internal pressure. A system has been designed to permit biaxial compression testing and to study the effect of hydrostatic pressure on yielding and deformation.

Basal pole figures have been determined for six lots of tube-reduced Zircaloy tubing. The texture coefficients were found to be a function of the wall- to diameter-reduction ratio in the final fabrication step. Unexpected differences were encountered in the textures of identically processed Zircaloy-2 and Zircaloy-4 tubing.

Plane stress yield loci have been constructed for Zircaloy-2 by: (1) a microhardness anisotropy technique; (2) a method using strain anisotropy constants and tension and compression yield strengths; and (3) a computer program developed from a theoretical study of yield criteria. Results of the three methods are in excellent agreement.

Shear tests have been performed in four orientations on three schedules of polycrystalline Zircaloy-2. The ultimate shear strengths and elastic limits have been examined in relation to uniaxial strengths in these same materials.

A single crystal of zirconium has been sheared in an attempt to produce $\{10\bar{1}1\}\langle 11\bar{2}3\rangle$ slip. First, second, and higher order twinning was seen, but none of the expected slip. A second specimen, tested at 200°C, showed less twinning but still no slip in the $\langle 11\bar{2}3\rangle$ direction.

A study of the variation of optical properties of zirconium alloys as functions of alloying element and content has been initiated. This study is a prerequisite to investigation of the partitioning of alloying elements between oxide and metal during oxidation-corrosion. In order

[redacted]

to pursue this study it was necessary to design, construct, and instrument equipment to perform highly accurate reflectivity measurements.

Single crystals of high-purity zirconium have been oxidized for 100 hr in 360°C water. It is observed that the weight gains are made up in large part from oxide protuberances rather than from the uniform film seen with the eye and the spectrophotometer.

Anodic film thickness on zirconium was investigated as a function of crystallographic orientation and the dissolution rates of these films into the metal at 500°C were measured.

The inhibition of oxidation by anodic oxide films was investigated by comparing 6-hr weight gains in 500°C steam for unanodized specimens of zirconium with those for specimens anodized in either 1% KOH or a phosphate containing solution that produces an anodic film incorporating phosphate ions. Anodizing in KOH slightly lowered the corrosion rate, but the phosphate anodized specimen showed only half the rate of the unanodized material. This corroborates previous suggestions that pre-anodizing in solutions containing phosphate might decrease oxidation rates at high temperatures.

Oxidation in 360°C water of specimens from known locations in three zone-refined bars of zirconium has shown that there is a distinct effect of purity on the oxidation rate. Specimens from near the head of the bar, purest except for oxygen and hafnium, show the least oxidation.

A method that allows quantitative detection of weld contamination in Zircaloy-2 without autoclaving has been developed. The weld specimens are anodized in a 1% solution of H_3PO_4 at 100 v direct current and examined under polarized light at low magnification. The inspection operation can be automated by use of a photometer to locate "corrosion bands".

7. Weldability of Nickel-Bearing Alloys

Studies are well under way on the program to determine the effects of minor elements, individually and combined, upon the cracking behavior and mechanical properties of welds in nickel-bearing alloys. Chemical analyses of the first three experimental aluminum- and titanium-containing

Incoloy 800 alloys show that excellent purity and reproducibility were obtained with the in-house melting and fabrication processes. Additional alloys for weldability testing are being prepared, and others are being procured.

Three ORNL-fabricated special heats of Incoloy 800 were weldability tested at Rensselaer Polytechnic Institute using their VARESTRAINT testing apparatus. Minor additions of titanium and aluminum produced a definite deleterious effect on the susceptibility to hot cracking. For example, the total length of cracks in a weld containing 0.15% Ti and 0.15% Al was 13 times as great as was the crack length in the simple iron-nickel-chromium ternary alloy. The cracking propensity of all the experimental heats tested to date is, however, considerably less than that of commercial Incoloy 800. It is proposed that this difference is due to other minor elements (such as C, Mn, Si, S, P, etc.) which are either eliminated or minimized in the special heats.

A modified VARESTRAINT specimen has been devised in order to minimize the costs and time delays incurred in preparing large amounts of special alloys. Numerous specimens are being prepared for hot-ductility testing and for fatigue testing; the purpose of the latter is to determine the influence of small flaws upon the mechanical properties of welds.

PART II. REACTOR CHEMISTRY DIVISION

8. Fission-Gas Release and Physical Properties of Fuel Materials During Irradiation

A hollow-cylinder specimen of single-crystal UO_2 is being irradiated for the purpose of measuring thermal conductivity and fission-gas release during irradiation. In these experiments the specimen is oscillated sinusoidally in the reactor so as to oscillate the neutron flux and thus oscillate the fission rate in the specimen in a sinusoidal manner. The specimen temperature, measured by axial thermocouples, will also oscillate in response to the changing fission power. The base specimen temperature can be controlled by air-cooling the outside of the specimen capsule.

The response of the specimen temperature will not be instantaneous with change of fission power, but will have a time lag depending on the specific heat, thermal conductivity, and emissivity of the specimen. The amplitude of the temperature oscillations will depend upon the amplitude of the fission-rate oscillations and the frequency of the oscillations. From measurements of phase shift and temperature amplitude as a function of frequency and amplitude of fission-rate oscillations, the thermal conductivity of the specimen can be calculated. By changing the base temperature and base fission rate, the thermal conductivity can be measured as a function of fission rate and temperature.

A literature survey confirmed and extended our defect-trap theory of fission-gas release from fuels. A review of our older data showed that the characteristics of fission-gas release did conform to our extended theory. Namely, the temperature dependence of escape from point defects could be distinguished from the escape of fission gas from clusters of point defects. Also, the effect of cluster formation on gas release could be detected.

The large mass of thermal diffusivity data obtained during flux and temperature oscillations has been analyzed once by hand calculations. The hand calculations contained some uncertainties and did not contain corrections for thermocouple responses. The raw data were therefore Fourier analyzed again with a different program designed to reject individual wild points caused by malfunctions of the tape punch. The results were then inspected and the data along with thermocouple corrections placed in another computer program to solve the complex algebraic equations that yield the thermal diffusivity values. The results from the second program are now being inspected and tabulated.

The equipment for a transient test has been designed, constructed, installed, and is now being checked out. The transient test will decrease the time required to obtain data by an order of magnitude if all goes well.

[redacted]

PART I.

METALS AND CERAMICS DIVISION

[redacted]

1. CONTROLLED PRECIPITATION IN NUCLEAR MATERIALS

J. L. Scott

The purpose of this program is to develop means of improving the performance characteristics of both fissionable and nonfissionable materials through controlled precipitation of stable dispersed phases. Recent emphasis has been placed on uranium nitride, which finds application in space nuclear reactors. Solid solutions of (Pu,U)N are long-range contenders for use in fast breeder reactors.

Production of Fine Precipitates in Uranium Nitride

T. G. Godfrey J. M. Leitnaker
R. A. Potter

We are investigating several possible ways of incorporating a fine dispersion of precipitate particles in uranium nitride that might enhance the irradiation performance of this nuclear fuel through provision of nucleation and pinning sites for fission-gas bubbles. Molybdenum and thoria are being considered as precipitate formers. We have been concerned also with the development and evaluation of replication and replica-stripping techniques for electron microscope examinations.

Molybdenum Additions

No significant results have been obtained on the effects of molybdenum additions to UN since those described previously in which an unusual behavior was observed at temperatures around 2350°C and a composition of 0.1 wt % Mo in UN.[1] Alloys of uranium and molybdenum containing up to 10 wt % Mo are being prepared for nitride powder synthesis and specimen fabrication in order to further study the reactions that occur in this system. A second batch of U–0.1 wt % Mo alloy is also

[1] T. G. Godfrey, J. M. Leitnaker, and R. A. Potter, Fuels and Materials Development Program Quart. Progr. Rept. Sept. 30, 1966, ORNL-TM-1700, pp. 4–10.

being prepared for additional sintering and annealing experiments to define the solid solubility relationships below 2300°C that might lead to formation of a fine precipitate dispersion.

Thorium and Oxygen Additions

Studies on the formation of a fine dispersion of precipitate particles through internal oxidation of solid solutions of (U,Th)N were continued. We modified our synthesis and mixing procedures to yield a more sinterable and homogeneous powder, and we have begun to study the effect of carbon additions on the solubility of thorium dioxide in uranium nitride.

In the modified synthesis work, a U–2% Th alloy was prepared by arc melting high-purity metal (< 300 ppm impurities); this material was then alternately hydrided and nitrided using a procedure that involved a final powder heat treatment at 1800°C. Previously we had treated these nitride powders at 2000°C in order to minimize oxygen contamination during subsequent handling, but the product was relatively coarse and did not sinter well. This coarseness also hindered the proper mixing of powders such as UO_2 and graphite that were subsequently added to the nitride powders. The 1800°C treatment represents a compromise between sinterability and susceptibility to oxygen contamination in our present equipment.

Further improvement in mixing was achieved by the use of a mortar and pestle with the acetone-base slurry instead of spatula stirring. As discussed below, this procedure leads to nearly ideal mixing of the oxide and nitride powders.

The properties of specimens of various compositions after sintering at 2300°C are presented in Table 1.1. The complete sintering cycle consisted of slowly heating to 1500°C under vacuum and to 2300°C under 1 atm N_2, holding for 2 hr at 2300°C, rapidly cooling to 1500°C, and cooling to room temperature after evacuating the system to 1×10^{-5} torr. Lattice parameters of the (U–2% Th)N samples indicated that the 1800°C powder treatment did not lead to formation of a single ideal solution (Sample 322), but that after sintering a pressed compact at 2300°C (Sample 328) an ideal solution was obtained within the accuracy of the

Table 1.1. Description and Properties of Uranium-Thorium Nitride Specimens Sintered at 2300°C

Sample Number	Nominal Composition (wt %)	Chemical Analysis, wt %				Bulk Density (% of theoretical)	Lattice Parameter (A)	ThN Content, mole %	
		Th	N	O	C			By Chemical Analysis[a]	By Lattice Parameter[b]
322 (reference powder)[c]	(U–2% Th)N	2.02	5.58	0.043	0.021		4.8940[d]	2.14	1.85
328	(U–2% Th)N	2.01	5.38	0.063	0.024	91.0	4.8948	2.13	2.15
329	(U–2% Th)N–2% UO_2	1.94	5.46	0.291	0.030	94.5	4.8922	2.05	1.18
324	(U–2% Th)N–5% UO_2	2.13	6.22[e]	0.650	0.008	97.7	4.8904	2.25	0.37
331	(U–2% Th)N–2% UO_2–0.3% C	2.03	5.28	0.085	0.107	86.5	4.8958[f]	2.15	2.52[f]

[a]Assuming all thorium is present as ThN.

[b]Assuming Vegard's law.

[c]Synthesized by hydride-nitride process with final heat treatment at 1800°C.

[d]Sample contained a minor face-centered cubic phase with a lattice parameter of 4.9108 A which might correspond to 8.08 mole % ThN in UN.

[e]High value probably in error.

[f]This large lattice parameter indicates solution of UC as well as ThN in UN.

measurements. The microstructure of the sintered (U–2% Th)N sample, as shown in Fig. 1.1a, was that of a single-phase material free of second-phase oxide. This observation is consistent with the low oxygen content (630 ppm) determined by chemical analysis. However, as is evident in Fig. 1.1b, this sample contained many areas of very large-grained material, typically surrounding a large void. We feel that the presence of these areas is related to the possibly thorium-rich second-phase material detected by x-ray diffraction on the as-synthesized powder, but we are unable to propose a possible mechanism for their formation at this time.

Samples 329 and 324, which contained 2 and 5 wt % UO_2, respectively, gave lattice parameters indicative of removal of thorium from the nitride phase. The addition of 2% UO_2 resulted in the oxidation of about one half of the thorium in the nitride phase while the addition of 5% UO_2 resulted in oxidation of about 80% of the thorium. The microstructure shown in Fig. 1.2 of the sintered sample containing 2% UO_2 exhibits a small amount of white oxide phase well distributed within the nitride grains. In an area close to the very large-grained region, the oxide is more abundant and more finely divided. The microstructure of the specimen with 5% UO_2, Fig. 1.3a, shows a greater concentration of the oxide phase throughout the specimen. A large portion of the precipitates are fine and the absence of porosity in this 97.7% dense material is apparent. Examination of this specimen at 2000× using an oil-immersion lens revealed areas with very fine oxide particles and platelets as shown in Fig. 1.3b. The platelets seem to be crystallographically oriented with respect to the nitride subgrains, suggesting a degree of coherency between the oxide and nitride phases.

The relative densities and grain sizes of the three specimens just described are of considerable interest. As shown in Table 1.1, oxide additions increased the density from 91.0 to 97.7% of theoretical. We estimate the grain sizes of these three specimens to be in the ratio of 7:5:3 for the reference nitride, the 2% oxide, and the 5% oxide samples, respectively. These results are consistent with theories of enhanced densification through grain-boundary pinning by inclusions. They also substantiate our ideas concerning the oxidation of the thorium within

[redacted]

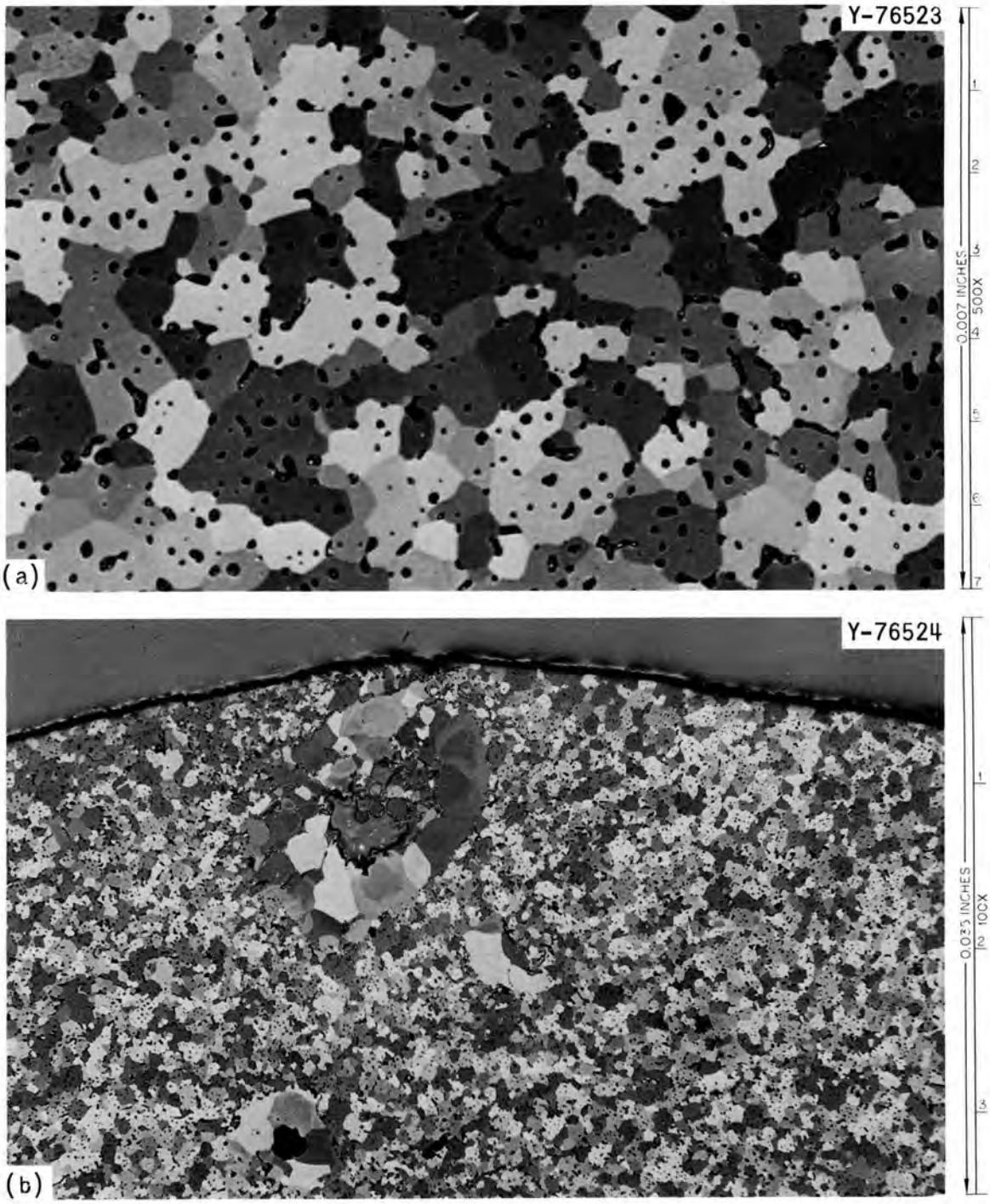

Fig. 1.1. Microstructure of (U–2% Th)N Sample Sintered at 2300°C. Etchant: 30 parts lactic, 10 parts HNO_3, and 1 part HF. (a) Typical area showing rather uniform large grains of nitride and no oxide. (b) Area showing regions of exaggerated grain growth with central voids.

[redacted]

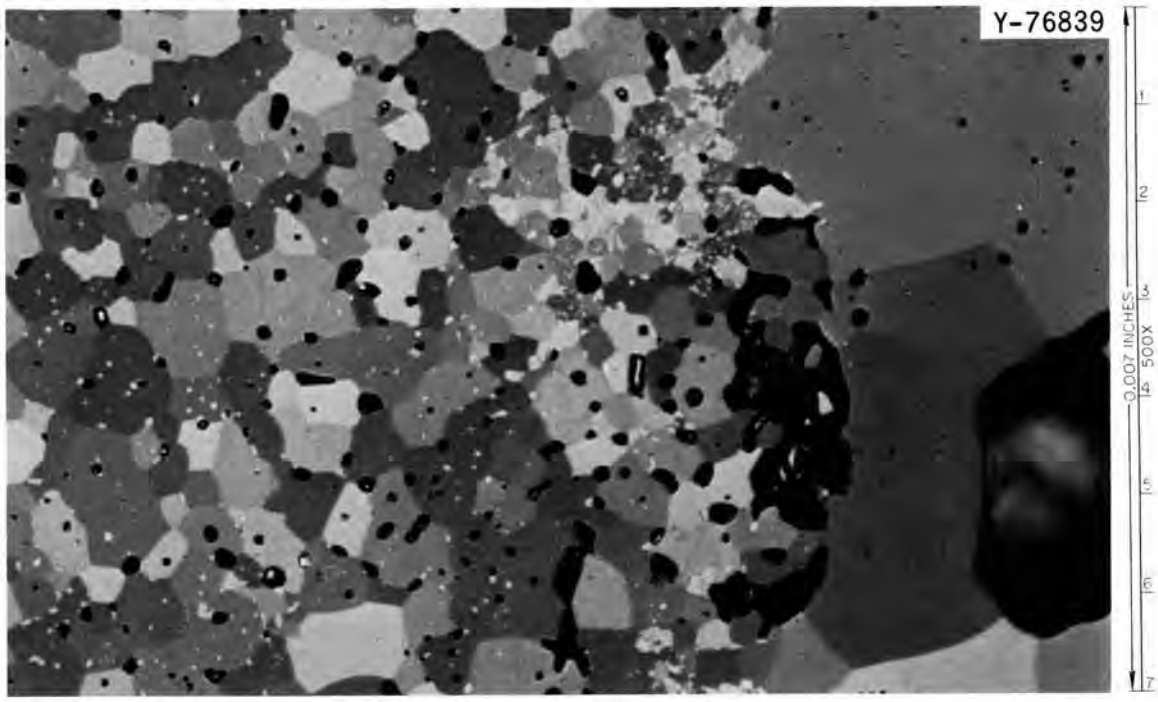

Fig. 1.2. Microstructure of (U–2% Th)N–2% UO_2 Sample Sintered at 2300°C, Showing Good Distribution of White Oxide Phase and Edge of a Very Large-Grained Area. Note that the fine oxide particles are more abundant next to the large-grained area. Etchant: 30 parts lactic, 10 parts HNO_3, and 1 part HF.

the nitride matrix. The UO_2 originally resides in grain-boundary areas of the compacted powders. On sintering, some of the oxygen diffuses into the grains and reacts with thorium as shown by the decrease in lattice parameters and the presence of an oxide phase within the nitride grains. Any excess UO_2 remains at the grain boundaries, effectively pinning them until all porosity is removed through the grain-boundary network. A further point suggested by these results is that UO_2 is not appreciably soluble in pure UN at 2300°C since a large amount of it must have remained in grain boundaries as UO_2 throughout the sintering process.

In an attempt to alter the solubility relationships between oxide and nitride phases, we prepared a (U–2% Th)N sample with 2% UO_2 and 0.3% C (Sample 331). During the initial heating under vacuum, considerable off-gassing was noted, indicative of the carbothermic reduction of the UO_2. Chemical analysis (Table 1.1) revealed that removal of oxygen was essentially complete. The microstructure, Fig. 1.4, shows no oxide

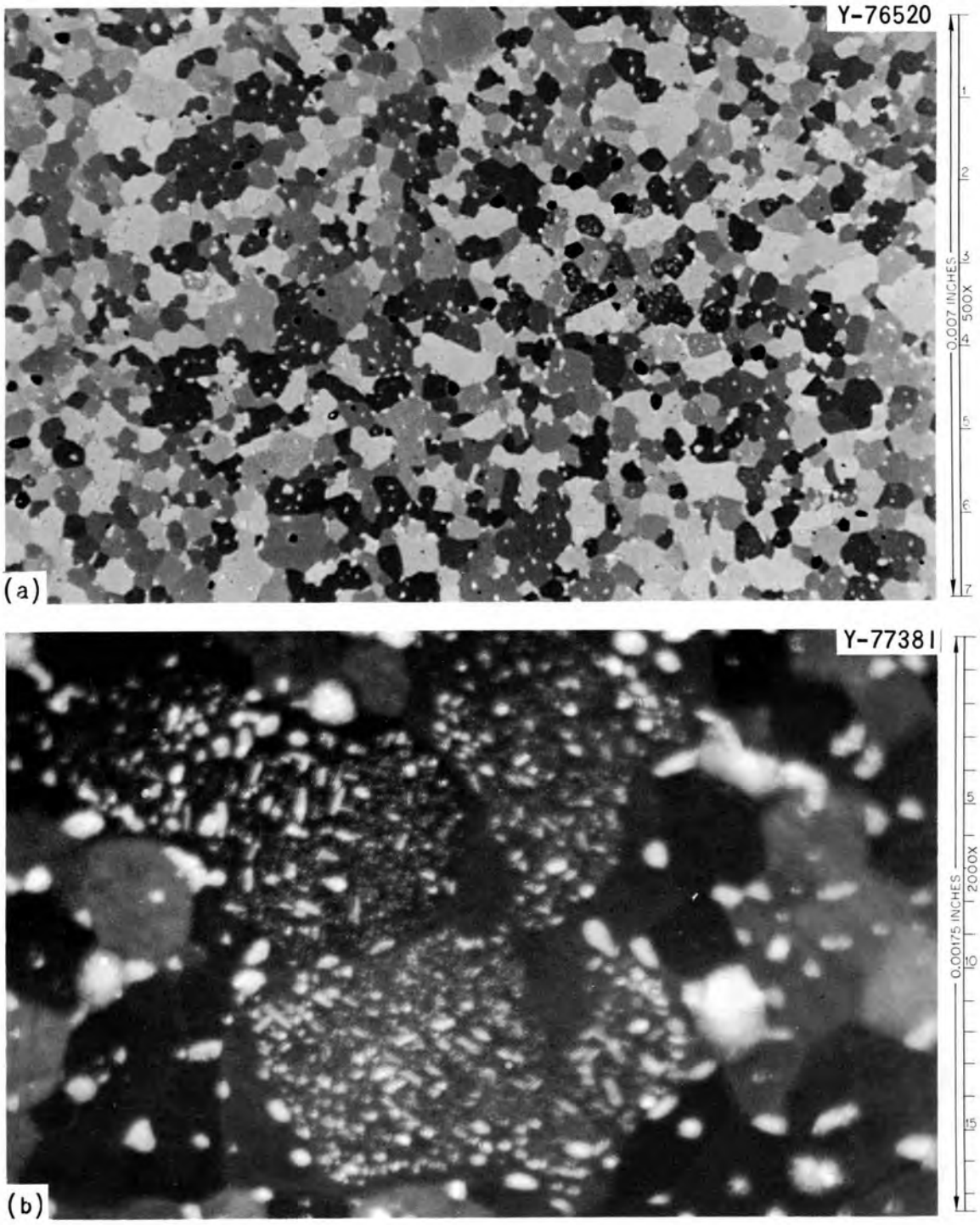

Fig. 1.3. Microstructure of (U–2% Th)N–5% UO_2 Sample Sintered at 2300°C, Showing Distribution of White Oxide Phase. Etchant: 30 parts lactic, 10 parts HNO_3, and 1 part HF. (a) Typical high-density, small-grained area. (b) Area showing very fine oxide particles and platelets within subgrains.

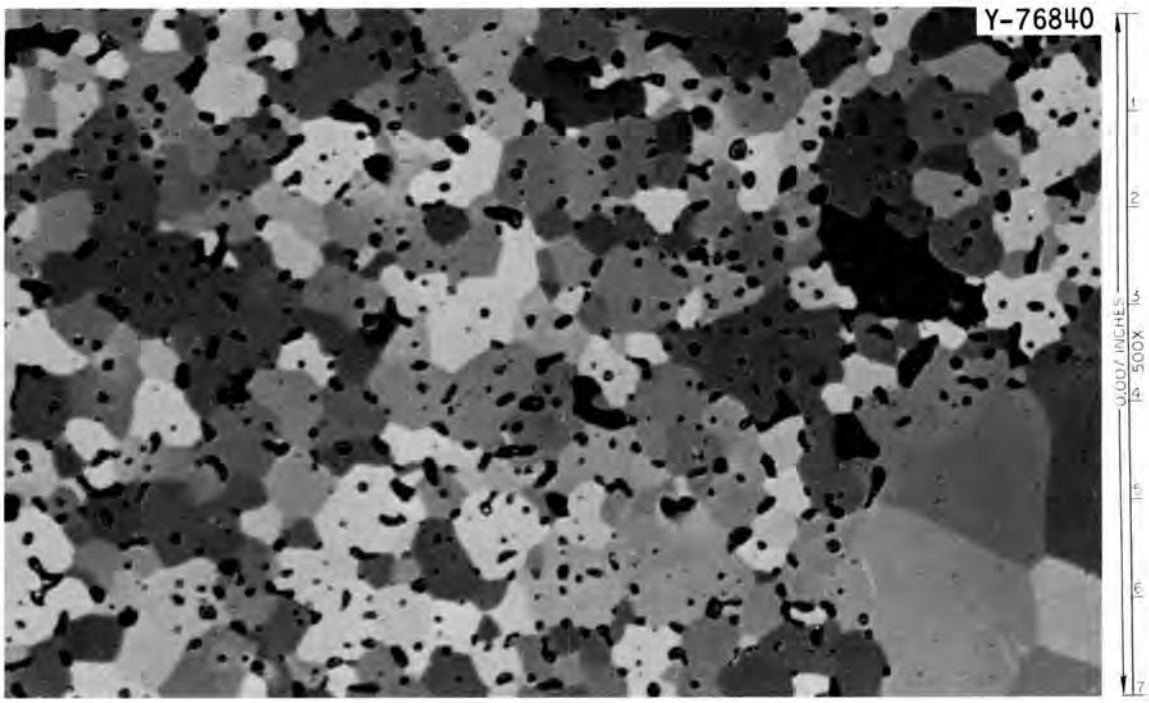

Fig. 1.4. Microstructure of (U–2% Th)N–2% UO_2–0.3% C Sample Sintered at 2300°C. Note the absence of oxide. Etchant: 30 parts lactic, 10 parts HNO_3, and 1 part HF.

phase and a large number of pores within the nitride grains. The lattice parameter of this specimen was unusually large, indicating that a considerable amount of UC was dissolved in the (U,Th)N. The low density of this specimen (86.5% of theoretical) indicates that removal of the oxide or the presence of the carbon (as UC) has a deleterious effect on the densification of UN. We cannot say with certainty which is the major cause, but are now conducting experiments on specimens in which carbon was added to (U–2% Th)N powders which were then heated to 1400°C to form a (U,Th)-(N,C) solution. Additions of UO_2 will be made to these carbon-treated powders. On sintering, removal of the oxygen should be less pronounced, and we may be able to observe the effects of carbon and oxygen independently.

Electron Microscopy

An important aspect of our work on precipitates in UN is the preparation of specimens for electron microscopy. Since our specimens typically contain from 5 to 15% porosity, we have little hope of being

able to prepare thin sections for direct transmission electron microscopy, which normally would be the preferred technique. Therefore, we have selected the technique of replicating with carbon a freshly fractured surface, preshadowed with platinum. We feel that this method is more apt to reveal the true nature of the sample than the alternate technique of replicating a selectively etched, metallographically prepared sample.

Two problems immediately arise in the application of this replication method. First, there is the problem of producing the fracture surface and keeping it free of artifacts such as might arise from oxidation of this pyrophoric material. As one possible way of preventing any alteration of the specimen surface, we have fractured specimens with a small chisel and hammer under zylene and toluene and transferred the chips still immersed in the liquid to the vacuum shadowing unit. The liquid was then removed through vaporization under vacuum and the specimen was immediately shadowed and replicated. In order to determine if any artifacts arise solely from the presence of the liquid, such as residue from vaporization, NaCl single crystals were similarly treated. Examination of the replicas from the NaCl revealed that apparently an oily or waxy residue had interfered with the platinum and carbon film deposition process. We are continuing these experiments with other organic liquids. Another possible approach is to carry out these operations in an inert atmosphere enclosure, but a suitable facility is not currently available.

The second problem encountered with the replication techniques is the removal of the carbon film from the UN substrate. Because of the porosity of the specimens, the film is rather lacey and is tenaciously held to the substrate. Solution of the surface of the UN by some process is the only feasible way to release the film. We have tried a variety of acids, singly and in combination, both at room temperature and with application of heat, with less than satisfactory results. The action of acids on UN leads to formation of soluble uranium complexes and compounds with the attendant release of gases. These gases form as bubbles on the surface of the sample and tend to tear and otherwise disrupt the carbon film. Our best results have been obtained in two

[redacted]

different ways: (1) by repeatedly dipping the specimen into 40% HNO_3 at 110°C, thus causing the film to be released in a matter of minutes and minimizing the troublesome bubble formation; and (2) by exposing the specimen to attack by hot HNO_3 vapor on a platinum gauze.

[redacted]

2. FUEL ELEMENT FABRICATION DEVELOPMENT

W. R. Martin

We have continued studying chemical vapor deposition as a technique for direct conversion of fissionable halides to refractory fuel compounds and as a means for fabrication of refractory-metal alloy tubing. Sufficient submicron-size UO_2 powder for irradiation specimens has been prepared and it has been demonstrated that UO_2 may be deposited directly onto thoria to give a fertile-fissile duplex pellet.

Experiments in producing UO_2 by thermochemical reduction of the chlorides have been terminated due to deaccentuation of the chloride fuel element reprocessing cycle. We have also completed sufficient work to demonstrate that UF_6 may be reduced by lithium vapor and ammonia to produce uranium nitride powder.

A facility for experimental conversion of PuF_6 to PuO_2 has been completed and preliminary testing by conversion of UF_6 to UO_2 is under way.

Deposition studies of tungsten-rhenium alloys have progressed to where it is feasible to produce tubing directly, and fabrication of sheet stock for mechanical properties studies is under way.

Deposition of Uranium Dioxide by Hydroreduction of Uranium Hexafluoride

R. L. Heestand

We have completed the conversion of 1 kg of 2.5% enriched UF_6 to UO_2 as submicron-size powder. After conversion, the powder was fired in wet hydrogen at 900°C to adjust the oxygen-to-uranium ratio and to remove excess fluorine. In this treatment the oxygen-to-uranium ratio was dropped to 2.002; however, the fluorine content could not be brought below 0.2%. On attempting adjustment in wet hydrogen at temperatures greater than 950°C, fluorine content is lowered; however, sintering of the powder becomes a problem.

It is assumed that the fluorine content will be lowered further on sintering the powder into pellets; therefore, the material was transferred

to the Ceramics Technology group for further fabrication into pellets. We have also prepared approximately 250 g of depleted UO_2 powder for this group to use in sintering studies.

High-density coatings of UO_2 have been deposited onto thoria pellets to prove the feasibility of fabricating a fertile-fissile duplex pellet. Fully enriched UF_6 was obtained for preparation of irradiation specimens; however, we have been unable to obtain homogeneous crack-free thoria pellets for use in the experiments. Preparation of the duplex pellets will proceed immediately as soon as suitable thoria pellets are available.

Preparation of Uranium Dioxide by Hydroreduction of Uranium Chlorides

F. H. Patterson W. C. Robinson

Direct conversion of uranium chlorides to uranium dioxide was studied as a means for fabricating fuels reclaimed by the chloride volatility process. We demonstrated that the recycle could be accomplished, and the results will soon be published.[1] We anticipate no further studies on this process, as the fluoride volatility process has been proved more advantageous than the chloride volatility process.

Preparation of Uranium Compounds by Lithium Vapor Reduction of Uranium Hexafluoride

W. C. Robinson

The feasibility of producing uranium nitride by lithium reduction of UF_6 and simultaneous nitriding with nitrogen gas was studied. It was proved that uranium nitride could be obtained; however, engineering difficulties in metering lithium vapor were encountered.

---

[1]F. H. Patterson, W. C. Robinson, and C. F. Leitten, Jr., Conversion of Uranium Chlorides to Urania by Gas-Phase Reduction Hydrolysis, ORNL-TM-1701 (in press).

It is apparent that considerable work in determining methods for handling lithium vapor would be required to fully evaluate the economic feasibility of the process. We have discontinued our work in this area, and a topical report on our study has been written.[2]

Preparation of Plutonium Dioxide Powder from Plutonium Hexafluoride by Thermochemical Reduction

R. L. Heestand W. C. Robinson

We have begun an investigation on the direct conversion of PuF_6 to PuO_2 using chemical vapor deposition. The process was selected due to its adaptability to remote handling and its requirement of a minimum amount of equipment and time. An apparatus similar to that used for conversion of UF_6 to UO_2 was assembled and is currently being checked out in Bldg. 4508 prior to use with PuF_6.

Trial runs have been made using UF_6 as feed material to determine the additional difficulties that may be encountered in working in the enclosures. Some modifications were necessary to reduce the internal heat generation of the apparatus, and it now appears that all components work satisfactorily. Disposal of the by-product hydrogen-fluorine gas is not permitted in the Bldg. 3019 alpha facility ventilation system; therefore, additional runs with UF_6 will be made to determine the effectiveness of removing hydrogen-fluorine gas with a sodium fluoride-potassium fluoride trap. At present it is permissible to vent the excess hydrogen into the building system since the amount is small (less than 500 cm^3/min).

It is anticipated that the apparatus will be moved to the Bldg. 3019 alpha facility upon completion of the UF_6 trial runs and approval of the Operations Safeguards Committee.

Considerable difficulty was encountered in obtaining plutonium fluorides. The hexafluoride, which is the most desirable compound for

---

[2]W. C. Robinson and W. R. Martin, A Feasibility Study — Formation of Uranium Nitride Compounds Using Chemical Vapor Deposition Techniques (report in preparation).

conversion, was not available due to shipping limitations. Therefore, we obtained a quantity of PuF_4 for conversion to PuF_6 before reduction to the oxide.

Deposition of Tungsten-Rhenium Alloys

J. I. Federer W. R. Martin

Experiments are continuing for the purpose of depositing tungsten-rhenium alloy flat stock by hydrogen reduction of WF_6 and ReF_6. The injector moving-hot-zone technique, as previously reported, produces deposits having axial uniformity of composition in tubular deposits.[3] Recent electron microprobe analysis showed that the composition was not as uniform through the thickness of the deposits, but much improved over deposits prepared without an injector. Tungsten and rhenium traces through the thickness of a deposit having an average rhenium content of 22% are shown in Fig. 2.1. Because different scale factors were used in obtaining the traces, values read from the ordinate at a given position do not indicate the composition of the alloy at that position. In addition, small variations in compositions are amplified more on the rhenium trace. Variation in composition through the thickness of the deposit can be obtained by relating the average alloy composition (W–22% Re) to the average value of either trace indicated on the ordinate of Fig. 2.1, approximately 30 and 50% for the rhenium and tungsten traces, respectively. In this way maximum variations of about ±6% Re through the thickness of the deposit were found.

Steel mandrels of octagonal cross section having 0.75- or 1-in.-wide flat sections have been fabricated for deposition of flat stock. Before using these mandrels, experiments were conducted in 1.8-in.-ID round mandrels having approximately the same surface area as the octagonal mandrel in order to properly locate the WF_6-ReF_6 injector in the hot zone and to determine flow rates consistent with smooth surface texture and satisfactory deposition rates. Total flow rates of WF_6 and ReF_6

[3] J. I. Federer and W. R. Martin, Fuels and Materials Development Program Quart. Progr. Rept. Sept. 30, 1966, ORNL-TM-1700, pp. 22–28.

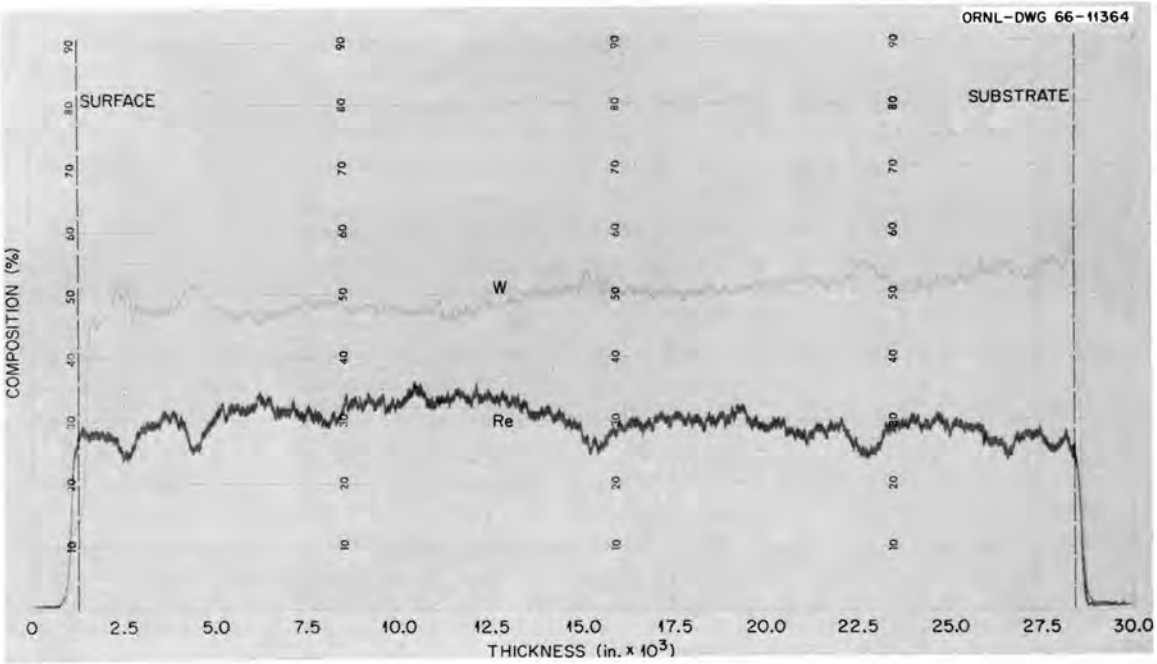

Fig. 2.1. Electron Probe Microanalyzer Traces for a Tungsten-Rhenium Alloy Deposited in a Moving Hot Zone at 900°C with a WF_6-ReF_6 Injector. Average composition 22% Re.

were about 33 cm^3/min in the 5/8-in.-ID mandrels used to establish the injector technique; therefore, flow rates were increased proportionally to 100 cm^3/min in the 1.8-in.-ID mandrels. Deposition conditions for nominal 5 and 25% Re alloys are given in Table 2.1.

Table 2.1. Deposition Conditions for Rhenium Alloys

Alloy	Flow Rates, cm^3/min			Pressure (torr)	Temperature[a] (°C)	Time (hr)
	H	WF_6	ReF_6			
W–5% Re	1500	95	5	5	750	2
	1500	95	5	50	850	2
W–25% Re	1500	75	25	5	950	2

[a]Uniform hot zone 8 to 10 in. long.

Deposits of both nominal compositions formed over a 10- to 12-in. length of mandrel, or slightly longer than the uniform hot zone.

Previous studies have shown that compositional uniformity precludes deposition in a temperature gradient.[4] An attempt was made, therefore, to confine the deposit to the uniform hot zone by increasing the pressure from 5 to 50 torrs and temperature from 750 to 850°C. These conditions resulted in powder formation, deposition of a dark coating on the injector, and only a thin coating on the mandrel. The surface texture of the other deposits was smooth except for a few small areas of nodules. The deposition rate, however, was only 3 mils/hr. Deposition of flat stock having a desired thickness of about 50 mils requires that the deposition rate be increased. Increasing the rate by increasing WF_6 and ReF_6 flow rates is the object of current experiments.

Concurrent with development of the technique for depositing alloys of uniform composition, a study is being made of the phases present in as-deposited material. Previous studies showed that tungsten-rich alloys deposited at 500 to 700°C contained two phases that coexist in certain compositional ranges, the body-centered cubic solid solution and a β-tungsten phase.[5] The β-tungsten phase, which has a hardness up to 2000 DPH compared with about 400 DPH for the solid solution, embrittles the deposits. The as-deposited W–25% Re alloys are quite hard and brittle. Therefore, the temperature and composition limits for formation of the β-tungsten phase are being investigated – in effect, an extension of the tungsten-rhenium phase diagram that is not established below 1500°C.

X-ray diffraction of powder samples was used to determine the presence of body-centered cubic solid solutions and the β-tungsten phase. The results of recent experiments are summarized in Table 2.2. The data for alloys deposited at 1000°C are not in complete agreement with previous data[6] but are considered more reliable because of an improved sampling method. The data in Table 2.2, along with data previously reported,[6] indicate that higher deposition temperatures require

---

[4] J. I. Federer and C. F. Leitten, Jr., Fuels and Materials Development Program Quart. Progr. Rept. Mar. 31, 1966, ORNL-TM-1500, pp. 14–18.

[5] J. I. Federer and C. F. Leitten, Jr., Metals and Ceramics Div. Ann. Progr. Rept. June 30, 1965, ORNL-3870, pp. 88–91.

[6] J. I. Federer and W. R. Martin, Fuels and Materials Development Program Quart. Progr. Rept. Sept. 30, 1966, ORNL-TM-1700, p. 28.

[redacted]

Table 2.2. Phases Occurring in Chemical Vapor-Deposited Tungsten-Rhenium Alloys

Deposition Temperature (°C)	Rhenium (%)	Solid Solution	β-Tungsten
1100	19.1	a	b
	21.9	a	a
	23.0	a	a
	25.6	a	a
	34.0	b	a
1200	11.1	a	b
	13.5	a	b
	16.6	a	b
	18.4	a	b
	25.8	a	a
1500	26[c]	a	b
	32[c]	a	b
	38[c]	a	a
	43[c]	d	d

[a]Found.

[b]Sought, not found.

[c]Estimate, analysis being obtained.

[d]X ray in progress.

higher rhenium contents for occurrence of the β-tungsten phase boundaries. Although sufficient data are not yet available to determine phase boundaries, the temperature and composition limits for formation of the β-tungsten phase are approximately known. The phase appears in coexistence with the solid solution in alloys containing about 20% Re deposited at 1000°C and in alloys containing about 35% Re deposited at 1500°C. The two-phase region extends over a range of about 5% Re before the alloys become single-phase β-tungsten. The high rhenium boundary of the β-tungsten phase is not yet known. Annealing treatments at 1800 and 2000°C have been performed on alloys containing 15 to 50% Re deposited at 1100 and 1200°C. During these anneals, the β-tungsten phase completely transformed to the equilibrium phases, solid solution and sigma.

[redacted]

[redacted]

3. MECHANICAL PROPERTIES

J. R. Weir, Jr.

One objective of this program is to determine the effect of irradiation on the mechanical properties of alloys of interest as fuel cladding and to find a metallurgical condition for the alloys that produces the least effect of subsequent irradiation on the mechanical properties. To accomplish this, our study concerns the interaction of radiation-induced defects and the substructure of the alloys, the effect of irradiation temperature, postirradiation test variables, and neutron dosimetry in the facilities used in the irradiations. The material selected for initial study is type 304 stainless steel.

Effect of Helium upon the Mechanical Properties of Type 304 Stainless Steel

R. T. King J. R. Weir, Jr.

Many authors currently attribute the high-temperature neutron irradiation-induced embrittlement of stainless steel and other alloys to helium generated by (n,α) reactions. It has been demonstrated that sufficient helium can be cyclotron-injected into aluminum and beryllium to produce observable bubbles of helium after a postbombardment anneal. In the experiment to be described, a uniform dispersion of helium in type 304 stainless steel is shown to cause a loss of high-temperature ductility.

The composition of the steel is given below:

Element	Content, wt %		Element	Content, wt %	
	Type 304 stainless steel	Heat 3756		Type 304 stainless steel	Heat 3756
C	0.046	0.019	Ni	9.60	11.22
Mn	1.77	1.05	Co	0.25	
P	0.023	0.006	Ti		0.22
S	0.010	0.017	Mo	0.33	
Si	0.62	0.046	Co	0.03	
Cr	18.15	19.23			

[redacted]

It was hot rolled from 0.060-in.-thick sheet to 0.040-in.-thick strip, cold rolled to 0.020-in.-thick strip, annealed 1 hr at 1038°C in argon, and tensile samples of 0.75-in.-gage length, 0.25-in.-gage width prepared. A final 1-hr anneal at 1038°C in argon was followed by cooling in the cold zone of the furnace.

Five samples were bombarded at the Oak Ridge Isochronous Cyclotron in the following manner: α-particles accelerated to 80 ± 0.5 Mev were moderated by a device designed to distribute the helium uniformly through the sheet thickness. Neglecting scattered electrons, beam-current monitors in vacuum indicated that the beam was uniformly intense over the sample within at least a factor of 2. The temperature of the samples at no time exceeded 200°C. The samples were irradiated to approximately 0.1 ppm (atom fraction) of helium, calculated from the total beam current and known losses.

In order to demonstrate that displacement damage caused by α-particles did not affect the properties of the type 304 stainless steel, a set of five samples was bombarded under identical conditions, except that the moderator was not used. This allowed the α-particles to pass completely through the samples.

These samples were tensile tested at a strain rate of 0.026 min^{-1} in air over the temperature range from 500 to 900°C in 100° increments. A minimum of three unirradiated control samples was also tested under the same conditions. These data are tabulated in Table 3.1.

The results indicate no change in the strength properties of the steel as a result of α-bombardment with and without the moderator in place. This is not surprising, since displacement damage in type 304 stainless steels may recover below 500°C.

Within experimental scatter, the uniform and total elongations of the samples bombarded without the moderator were not affected by the bombardment, nor were the uniform elongations of the samples bombarded with the moderator in place altered.

However, the total elongations of the samples containing helium, irradiated with the moderator in place, were decreased substantially over the temperature range from 700 to 900°C, where neutron irradiation causes embrittlement of stainless steel. This provides strong evidence

Table 3.1. Effect of α-Particle Bombardment on Type 304 Stainless Steel

Sample	Test Temperature (°C)	Yield Strength (psi)	Ultimate Tensile Strength (psi)	Uniform Elongation (%)	Total Elongation at Fracture (%)
		$\times 10^3$	$\times 10^3$		
Control	500	17.0–18.0	68.8–71.6	44.1–45.6	45.4–47.8
	600	12.4–14.4	48.0–52.4	35.5–39.5	40.9–41.9
	700	12.8–13.6	29.6–33.2	21.9–25.2	48.3–52.5
	800	11.0–14.4	18.3–23.2	9.36–17.1	34.1–49.1
	900	8.6–8.8	10.1–10.8	11.0–16.3	36.1–39.5
Irradiated with moderator	500	15.0	59.0	43.2	44.3
	600	15.6	52.0	33.6	42.7
	700	15.0	31.6	20.6	31.0
	800	11.2	17.0	11.6	19.9
	900	8.4	9.4	6.5	13.9
Irradiated without moderator	500	14.4	60.8	44.1	47.5
	600	12.8	51.8	40.8	43.2
	700	14.2	43.0	30.3	41.9
	800	12.4	21.4	17.9	44.7
	900	8.6	11.0	12.2	26.5

that the presence of helium can be responsible for the high-temperature loss of ductility of stainless steel.

Effect of Helium upon the Mechanical Properties of Titanium-Modified Type 304 Stainless Steel

R. T. King J. R. Weir, Jr.

Martin and Weir[1] have demonstrated that small additions of titanium reduce the magnitude of neutron irradiation-induced embrittlement of type 304 stainless steels. A heat of type 304L stainless steel modified with 0.2% Ti, Heat 3756, has been cyclotron bombarded with α-particles.

The composition of the titanium-modified stainless steel has been given on page 20 of this report. The type 304L stainless steel was hot rolled from 0.50-in.-diam rod to 0.040-in.-thick strip, cold rolled to

[1]W. R. Martin and J. R. Weir, Solutions to the Problems of High-Temperature Irradiation Embrittlement, ORNL-TM-1544 (June 1966).

0.020-in.-thick strip, and tensile samples prepared. Sets of samples were annealed at 925, 1038, and 1225°C for 1 hr in argon and cooled in the cold zone of the furnace. One set of samples was annealed for 1 hr at 1038°C and water quenched. These samples were irradiated to approximately 0.1 ppm of helium and tensile tested in the same manner as the standard type 304 stainless steel of the previously described experiment.

Testing of nonbombarded control samples is in progress, and only data for the control samples annealed for 1 hr at 1038°C in argon are now available. These data and data from bombarded samples are presented in Table 3.2.

Table 3.2. Tensile Ductility of 0.2% Ti-Modified Stainless Steel[a]

Sample Condition	Total Elongation (%) at Temperature (°C)				
	500	600	700	800	900
Not bombarded, annealed 1 hr at 1038°C	33.4	34.4	55.5	55.3	> 33.7
Annealed 1 hr at 1038°C, water quenched, bombarded	32.0	33.7	56.9	65.9	58.4
Annealed 1 hr at 925°C, bombarded	33.5	41.4	65.3	84.9	86.1
Annealed 1 hr at 1038°C, bombarded	33.1	35.5	63.2	61.9	61.1
Annealed 1 hr at 1225°C, bombarded	33.9	31.5	35.4	48.4	38.8

[a]Heat 3756.

It is noteworthy that the titanium-modified stainless steel has higher tensile ductility from 700 to 900°C than the type 304 stainless steel. However, while 0.1 ppm of helium causes drastic reductions in the ductility of the type 304 stainless steel, the titanium-modified steel annealed at 1 hr at 1038°C undergoes no experimentally detectable change in ductility as a result of bombardment to 0.1 ppm of helium. Further, the properties of the material are the same in the water-quenched and furnace-cooled conditions.

At test temperatures above 500°C, the ductility of the titanium-modified stainless steel consistently decreases with increasing

preirradiation annealing temperature. Two factors that may influence the ductility of these samples are: (1) as the annealing temperature increases, the grain size becomes larger; and (2) there is a noticeable decrease in the amounts of secondary phases present with increasing temperature.

Further bombardment experiments will be performed soon in which samples containing from 1 to 50 ppm of helium should be obtained. In these samples, the helium distribution uniformity should be greatly improved due to better injection techniques. Electron microscopy is in progress to attempt to find bubbles of helium gas in material annealed after cyclotron injection of helium.

Elevated-Temperature Irradiation Embrittlement in the Austenitic Stainless Steels

E. E. Bloom J. R. Weir, Jr.

Investigation of the problem of elevated-temperature irradiation embrittlement of the austenitic stainless steels is continuing. Recent studies on two commercial heats of type 304 stainless steel containing 0.14 wt % Ti indicate that the resistance to elevated-temperature irradiation embrittlement is strongly dependent on the microstructure present prior to irradiation. Table 3.3 shows the effect of preirradiation heat treatment on the postirradiation ductility for specimens irradiated at 50°C to an exposure of 1×10^{20} neutrons/cm^2 (thermal).

Postirradiation tensile and creep-rupture tests on type 304L stainless steel specimens containing 0.14 wt % Ti that were irradiated to a total exposure of 1.3×10^{21} neutrons/cm^2 (thermal) and 1.0×10^{21} neutrons/cm^2 ($E > 1$ Mev) are in progress. Preirradiation heat treatments of 1 hr at 900°C and 1 hr at 1215°C were used. Irradiation temperatures were 650 and 800°C. Results of tensile tests are listed in Table 3.4.

The important difference between microstructures appears to be a very fine dispersion of intragranular precipitates which are present when the alloy is annealed 1 hr at 900°C and are not present when higher annealing temperatures, such as 1038 and 1215°C, are used. A second

Table 3.3. Effect of Preirradiation Heat Treatment on the Tensile Properties of Titanium-Modified Type 304 Stainless Steel Tested at 871°C

Alloy	Annealing Temperature (°C)	Yield Strength (psi)		Total Elongation, %	
		Unirradiated	Irradiated[a]	Unirradiated	Irradiated[a]
		$\times 10^3$	$\times 10^3$		
Type 304 stainless steel containing 0.014 C and 0.14 Ti (wt %)	900	10.1	11.0	64.7	34.1
	1036	8.7	9.4	75.5	17.7
Type 304 stainless steel containing 0.05 C and 0.15 Ti (wt %)	900	11.5	12.6	60.9	28.1
	1036	10.8	9.4	71.5	23.7

[a]Irradiated at 50°C to an exposure of 1×10^{20} neutrons/cm^2 (thermal).

Table 3.4. Effect of Irradiation on the Postirradiation Ductility of Type 304L Stainless Steel Containing 0.14 wt % Ti[a]

Preirradiation Annealing Temperature (°C)	Irradiation Temperature (°C)	Total Elongation (%) at		
		600°C	700°C	800°C
900	650	29.0	18.7	20.9
900	800	34.8	24.6	19.0
1215	650	14.0	11.8	7.4
1215	800	12.4	5.0	3.8

[a]Specimens irradiated to exposure of 1.3×10^{21} neutrons/cm^2 (thermal) and 1.0×10^{21} neutrons/cm^2 ($E > 1$ Mev).

factor which cannot be ignored is the different grain sizes that result from the different heat treating temperatures. Work is continuing to develop a precipitate structure in the titanium-bearing alloys such that we may compare material with equivalent grain sizes with and without the precipitate.

Table 3.5 lists the results of three postirradiation creep-rupture tests that have been completed to date.

Table 3.5. Postirradiation[a] Creep-Rupture Properties of Type 304L Stainless Steel Containing 0.14 wt % Ti[a]

Preirradiation Annealing Temperature (°C)	Irradiation Temperature (°C)	Creep-Rupture Properties at 704°C and 15,000 psi		
		Rupture Life (hr)	Minimum Creep Rate (%/hr)	Fracture Elongation (%)
900	650	31.2	0.68	27.5
900	800	37.0	0.61	38.1
1215	650	28.1	0.17	7.3

[a]Specimens irradiated to exposure of 1.3×10^{21} neutrons/cm^2 (thermal) and 1.0×10^{21} neutrons/cm^2 ($E > 1$ Mev).

4. NONDESTRUCTIVE TEST DEVELOPMENT

R. W. McClung

This program is intended to develop new and improved methods of nondestructively evaluating reactor materials and components. To achieve this we are studying various physical phenomena, developing instrumentation and other equipment, devising application techniques, and designing and fabricating reference standards. Among the methods being actively pursued are electromagnetics (with major emphasis on eddy currents), ultrasonics, and penetrating radiation. These and other methods are being evaluated for both normal and remote inspection.

Electromagnetic Test Methods

C. V. Dodd

Analytical Studies

We have continued research and development on electromagnetic phenomena on both analytical and empirical bases. We have obtained a closed-form solution of the vector potential for the case of a probe coil positioned a distance above a semi-infinite conducting plane, consisting of one conductor clad on another. The solutions apply for all values of lift-off (coil-to-metal spacing), coil length and thickness, conductivity for the two metals, and thickness of the cladding metal. We are now working on the closed-form solution for the case of a coil encircling a rod. However, the solutions to both these problems take the form of a number of unevaluated functions. The actual work involved in determining these solutions may be as time-consuming as working the problem by the relaxation method. While the closed-form solution should be more accurate, the relaxation solution is more versatile.

The relaxation technique was used to determine the shaping effects on the eddy-current distribution by the use of a ferrite cup around the

[redacted]

coil. Figure 4.1 shows the vector potential, hence the distribution of eddy currents in the metal (the currents are directly proportional to the vector potential). When the ferrite cup is added, as shown in Fig. 4.2, the currents are concentrated and a greater sensitivity to defects is achieved.

Phase-Sensitive Eddy-Current Instrument

In our continued development on the portable phase-sensitive eddy-current instrument, we designed optimum probe coils for both the 50- and 500-kilohertz frequencies. The 500-kilohertz-frequency circuits have been improved to further decrease the effects due to lift-off. For instance, on stainless steels the instrument will measure the conductivity within ±0.5% with a 0- to 30-mil lift-off variation. The instrument is undergoing final stability tests, and circuit diagrams are being prepared for distribution to the Division of Technical Information for external distribution.

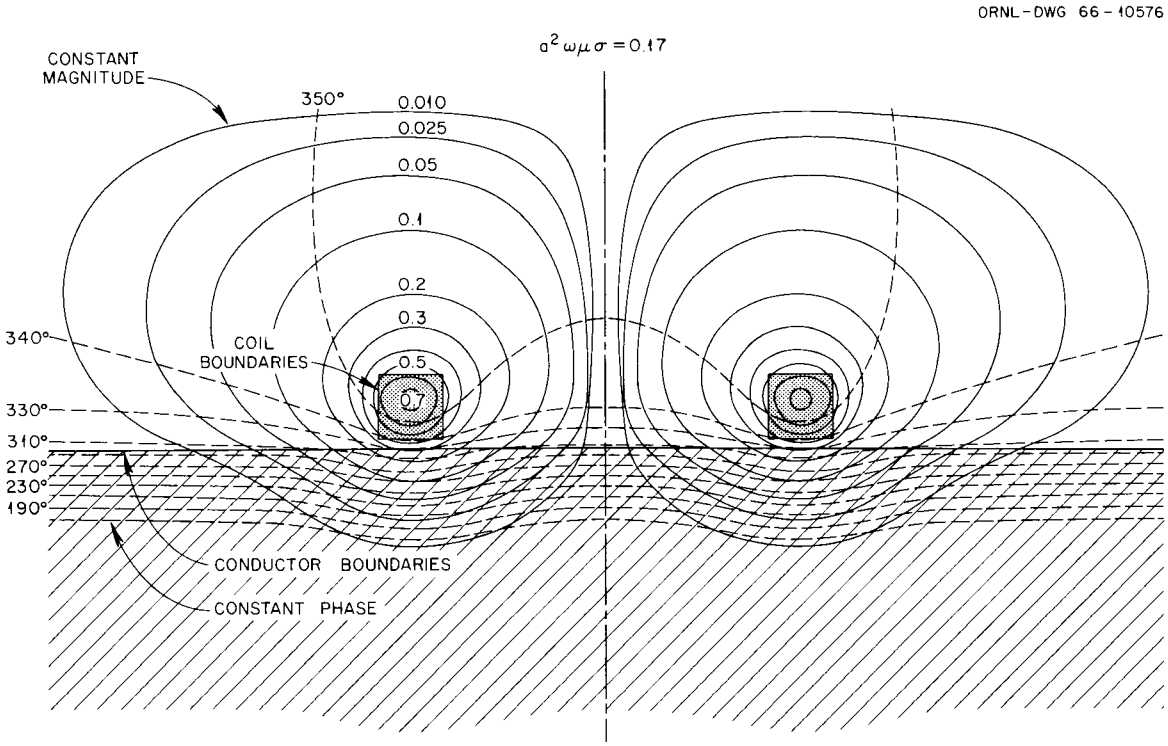

Fig. 4.1. Field of a Coil Above a Conducting Plane.

[redacted]

[redacted]

ORNL-DWG 66-10577

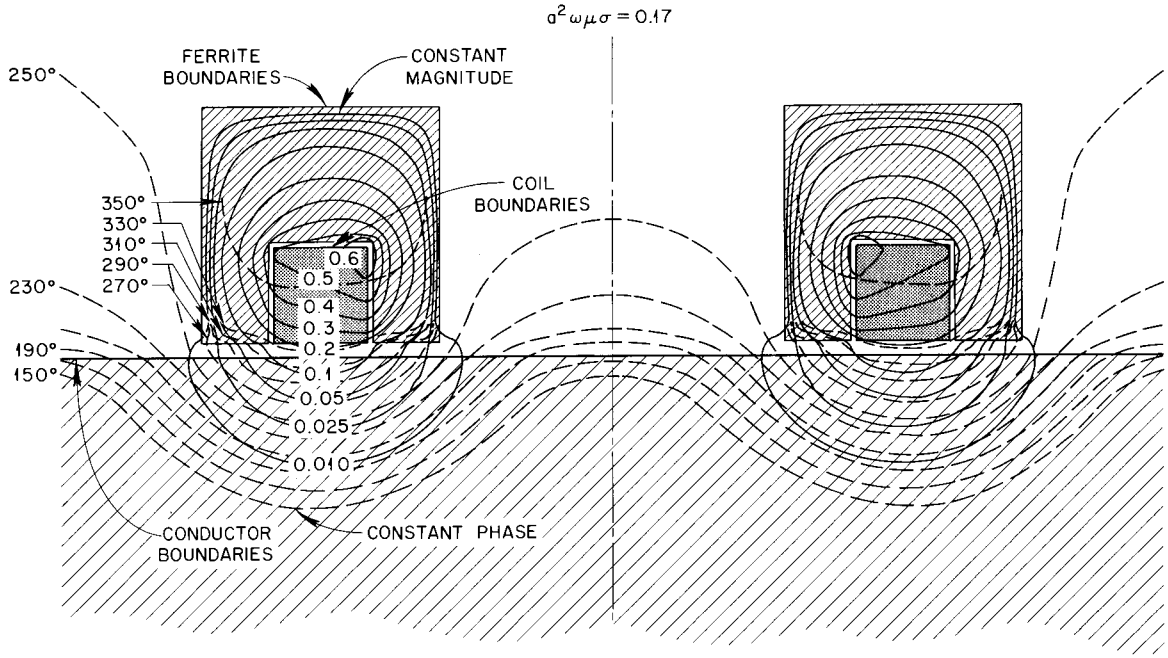

Fig. 4.2. Field of a Coil with a Ferrite Cup Above a Conducting Plane.

We have continued work on applications of the phase-sensitive eddy-current instrument. Since the phase-sensitive instrument eliminated the error due to lift-off over such a wide range, it has allowed applications previously impossible. For instance, many problems require very small coils. (Since the effect of lift-off can be scaled in terms of coil diameters, the smaller the coil, the greater the effect due to an absolute displacement.) We have been developing techniques and skill for making miniature probe coils and recently wound probes (consisting of a driver coil enclosing two small pickup coils) with an outer diameter of 0.055 in. and a length of 0.250 in. These small coils allow us to inspect small parts without effects due to curvature and the proximity of the specimen edge in relatively inaccessible locations.

[redacted]

Ultrasonic Test Methods

K. V. Cook

Fabrication of Reference Notches

We are continuing to work on the problems encountered in tubing inspection. A major problem is the establishment of realistic ultrasonic notch standards for calibration. Since electrical-discharge machining appears to be a reliable method for making both inner- and outer-surface notches, we are continuing our fabrication studies.[1] A paper on this subject has been prepared and accepted for publication.[2] The abstract follows:

> Electro-discharge machining was investigated for the preparation of artificial defects in reference materials of plate, sheet, bar, and tubing configurations.
>
> Difficulties were overcome in machining these reference discontinuities by developing reproducible methods of establishing a start-of-cut position and by preshaping the cutting tool. Techniques were also developed for measuring depths of notches, using replication methods and/or subsequent differential focusing techniques with a microscope.
>
> Longitudinal notches were machined within ±0.0001 in. of nominal depths and have been placed in tubing with an inner diameter as small as 0.065 in. Circumferential notches were machined within ±10% of nominal depths and have been placed in tubing with an inner diameter of 0.380 in.

Reference Standards

We have initiated a study which will attempt to correlate ultrasonic response from EDM notches, drilled holes, and flat-bottomed holes of various sizes machined in thin materials. At the present time we are working with sheet material; however, we plan to make a similar study with small-diameter tubing.

Four sheets of 1100 aluminum (0.019, 0.050, 0.063, and 0.080 in. thick) were selected and EDM notches of 0.001-, 0.002-, and 0.004-in.

---

[1] K. V. Cook, Fuels and Materials Development Program Quart. Progr. Rept. Dec. 31, 1964, ORNL-TM-1000, pp. 39–41.

[2] K. V. Cook and R. W. McClung, "Electro-Discharge Machined Reference Discontinuities," to be published in Materials Evaluation.

depths were machined into the samples. Holes of 1/64, 1/32, and 1/16 in. in diameter were drilled through the sheets, and 1/32-in.-diam flat-bottomed holes were machined halfway through the three thicker samples. We are generating and compiling data on reflection amplitude vs incident angle of the ultrasonic beam from the reference discontinuities in these sheets.

Penetrating Radiation Methods

R. R. Wamorkar[3] R. W. McClung

We are conducting quantitative studies on radiographic sensitivity as various parameters, such as x-ray energy, specimen thickness, and lead intensifying screens, are varied. The materials being examined are stainless steel, aluminum, and copper. Special penetrameters for the steel and aluminum have been prepared to allow evaluation of small changes in sensitivity. The penetrameters are thin sheets containing many small drilled holes varying in small increments of diameter and depth in an ordered array. For copper we are using small-diameter wire to indicate image quality. Preliminary results indicate that thin lead screens are beneficial at energies as low as 70 kvp. This contrasts with previously accepted values of approximately 120 kvp.

---

[3]Visitor from the Atomic Energy Establishment, Trombay, Bombay, India.

5. SINTERED ALUMINUM PRODUCTS DEVELOPMENT

E. A. Franco-Ferreira

Sintered aluminum products material has been designated as the construction material for the fuel rods and pressure tubes of the Heavy-Water Organic-Cooled Reactor.

Our program is to study the problems and parameters associated with primary billet fabrication. The purpose of these studies is to arrive at a more reliable and consistent product having the strength of a commercial 10 wt % Al_2O_3-SAP alloy. General process steps of importance are feed-powder characterization, dispersion preparation, and consolidation. Work is continuing on the investigation and optimization of all these steps. The progress of our program during the last three months is summarized in the following report.

Dispersion Preparation

W. R. Martin

We have, in general, considered three methods of dispersion preparation. These are (1) ball milling, (2) controlled oxidation, and (3) mechanical blending. The first two were selected for further investigation at ORNL. These investigations have indicated that ball milling is the most logical approach to be used for industrial production of SAP-like materials today.

Ball Milling (G. L. Copeland)

In order to determine the maximum efficient milling capacity of the 10-in.-diam laboratory mill, a series of batches was run with variations in the amount of aluminum powder from 2 to 11% of the weight of the steel balls. At a loading of 6%, an oxide content of 2% was produced after 15 hr of milling. The milling conditions were 33% ball charge in ribbed mill, 3% stearic acid as lubricant, with the mill filled to 50% with Varsol milling vehicle. Similar milling conditions with 2 to 3% loadings of aluminum powder produced 10% oxide after 10 to 12 hr. Thus, the 3% powder loading seems to be a reasonable maximum

for the 10-in.-diam mill under present milling conditions. The expected increase in milling action in a larger mill may increase the practical loading range. Several identical runs were made with −100, −120, and −325 mesh air-atomized aluminum powders chosen for use in the large prototype mill. The milling characteristics were the same for the three powders. The oxide content produced for a given milling time was less than for the smaller helium-atomized powders that have been used extensively thus far in the milling studies.

Fabrication of the 36-in.-diam by 16-in.-long prototype ball mill is completed. The mill and associated cleaning equipment should be installed and ready for use the first week in January.

Magnetic Separation of SAP Flake (D. H. Turner)

Magnetic separation of tramp iron from SAP flake was evaluated to determine the feasibility of reducing the iron content of the ball-milled product. A 60-g sample of MD 3100 was mixed in 200 ml of Varsol to simulate a ball-milled product. Two small permanent magnets were encased in a polyethylene bag and suspended in the slurry and agitated for two cycles of 3-min duration. After each cycle the magnets were withdrawn and the sheath was rinsed with acetone to remove the bulk of the nonmagnetic material. Magnetic particles were observed along the magnet edges after the first cycle. The magnet sheath was replaced for the second cycle. Iron analyses of the various fractions are listed below:

	Iron (wt %)
As-received MD 3100	0.35
First-cycle product	0.17
Second-cycle product	0.16

Further reduction of the amount of tramp iron is doubtful because the iron content of the aluminum powder from which the flake is made is on the order of 0.2%. This experiment suggests the possibility of utilizing a magnetic filter on the ball-milled product prior to separation of the Varsol. An improved separator is planned to evaluate this technique further.

Powder Consolidation

M. M. Martin D. H. Turner[1]

The primary purpose of consolidation is to get SAP powder into a convenient geometric shape for subsequent extrusion to a semifinished product while retaining and/or converting the aluminum oxide to a stable form of predictable morphology. Processes under investigation include combinations of cold pressing, vacuum annealing, vacuum hot pressing, and vacuum fusion. The process that exhibits superior mechanical properties with minimum variability will be selected for more detailed evaluation and scale-up for pilot production of 10% Al_2O_3-SAP billets.

A series of 2-in.-diam SAP billets was produced by six different consolidation processes from commercially produced Al–6 wt % Al_2O_3 flake[2] and evaluated on the basis of mechanical properties. The consolidation processes and variables used are described in Table 5.1. Equipment limitations necessitated the stacking of cold-pressed compacts to form billets of adequate length for processes A, C, and E. However, lubricant entrapment at the compact interfaces proved to be a problem with this technique. The density of all billets immediately prior to extrusion was 70 to 80% of theoretical; all nonfused billets were approximately 79% of theoretical. Billet length was 2.5 in. except for the fused billets, which varied because of leakage around the hot press die punches during the fusion process.

All billets were extruded at 436°C with a reduction ratio of 30:1 to 3/8-in.-diam rod. Following extrusion, the rods were straightened by swaging at 450°C with a reduction ratio of 1.02:1. Mechanical properties tests were performed at 450°C using a strain rate of 0.0002 min^{-1}. Maximum and minimum mechanical properties values along the length of each extruded SAP rod are presented in Table 5.2. Consolidation process E-1 showed the best ductility. This was 0.8% minimum and 1.1% minimum for

[1]On loan from Atomics International.

[2]Metals Disintegrating Type MD 3100.

[redacted]

Table 5.1. Details of Consolidation Processes and Attributes of MD 3100 SAP Billets under Investigation

Process	Description	Billet Attributes		
		Density (% of theoretical)[a]	Surface Condition	Number of Layers
A	As-received powder + cold press (14.2 tsi) + vacuum anneal (20 hr at 600°C; < 10^{-1} torr)	78	Numerous circumferential cracks	4
B	As-received powder + vacuum hot press (2.5 hr total time at 600°C; 0.8 tsi applied for 0.5 hr; less than 10^{-1} torr) + vacuum anneal (17.5 hr at 600°C; < 10^{-1} torr)	78	Excellent	1
C-1	Vacuum annealed powder (600°C for 20 hr) at < 10^{-2} torr + cold press at 13 tsi	79	Excellent	4
C-2	Vacuum annealed powder (600°C for 20 hr) at < 10^{-1} torr + cold press at 13 tsi	79	Excellent	4
D	Vacuum annealed powder (20 hr at 600°C; < 10^{-1} torr) + vacuum hot press (2.5 hr total time at 600°C; 0.8 tsi applied for 0.5 hr; < 10^{-1} torr)	77	Some circumferential striae	1
E-1	As-received powder cold pressed at 13 tsi followed by vacuum fusing for 1 hr at 700°C at a pressure < 1 torr	75	Some circumferential cracks	1[b]
E-2	As-received powder cold pressed at 13 tsi followed by vacuum fusing for 1/4 hr at 700°C at a pressure < 1 torr	75	Some circumferential cracks	1[b]
F-1	Vacuum annealed powder at 600°C for 20 hr followed by vacuum fusing for 1 hr at 700°C at a pressure < 1 torr	71	Excellent	1[b]
F-2	Vacuum annealed powder at 600°C for 20 hr followed by vacuum fusing for 1/4 hr at 700°C at a pressure < 1 torr	71	Excellent	1[b]

[a]Theoretical density = 2.74 g/cm^3.

[b]Billets composed of four cold-pressed compacts fused together in vacuum hot press.

[redacted]

Table 5.2. Maximum and Minimum Mechanical Properties of SAP Rods[a]

Process	SAP Number	Tensile Strength, psi		Uniform Elongation, %		Total Elongation, %		Number of Specimens
		Maximum	Minimum	Maximum	Minimum	Maximum	Minimum	
		$\times 10^3$	$\times 10^3$					
A	173	16.2	14.3	0.8	0.5	1.0	0.6	8
	174	13.6	9.8	0.7	0.4	1.0	0.5	9
	175	9.6	8.9	0.7	0.4	0.8	0.4	9
	176	10.0	9.2	0.7	0.4	0.7	0.5	8
B	177	11.7	9.8	0.9	0.5	1.4	0.6	9
	178	12.0	9.4	1.0	0.4	1.7	0.5	8
C-1	169	14.2	11.9	0.5	0.3	1.0	0.4	9
	170A	14.0	11.9	0.8	0.4	1.0	0.4	8
C-2	188	15.3	12.0	0.7	0.3	1.0	0.3	8
	189	15.3	12.0	0.6	0.4	0.9	0.4	9
D	171	12.2	11.5	0.6	0.4	1.0	0.6	9
	172	12.3	11.4	0.6	0.4	1.1	0.6	9
E-1	196	12.8	11.4	1.0	0.8	1.4	1.1	5
E-2	197	13.3	11.3	0.7	0.4	1.3	0.7	6
F-1	193	12.9	12.1	0.8	0.7	0.9	0.9	2
F-2	194	13.0	10.7	0.7	0.5	1.1	0.7	4
Commercial SAP 895	210	12.4	11.9	0.7	0.5	1.3	0.8	6

[a]Tested at 450°C and 0.0002 min^{-1} strain rate.

uniform and total percent elongation, respectively. As shown in Table 5.3, processes B and C produced material whose tensile strength had a high degree of length dependency. Subject to the limitations of footnote d in Table 5.3, it appears that the products of processes E-2 and F-2 behaved similarly. However, this may be related to a high oxide content at the nose of the extrusions. Elimination of the high-oxide area from the evaluation yielded the tensile values presented in Table 5.3 for the fused SAP. Based on its strength and lack of variability, process D appears to be the most attractive in that it closely approximates the properties of SAP 895 at an oxide content significantly lower.

Table 5.3. Ultimate Tensile Strengths and Expected Deviations of SAP Rods Expressed as a Linear Function of Extruded Rod Length[a]

Process	Procedure	Ultimate Tensile Strength (psi)	Expected Deviation[b] (psi)	(%)
		$\times 10^3$	$\times 10^3$	
A	ARP + CP + VA	9.4	±0.65	6.9[c]
B	ARP + VHP + VA	12.2 − 0.55L	±0.96	8.6[c]
C-1	VAP(HV) + CP	13.7 − 0.039L	±1.34	10.4[c]
C-2	VAP(LV) + CP	15.5 − 0.086L	±0.75	5.4[c]
D	VAP(HV) + VHP	11.9	±0.82	6.9
E-1	ARP + CP + F (1/4 hr)	11.9	d	d
E-2	ARP + CP + F (1 hr)	11.5	d	d
F-2	VAP + CP + F (1 hr)	10.9	d	d
Commercial SAP 895		12.1	±0.77	6.4

[a]L = distance from nose of extruded rod, inch.

[b]Statistical tolerance limits, pounds per square inch.

[c]Value applies at midlength of rod.

[d]Insufficient tests to derive a meaningful value.

Chemical analyses of the products of the various processes are presented in Table 5.4. The high iron content is attributable to the utilization of the MD 3100 flake for the experiments. No explanation can be offered for the high oxide analyses at the nose of the extruded fused products. The oxide content of the products of all processes was significantly higher than the 6.3% oxide content of the MD 3100 flake.

We have examined the rods from this extrusion for texture differences. The results for as-extruded rods may be divided into three groups, as shown in Table 5.5. Deviations within a particular set are not great;

[redacted]

Table 5.4. Chemical Analyses of SAP Rods[a]

Process	Chemical Composition, wt %			Total Gas Content (cm^3/100 g)	Gas Content, ppm	
	Al_2O_3	Carbon	Iron		Hydrogen	Nitrogen
A	7.7–9.6	0.24–0.36	0.18	8.4		
B	6.6	0.26–0.29	0.18	3.4		18–25
C	8.2–9.4	0.12–0.29	0.19–0.20	5.7–19.0	5–15	
D	8.2	0.29	0.19	7.4		
E	7.7–11.5	0.53	0.16		7–11	29
F	10.1–14.3	0.30–0.36	0.15–0.16		8–16	186
Commercial SAP 895	11.5	0.24	0.06		2–4	220

[a]The range of values represent the maximum and minimum of at least four determinations along the rod length.

Table 5.5. Texture Variation of As-Extruded SAP Rods[a]

Process	SAP Number	Tensile Strength (psi)	Relative Degree of Texture
		$\times 10^3$	
A	176-F	9.5	Highest ⟨111⟩ component
B	177-F	11.6	
C	170A-F	12.3	In between
D	171-F	11.7	
E	189-F	13.5	
A	173-F	15.5	Lowest ⟨111⟩ component

[a]From extension set 10.

variations between groups, however, are very significant. Further interpretation awaits electron micrographs and texture determinations on annealed samples.

On the basis of the above data, we conclude that the process of vacuum annealing SAP powder and vacuum hot pressing produces the most

[redacted]

consistent product, the properties of which closely approximate those of SAP 895. The fusion consolidation process appears to improve ductility somewhat, but expected variability within the product is unknown. The VAP and VHP processes have therefore been selected for scale-up and further optimization studies.

Tooling is being designed and procured for consolidation and primary extrusion of 5.6-in.-diam billets as well as secondary extrusion of tubing and rod for strength evaluation. In the interim, optimization studies on 4-in.-diam billets for which tooling exists will be initiated.

Evaluation of Product

W. R. Martin

Standard techniques were used to evaluate the SAP produced and procured by ORNL. These include metallography, electron microscopy, x-ray diffraction, chemical analysis, nondestructive testing techniques, and mechanical properties measurements.

High-Temperature Stability (G. L. Copeland)

Several samples of extruded rods were annealed at 600°C in vacuum and air to determine if ball-milling lubricant is a controlling factor in the stability of the alloy at this temperature. These rods were made from flake ball milled at ORNL with the only variable being the use of either oleic or stearic acid as the milling lubricant. In a previous annealing experiment, rods from commercial flake milled in oleic acid were unstable, whereas rods from flake of equivalent oxide content milled in stearic acid at ORNL and fabricated in the same manner were stable at 600°C. In addition, samples were included from rods made from spherical powder. The oxide content of these rods was increased by high-temperature oxidation or by forming a low-temperature hydrate and converting this to oxide. The samples tested, their fabrication schedule, and their hydrogen contents as-extruded and after a 20-hr vacuum anneal are shown in Table 5.6. A sample of each rod was annealed in air for 20 hr at 600°C, under vacuum for 20 hr at 600°C, and then in air for 20 hr at 600°C. The diameter of each sample was measured before

Table 5.6. Samples Annealed to Determine Structural Stability of Extruded SAP

SAP Rod Number	Oxide Content (%)	Fabrication Process[a]	Hydrogen, ppm	
			As Extruded	Vacuum Annealed
102	6.5	BM(o)-VHP-EXT	1	2
121	9.2	BM(S)-VHP-EXT	4	2
129	14.3	Filing-BM(S)-VHP-EXT	18	5
134	6.6	BM(o)-CP-VA-EXT	6	3
145	9.5	BM(S)-VHP-EXT	2	
166	9.4	HT oxidized-CP-VA-EXT	15	2
167	12.0	Hydrated-CP-VA-EXT	12	4
168	20.9	Hydrated-CP-VA-EXT	21	4

[a]BM — Ball milled at ORNL: (o) oleic acid lubricant; (S) stearic acid lubricant.

VHP — vacuum hot pressed, 2 1/2 hr at 600°C under vacuum, 2- × 2-in. cylindrical compact.

EXT — extruded at 500°C, 30:1 ratio.

Filing — commercial — granulated by filing.

CP — cold pressed at approximately 17 tsi.

VA — approximately 80% dense compact vacuum annealed at 600°C for 20 hr.

HT oxidized — spherical H-3 powder oxidized at 550°C under partial pressure of oxygen.

Hydrated — spherical H-3 powder hydrated at low temperature under controlled conditions.

and after each annealing treatment. Metallographic examination was done after the annealing treatments. Hydrogen analysis was done by vacuum fusion and mass spectrometry on the as-extruded rod and after the vacuum treatment.

The rods numbered 102, 121, 134, and 145 developed a few fissures and small voids during annealing, but there was no gross structural change. This indicates that ball-milling lubricant is not the controlling factor in high-temperature stability of the extruded rods. The behavior of rod 129 was similar to that of the other rods, but it developed more fissures and voids. Rods 166, 167, and 168 developed many more fissures and voids and rod 168 was cracked extensively after annealing. The

higher hydrogen contents of these rods may indicate that some hydrate is still present in the extruded rod. None of the samples showed measurable volume change (accuracy of measurement was approximately 1%) during annealing.

Al_2O_3 Analysis of SAP (D. H. Turner)

During the ORNL SAP development program the accuracy of the aluminum oxide analysis has been frequently questioned. In order to evaluate the analytical techniques for oxide content and to provide a common analytical base between ORNL and AI, a series of SAP 895 cladding samples was interchanged to obtain comparative results. Three cladding samples were each cut in half. Each half-sample was analyzed using fast neutron activation analysis at AI and subsequently analyzed at ORNL by the same technique and by the conventional anhydrous HCl technique, modified to include a nitrogen flush to remove any residual aluminum chloride. The results, which are presented in Table 5.7, show excellent agreement between techniques and sites.

Table 5.7. Al_2O_3 Analyses of Interchanged Samples

Sample Number[a]	Al_2O_3 (wt %) and Standard Deviation					
	Neutron Activation				ORNL Anhydrous HCl[d]	
	AI[b]		ORNL[c]			
1,2	10.50	±0.36	10.44	±0.23	10.62	±0.04
3,4	10.61	±0.34	10.40	±0.25	10.26	±0.41
5,6	10.43	±0.29	10.51	±0.32	10.20	±0.27

[a]Numbers 1 and 2, 3 and 4, and 5 and 6 are halves of the same sample.

[b]Five determinations on each half-sample.

[c]Four determinations on each half-sample.

[d]Two determinations on each half-sample.

Evaluation of Commercial Product (D. G. Harman and D. H. Turner)

In order to provide base-line data to establish minimum requirements for ORNL semifinished SAP products, current commercial products are being evaluated. A 2-in.-diam SAP 895 billet produced by Montecatine was obtained from Atomics International. The billet was from the tail end of an 18-ft-long bar. A 2-in. length of the billet was extruded at ORNL at 436°C with a 30:1 reduction ratio to 3/8-in.-diam rod. Evaluation of this specimen included metallography, electron microscopy, chemical analysis, and mechanical properties. The longitudinal and transverse mechanical properties of a second 2-in. length were measured in the as-received condition.

The microstructures of SAP 895, both transverse and longitudinal, are shown in Fig. 5.1. The material exhibited some banding in the longitudinal section, but was almost completely free of inclusions. The SAP 895 was examined by transmission electron microscopy in the transverse direction. The structure at 32,000×, shown in Fig. 5.2, exhibits some tendency toward clustering of the oxide particles, but this is not severe. Average oxide particle size and center-to-center spacing were determined by linear analysis to be 0.2 and 0.4 μ, respectively.

The chemical analysis of the 3/8-in.-diam SAP 895 rod is given in Table 5.8 as a function of position in the rod. The material appears to be very uniform.

Elevated-temperature mechanical properties were determined along the length of the 3/8-in.-diam SAP 895 rod. The rod, after extrusion at ORNL, had a total reduction of approximately 750:1 from the original compact. No significant lengthwise variation in properties was noted. The results of the mechanical property tests are presented in Table 5.9.

In addition to these tests, a short section of the as-received 2-in.-diam 895 extrusion was sectioned and specimens machined parallel and transverse to the extrusion direction. These specimens were tensile tested at ambient and elevated temperatures at three strain rates.

The test results are shown in Table 5.10 and compared with our data from a similarly tested XAP-001 extrusion. The transverse-to-longitudinal

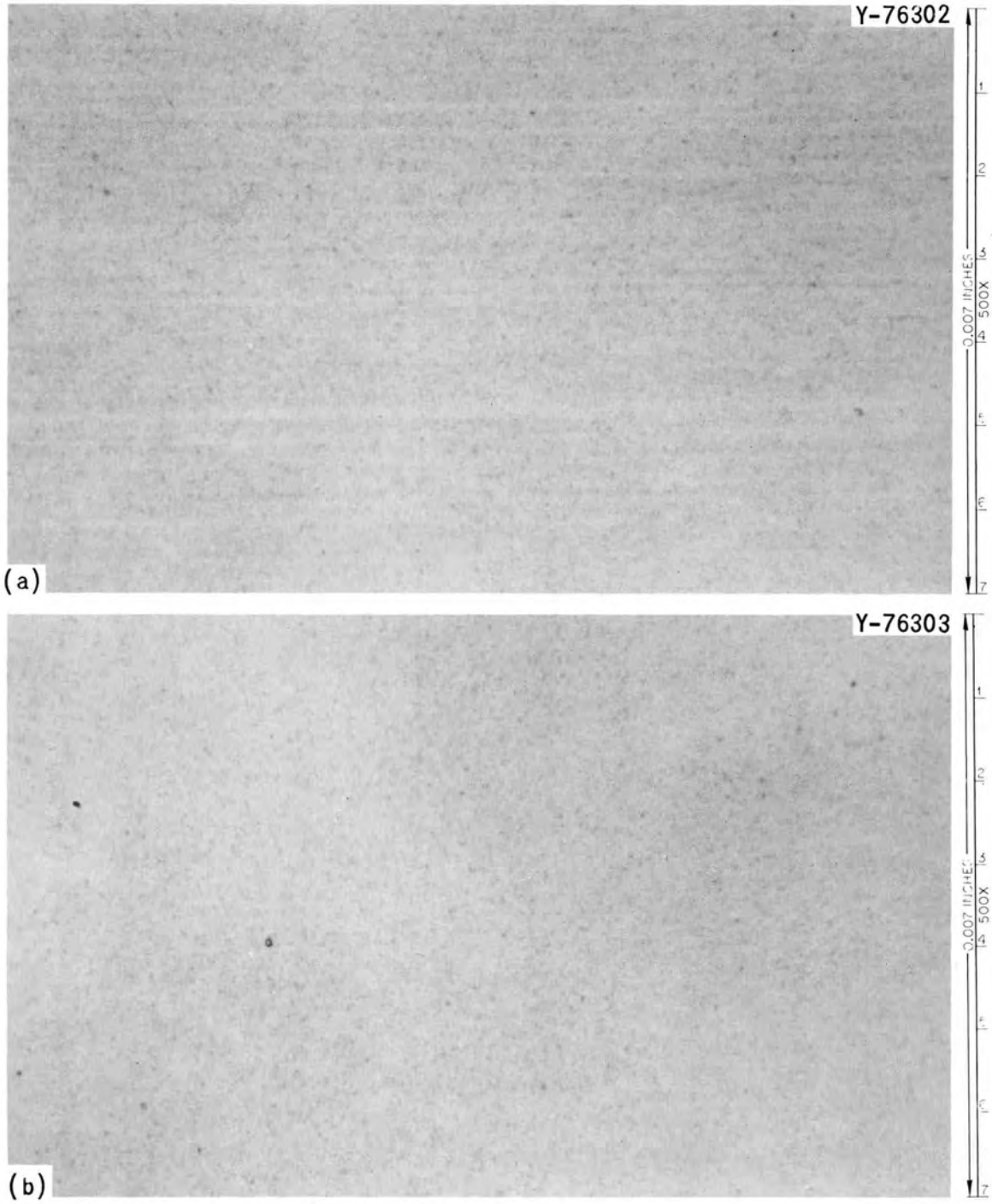

Fig. 5.1. Microstructures of SAP 895 Extruded at ORNL in the (a) Longitudinal and (b) Transverse Directions. As polished.

[redacted]

Fig. 5.2. Typical Structure of SAP 895 in Transverse Direction. 32,000X.

[redacted]

[redacted]

Table 5.8. Chemical Analysis of SAP 895 Rod (ORNL SAP 210)

Sample Location	Chemical Composition, wt %				
	Al_2O_3	C	Fe	H_2	N_2
Nose	11.5	0.244	0.057	0.0003	
Center	11.4			0.0003	0.022
Tail	11.3			0.0002	

Table 5.9. Mechanical Properties of SAP 895 Extruded at ORNL[a]

Specimen Number	Distance from Nose to Center (in.)	Strain Rate (min^{-1})	0.2% Yield Strength (psi)	Ultimate Tensile Strength (psi)	Elongation, %	
					Uniform	Total
4	12 5/8	0.02	13,800	14,440	0.91	2.5
7	14 3/4	0.002	12,800	13,060	0.8	2.1
1	3 5/8	0.0002	11,600	11,980	0.68	0.8
2	6 5/8	0.0002		12,190	0.70	1.3
8	17 3/4	0.0002	11,200	12,080	0.64	1.1
16	31	0.0002	12,000	12,200	0.53	0.9
17	34	0.0002	11,030	11,940	0.76	1.0
19	40	0.0002	11,510	12,420	0.62	0.8
Mean values at lowest strain rate			11,470	12,130	0.65	1.0

[a]30:1 reduction ratio, tested at 450°C (ORNL No. SAP 210).

ratio of properties is also listed in the table for these two commercial alloys. This ratio for the strength values is very low at the slowest strain rate.

The effect of strain rate on the elevated-temperature mechanical properties of the two alloys is shown graphically in Figs. 5.3 and 5.4. Figure 5.3 shows that as the strain rate is decreased the difference in strength between the 2-in.-diam longitudinal and transverse directions remains essentially constant for each alloy. This difference was about 3500 psi for the SAP 895 and about 2000 psi for the XAP-001. Notice

[redacted]

Table 5.10. Longitudinal and Transverse Mechanical Properties of XAP-001 and SAP 895 Alloys[a]

Material	Test Temperature (°C)	Strain Rate (min^{-1})	Longitudinal Properties			Transverse Properties			Transverse-to-Longitudinal Ratio		
			0.2% Yield Strength (psi)	Ultimate Tensile Strength (psi)	Total Elongation (%)	0.2% Yield Strength (psi)	Ultimate Tensile Strength (psi)	Total Elongation (%)	0.2% Yield Strength	Ultimate Tensile Strength	Total Elongation
SAP 895	25–29	0.02	33,310	40,220	9.9	29,780	38,050	8.6	0.89	0.95	0.87
	450	0.02	13,490	14,650	2.0	11,320	11,490	0.6	0.84	0.89	0.30
	450	0.002	12,410	12,900	1.4	9,080	9,240	0.9	0.73	0.72	0.64
	450	0.0002	10,720	11,390	1.1	6,690	7,430	1.0	0.62	0.65	0.91
XAP-001	25–29	0.02	32,000	38,270	11.5	23,680	33,590	6.0	0.74	0.88	0.52
	450	0.02	10,280	11,280	2.7	9,190	9,650	0.7	0.89	0.86	0.26
	450	0.002	9,690	10,400	1.8	7,990	8,450	1.1	0.82	0.81	0.61
	450	0.0002	8,650	9,170	1.3	6,740	6,990	0.9	0.78	0.76	0.69

[a]Rods extruded to 2 in. in diameter.

[redacted]

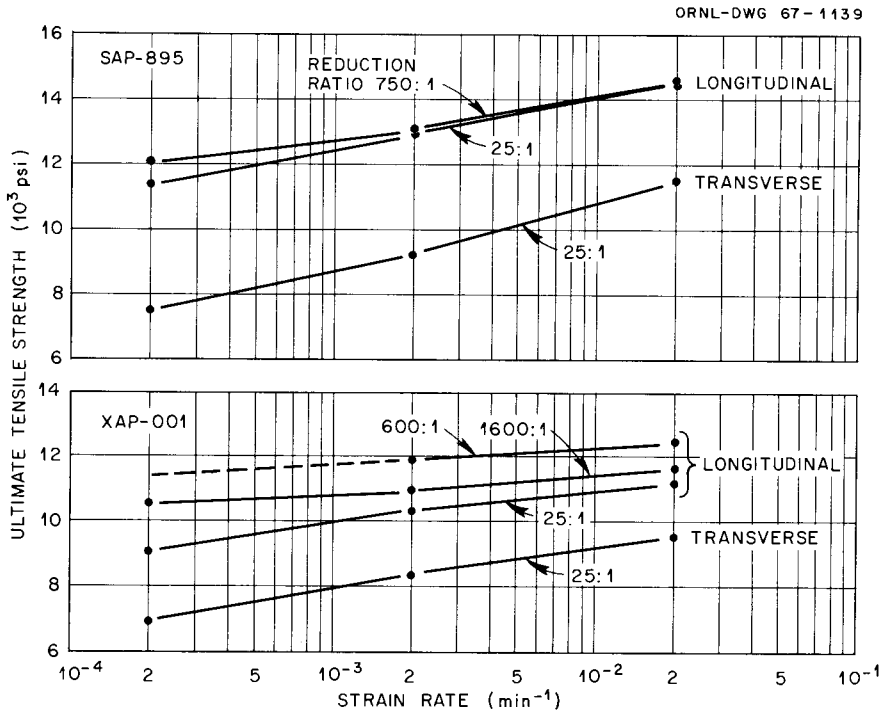

Fig. 5.3. Tensile Strength of Commercial SAP Alloys of Various Reduction Ratios at 450°C.

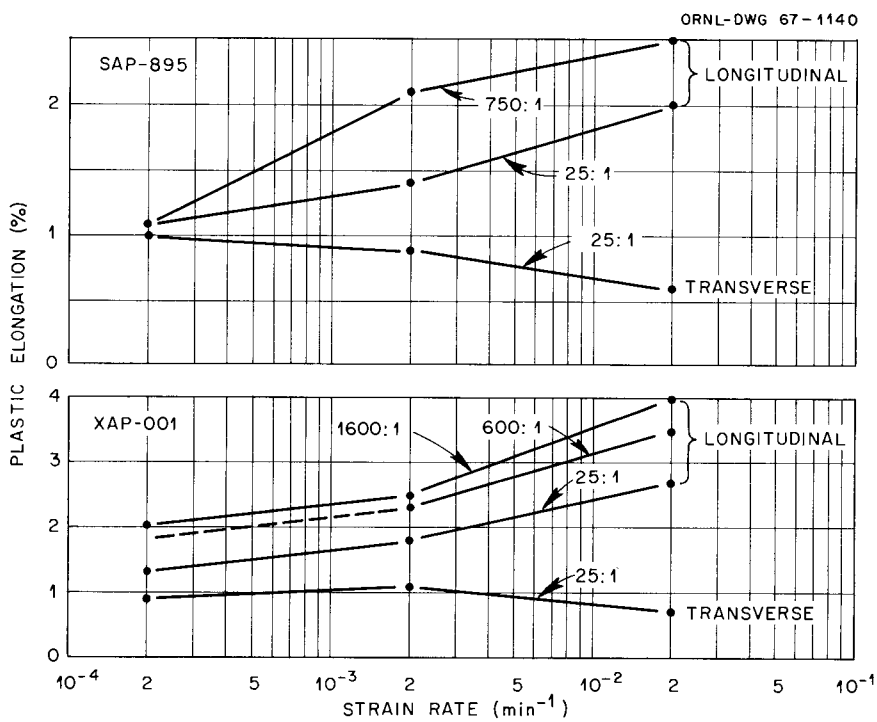

Fig. 5.4. Ductility of Commercial SAP Alloys of Various Reduction Ratios at 450°C.

[redacted]

that the SAP 895 is only 440 psi stronger in the transverse direction than is the XAP-001. Figure 5.4 shows that changing the strain rate by two orders of magnitude had very little effect on the ductility for either alloy as measured in the transverse direction. The material showed transverse elongations of 1% or less at all strain rates. On the other hand, a pronounced strain rate effect was noted on the longitudinal ductility. The elongation values essentially doubled with the two-order-of-magnitude increase in strain rate.

Additional billet samples from the center and nose of the 18-ft SAP 895 rod have been obtained for testing. Samples of recently produced SAP 930 and XAP-005 have also been obtained for evaluation.

SAP-UC Compatibility Experiments (J. T. Venard)

A recent review of the literature concerning reactions between SAP and UC revealed that a few inconsistencies exist among the data of various investigators.[3] This same review suggests that compatibility curves, similar to those of Figs. 5.5 and 5.6, may be valid for design use. A limited test program, using the compatibility capsule design shown in Fig. 5.7, has been initiated to investigate the validity of those curves. Table 5.11 is a listing of the proposed experiments. At present, we have completed all the anneals except those of 10,000-hr duration. These tests will be completed in March 1968. No metallographic or other analytical results are presently available on the completed anneals, but we anticipate obtaining these during the coming quarter.

Nondestructive Test Development (H. L. Whaley)

We have been concerned with development of systems and techniques for determination of flake thickness and oxide content of the aluminum powders. An air-settling device is being developed for the flake thickness measurements, and eddy-current conductivity measurements on fused compacts of SAP are being employed on the oxide content problem.

---

[3] J. T. Venard, Compatibility of Dispersion Strengthened Aluminum with Uranium Monocarbide — A Review of the Literature, ORNL-TM-1705 (January 1967).

[redacted]

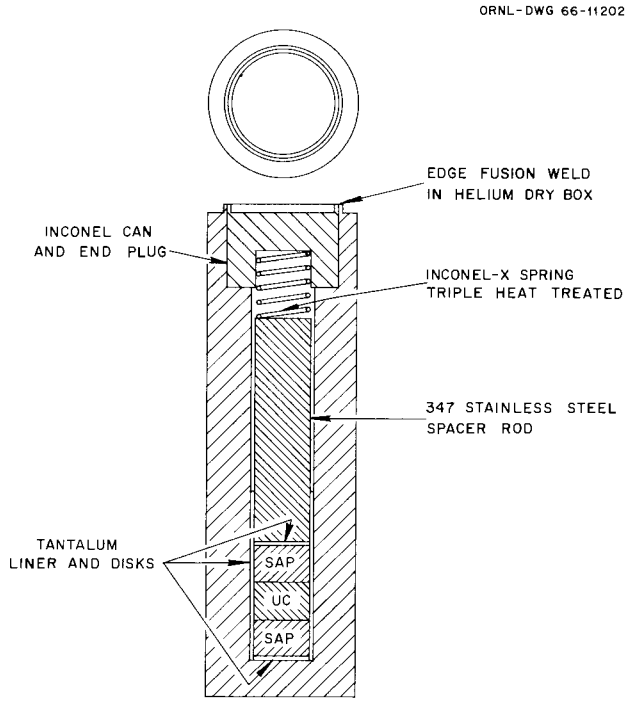

Fig. 5.5. Temperature-Time Compatibility Limits for the SAP-UC (4.8 wt % C) System.

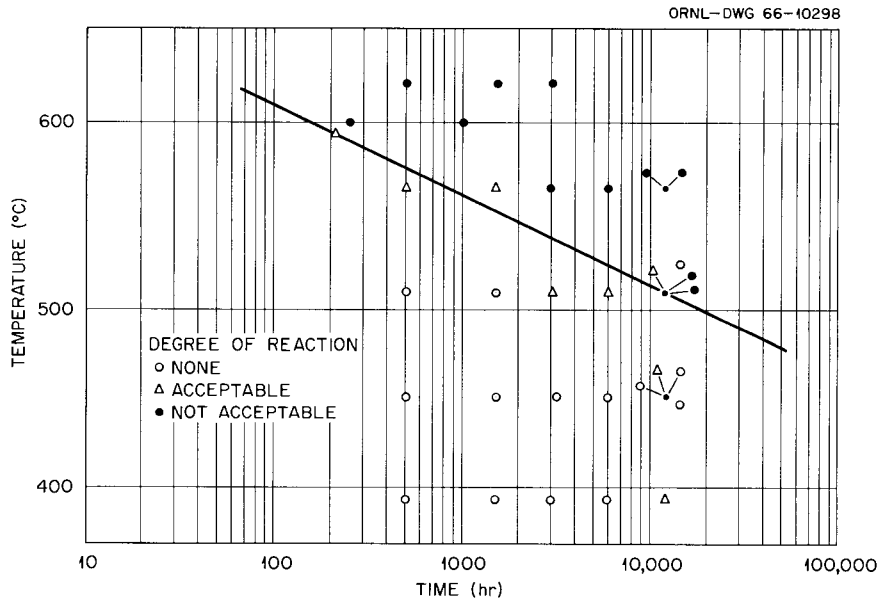

Fig. 5.6. Temperature-Time Compatibility Limits for the SAP-UC (> 4.8 wt % C) System.

[redacted]

[redacted]

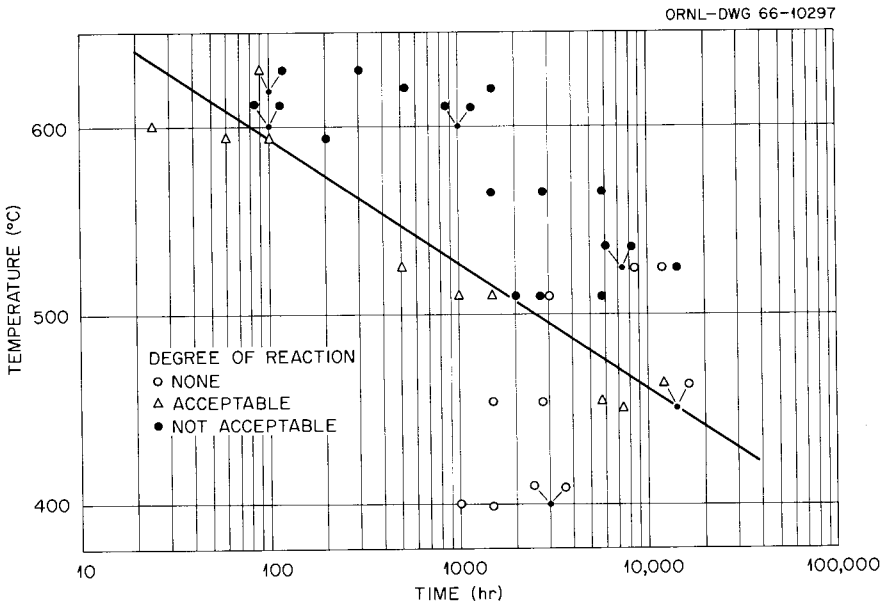

Fig. 5.7. Compatibility Capsule.

Table 5.11. Temperatures and Times for SAP-UC Compatibility Capsules

UC Chemistry, wt %					
< 4.8 C		4.8 C		> 4.8 C	
Temperature (°C)	Time (hr)	Temperature (°C)	Time (hr)	Temperature (°C)	Time (hr)
600	10	575	100	625	100
575	10	550	100	600	100
550	10			575	100
		525	1,000		
500	100	500	1,000	575	1,000
475	100	475	1,000	550	1,000
450	100			525	1,000
		475	10,000		
		450	10,000	550	10,000
		425	10,000	525	10,000
				500	10,000

[redacted]

Work is continuing with the settling apparatus for flake thickness measurements. An overall view of this unit is shown in Fig. 5.8. Metallographic examination of powder samples collected in the settling chamber has confirmed the dependence of settling position of a given particle on its thickness. Not enough particles were collected in the samples, however, to establish the exact nature of this dependence. It was impractical to spend the large amount of time needed to collect such large samples at this time because many particles were still observed passing completely through the chamber without settling out even though the horizontal air velocity had reached the practical lower limit. Metallographic inspection disclosed that the thinnest particles collected were 4 μ thick; the ones not settling out in the air chamber, then, were assumed to be those thinner than 4 μ since the settling distance increases as thickness decreases. Since we wished to collect particles thinner than 1 μ, a practical means of increasing the settling rate (and thereby collecting thinner particles) was needed. Two approaches investigated were: (1) use of a gas other than air in which to settle the flakes and (2) use of reduced air pressure in the settling chamber. Calculations eliminated gases other than helium and hydrogen. Next, the thinner particles were observed to remain suspended in still helium for several minutes, thus requiring a very long settling chamber. Hydrogen offered only a factor of 2 increase in settling rate as compared to helium. Therefore, the reduced pressure approach was taken. A large reinforced lucite box to enclose the settling chamber in a reduced air-pressure environment has been designed, and shop construction has commenced.

Cold compacts of SAP have been shown to be unsuitable for measurements of oxide content using eddy currents since the compacts have very poor electrical conductivity even when compacted to the highest practical pressures. Preliminary results obtained with the fused compacts are, however, encouraging. Two 1-in. fused compacts of MD 3100 about 0.130 in. thick were tested and found to have a conductivity between that for 2024 and 1100 aluminum. After demonstration that compacts of a given powder can be reproducibly made, compacts of powder of chemically determined oxide contents for the oxide range of interest will be made for calibration purposes.

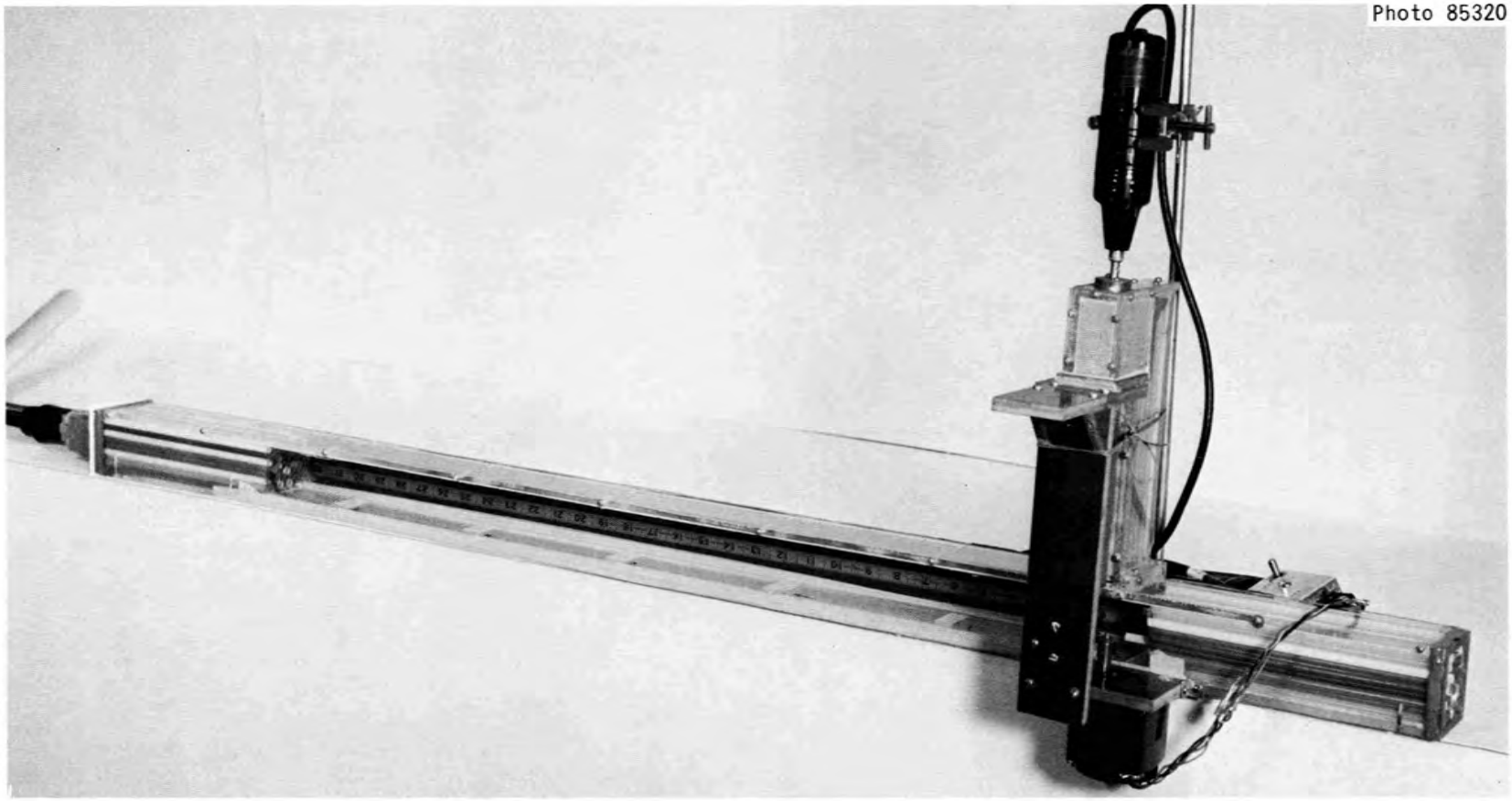

Fig. 5.8. Settling Apparatus for Flake-Thickness Measurements

Gamma attenuation is being investigated as a backup approach to the eddy-current technique for oxide content measurement. Its chief advantage is that the density of the compact is not critical as long as the same weight of starting powder is used for each compact. The gamma attenuation approach is, however, more expensive and involves a potential radiation hazard.

Development of Advanced SAP Materials

D. G. Harman G. L. Copeland

Work on advanced SAP materials is continuing using powders produced by two different methods: metal filings and ribbon casting. Both of these involve the milling, consolidation, and fabrication of a unique starting material.

The milling and consolidation steps are those developed at ORNL and reported previosly.[4] Final fabrication is by either hot extrusion or hot swaging.

Metal Filings

The initial work in this area included metal filings of four wrought aluminum alloys – 1100 aluminum (99.9% Al), 5052 (Al–2.5% Mg) 5154 (Al–3.5% Mg), and 5056 (Al–5.2% Mg). The resulting mechanical properties have been reported.[4] The essential conclusions were the following:

1. The 1100 aluminum filings produced a SAP product superior in strength to commercial SAP of equivalent oxide content.

2. The elevated-temperature strength of the aluminum-magnesium alloys decreased with increasing magnesium content.

3. Both the uniform and total elongations were considerably greater than those for commercial SAP and both of these properties increased with increasing magnesium content.

---

[4] G. M. Adamson, Jr., Fuels and Materials Development Program Quart. Progr. Rept. Sept. 30, 1966, ORNL-TM-1700, pp. 54–89.

[redacted]

Filings of these aluminum-magnesium alloys were milled using tungsten carbide balls and an overabundance of Varsol. The purpose of this was to produce a finer flake (smaller interparticle spacing), and thus, a stronger product. Preliminary oxide analyses from the initial 6-hr milling runs indicate that the additional Varsol successfully retarded the oxidation rate. One-inch billets of this material were hot swaged into rod for mechanical testing.

In addition to the commercially available alloys discussed above, the production of powder from filings of five experimental alloys is being studied. These alloys, which contain molybdenum, iron, and zirconium as their major alloying elements, are listed in Table 5.12. Alloys A-602 and A-204 have been successfully filed and are ready for milling. A small amount of oxidation will be allowed during milling to promote creep resistance.

Table 5.12. Experimental Aluminum Alloys for Filing Studies

Alloy	Nominal Composition, wt %				
	Molybdenum	Iron	Zirconium	Chromium, Titanium, Vanadium	Aluminum
A-602	6.0		2.0	0.2 each	Balance
A-204	2.0		4.0	0.2 each	Balance
A-222	2.0	2.0	2.0	0.2 each	Balance
A-620	6.0	2.0	0.2	0.2 each	Balance
A-440	4.0	4.0	0.2	0.2 each	Balance

Ribbon Casting

The starting material for this type of powder is a very thin metal ribbon produced by spraying a capillary stream of molten metal onto a rotating, water-cooled wheel. This technique has been developed commercially for aluminum and other metals by R. Pond of Johns Hopkins University, and the patents belong to Marvalaud Corporation.

The alloys presently being investigated microstructurally include aluminum alloyed with silicon (11.5, 15, and 20% Si), magnesium (5 and 18% Mg), zinc (78% Zn), nickel (4 and 8% Ni), iron (5 and 10% Fe), and a combination of molybdenum and zirconium (7% Mo + 2% Zr).

[redacted]

[redacted]

Aluminum ribbon purchased from Marvalaud Corporation has been milled in Varsol plus stearic acid using tungsten carbide balls. This has produced a flake powder that appears to be suitable for producing SAP material.

[redacted]

6. ZIRCONIUM METALLURGY

M. L. Picklesimer

Zirconium-base alloys are of potential use as structural materials for water-cooled and/or moderated and organic-cooled reactor systems. At present most of our work is directed toward the effective use of the anisotropy of mechanical properties of α-zirconium alloys and study of their basic oxidation-corrosion mechanisms. In particular, we are investigating: (1) the effects of fabrication variables on the resulting crystallographic texture; (2) the effect of texture on the anisotropy of mechanical properties in uniaxial and biaxial stress states; (3) the deformation systems operating in zirconium and its alloys as functions of stress relative to crystallographic directions, stress state, restraint to flow, temperature, and alloying additions; and (4) the mechanisms of the oxidation-corrosion processes from considerations of the mode of formation, rate of growth, composition, and structure of the corrosion films and the composition and crystallography of the underlying metal.

Anisotropy in Zircaloy-2 and Zircaloy-4

P. L. Rittenhouse

Multiaxial Testing of Tubing

Two preliminary tension-tension tests have been run on Zircaloy-2 tubing. The first test was terminated prematurely because of leakage of hydraulic fluid, but the second was carried to completion after several seals were installed. There was, as expected, a considerable decrease in internal pressure as the test proceeded so that the final stress ratio is in doubt. A servo-valve and pressure transducer are presently being installed to allow programming of the internal pressure.

A system has been designed to allow biaxial testing in compression-compression stress states. It consists primarily of a high-pressure double-acting cylinder with a labyrinth seal and a 20,000-psi hydraulic pressure intensifier. The cylinder will be provided with fixtures for

gripping the specimen and applying external and/or internal pressure. The system will also permit determination of the effect of hydrostatic pressure on yielding and deformation.

Preferred Orientation in Zircaloy Tubing

Average basal pole figures have been determined by the Knoop microhardness method[1,2] for six more lots of tube-reduced Zircaloy tubing. These materials are the first lots on which we have complete fabrication details from ingot to finished product. All of the materials were forged from ingot to 6 in. in diameter at 1015°C, forged to 4.25 in. in diameter at 840°C, and extruded to 1.53 in. in diameter and 0.28-in.-wall thickness at 580°C. Tube-reduction was accomplished in two steps for one material (WC-C) and in three steps for all others. Each tube-reduction step was done at room temperature with anneals between each step at approximately 700°C. Table 6.1 gives some of the tube-reduction details and the resulting texture coefficients. The times random intensity of the basal pole (texture coefficient) in the radial direction, $R_{(0001)_{\bar{R}}}$, is seen to be proportional to the total wall- to diameter-reduction ratio, Q_t. The correlation is better, however, with the wall- to diameter-reduction ratio in the final working operation, Q_f (see Fig. 6.1).

A surprising aspect of this data is the difference between the texture coefficients for Zircaloy-2 and Zircaloy-4. This is most striking when one compares the ζ ratio $[R_{(0001)_{\bar{R}}}/R_{(0001)_{\bar{\theta}}}$ where $R_{(0001)_{\bar{\theta}}}$ is the tangential direction texture coefficient] for the two materials. The two lots of Zircaloy-2 have a ζ ratio of about 3.6 while Zircaloy-4 fabricated by the same method has ζ equal to 1.6. Only two seemingly minor differences exist in the entire fabrication procedure. The diameter of the Zircaloy-2 ingot was 17 in. as opposed to 13 in. for

---

[1]P. L. Rittenhouse and M. L. Picklesimer, "Comparison of Pole-Figure Data Obtained by X-Ray Diffraction and Microhardness Measurements on Zircaloy-2," Trans. Met. Soc. AIME 236, 496–501 (April 1966).

[2]P. L. Rittenhouse and M. L. Picklesimer, Fuels and Materials Development Program Quart. Progr. Rept. Sept. 30, 1966, ORNL-TM-1700, pp. 34–35.

[redacted]

Table 6.1. Fabrication Parameters and Texture Coefficients for Tube-Reduced Zircaloy Tubing

Alloy	Code	Nominal Dimensions: Outside Diameter (in.)	Nominal Dimensions: Wall Thickness (mils)	Reduction in Area (%)	Q_t	Q_f	$R_{(0001)}$: $\bar{\theta}$	$R_{(0001)}$: $\bar{R}$	ζ
Zircaloy-4	WC-B	9/16	20	97	1.5	2.0	1.4	3.6	2.6
	WC-C	7/8	65	85	1.8	2.6	1.6	4.2	2.6
	WC-F	9/16	40	94	1.4	1.1	1.4	2.3	1.6
	WC-G	9/16	40	94	1.4	1.0	1.2	1.9	1.6
Zircaloy-2	WC-D	9/16	40	94	1.4	1.0	0.8	2.7	3.4
	WC-E	9/16	40	94	1.4	1.1	0.5	1.9	3.8

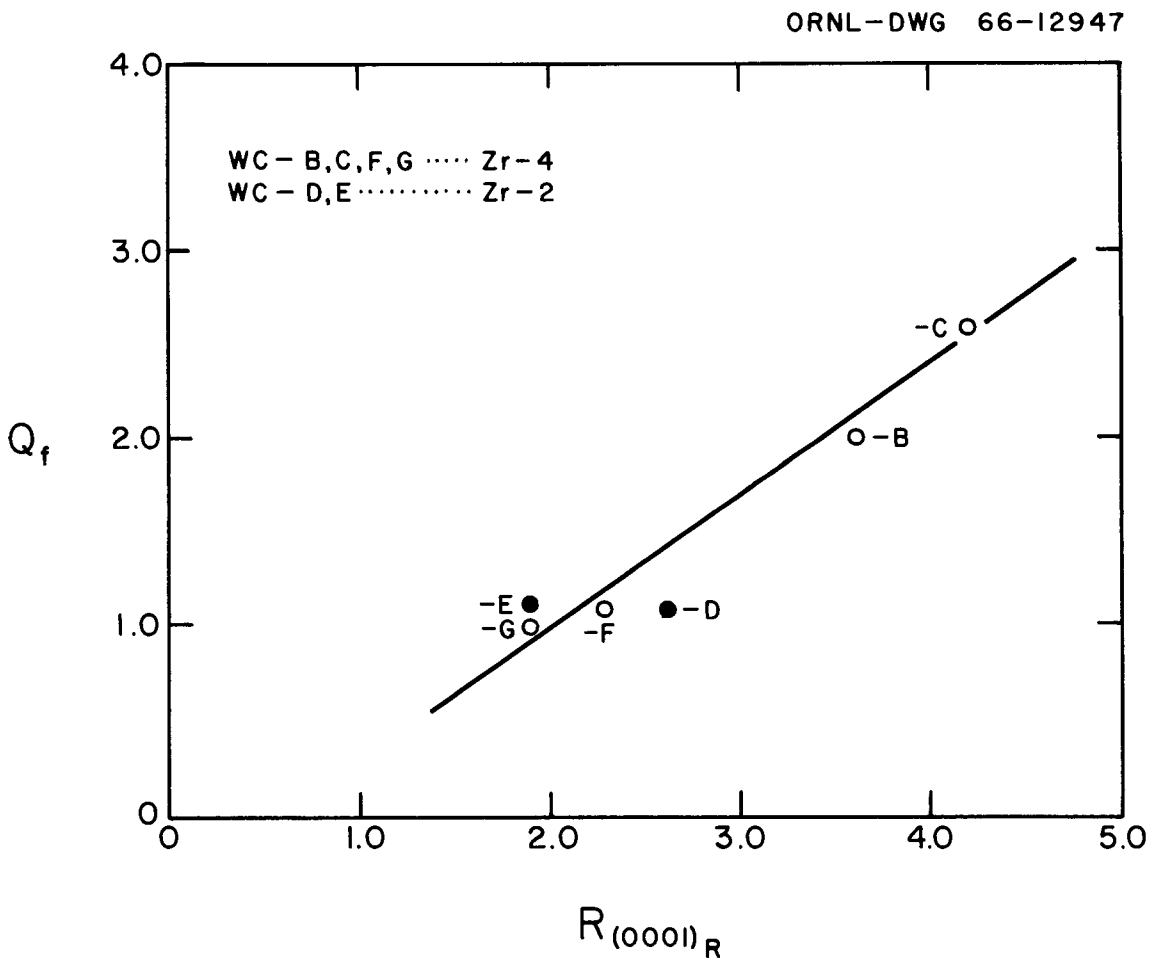

Fig. 6.1. The Effect of Q_f on the Texture Coefficient for the Radial Direction.

[redacted]

Zircaloy-4 and intermediate annealing temperatures were 50°C higher for Zircaloy-2. There is the possibility that the texture varies from head to tail of the stock, but the probability of material selection to give the results observed is relatively low. Further sampling of these materials will be done to check the results.

Yield Loci

Prediction of yield loci for anisotropic materials, α-zirconium alloys in particular, has been attempted by several methods. The first, described previously,[3] is based on the anisotropy of Knoop microhardness. A second method has been developed, based on a procedure used by Lee and Backoften.[4] This method requires the determination of the tension and compression strain anisotropy constants, k's, and yield strengths for three orthogonal directions. It is based on the condition that, in yield locus construction, the plastic strain vector, $\bar{\epsilon}_p$, must everywhere be normal to the locus.[5] In Fig. 6.2a, it is seen that $\bar{\epsilon}_p$ can be represented by its two component vectors $\bar{\epsilon}_{+ii}$, the strain parallel to the uniaxial test direction, (i) and $\bar{\epsilon}_{+ij}$, the strain perpendicular to i in the j direction. The cotangent of the angle between the σ_{+i} axis and the tangent to the yield locus at σ°_{+i}, the uniaxial yield strength in the i direction, is equal to the strain anisotropy constant k_{+ij}. The yield locus slopes at σ°_{-i}, σ°_{+j}, and σ°_{-j} are defined similarly in Fig. 6.2b. Yield at the point of balanced biaxial tension is fixed by its equivalence to yield in compression normal to both the i and j directions ($\sigma_{+i} = \sigma_{+j} = \sigma^{\circ}_{-k}$). For balanced biaxial compression σ_{-i} and σ_{-j} are equivalent to σ°_{+k}.

---

[3]P. L. Rittenhouse and M. L. Picklesimer, Fuels and Materials Development Program Quart. Progr. Rept. Mar. 31, 1966, ORNL-TM-1500, pp. 28–38.

[4]D. Lee and W. A. Backoften, "An Experimental Determination of the Yield Locus for Titanium and Titanium-Alloy Sheet," Trans. Met. Soc. AIME 236, 1077–1084 (July 1966).

[5]D. C. Drucker, U.S. Congress of Applied Mechanics, First Proceedings, 1951, pp. 487–491, American Society of Mechanical Engineers, New York, 1952.

[redacted]

ORNL-DWG 66-11268

(a)

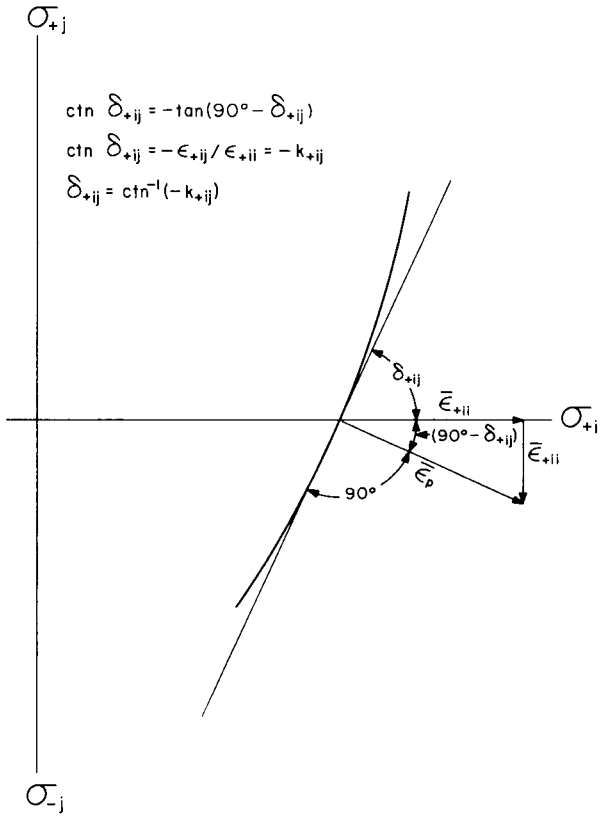

ORNL-DWG 66-11267

(b)

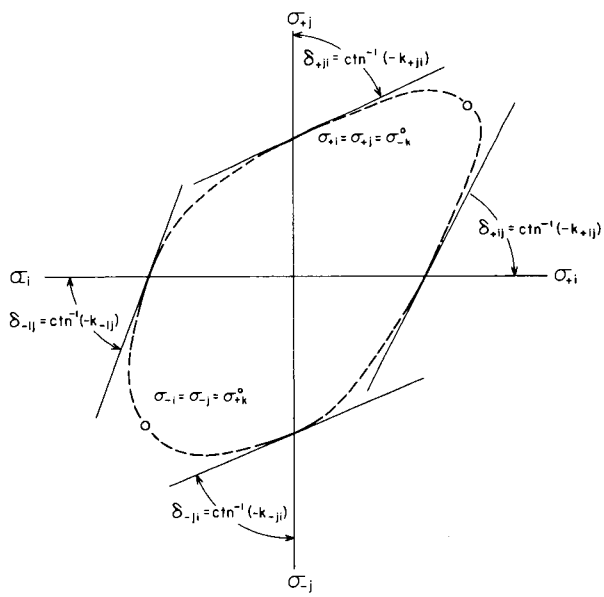

Fig. 6.2. Construction of the Plane Stress Yield Locus. (a) The plastic strain vector and its two component vectors. (b) Yield locus slopes and balanced biaxial stress states.

[redacted]

[redacted]

A third approach to the problem has been through a theoretical study of a yield criterion based on a broad generalization of the von Mises theory. The first phase of this study has resulted in the prediction of yield loci in terms of multidimensional stress experiments. A computer program has been developed that takes as its input uniaxial tension and compression yield strengths and prints out the yield loci on three biaxial stress planes. A single-yield locus for a Zircaloy-2 material determined by each of the three methods described is shown in Fig. 6.3. All results to date have been very satisfying but most await confirmation by biaxial testing.

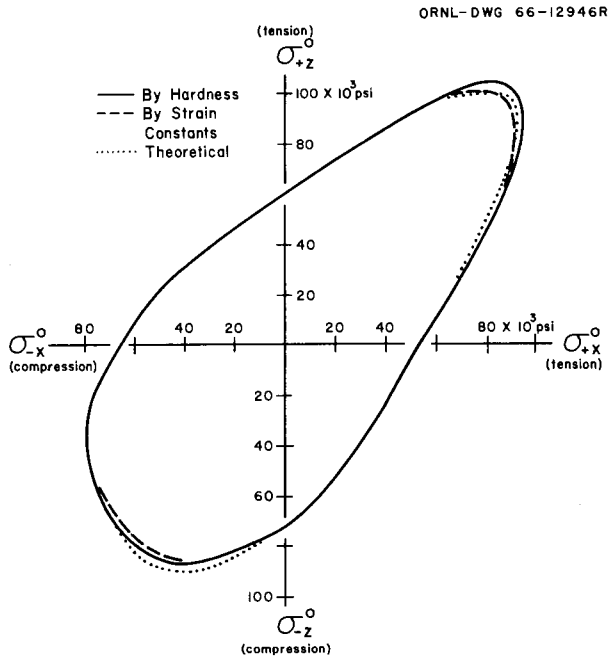

Fig. 6.3. Plane Stress Yield Locus for Zircaloy-2 Determined by Three Methods.

Studies of Zirconium and Its Alloys in Shear

D. O. Hobson

Zircaloy-2 Shear Studies

Zircaloy-2 specimens of schedules 9, 18, and 62 were machined into 1/8 × 1/8 × 1/2 in. shear specimens. The textures of these materials

[redacted]

have been reported previously,[6,7] but can be described briefly as basal poles predominantly in the normal direction (schedule 9), basal poles distributed between the normal and transverse directions (schedule 18), and relatively random (schedule 62). The specimens were sheared in a previously described jig[8] mounted in an Instron testing machine. A set of load-elongation curves for schedule 62 material tested in four shear orientations is shown in Fig. 6.4. The nomenclature describing the shear specimen orientation is based on the fabrication directions. The first letter (barred) identifies the direction perpendicular to the shear plane and the second designates the shear direction. Even though the texture of schedule 62 is the most "random" of the three studied, the load-elongation curves for the four shear orientations vary considerably.

Values for the ultimate shear strengths and elastic limits of the three schedules are given in Table 6.2 together with data from tensile tests on the same materials. No really direct comparison can be made between values for the two types of test because the shear tests involve biaxial stresses while the tensile test is one of uniaxial stress. In the case of an isotropic material, the yield strength in a pure shear state is theoretically $\sqrt{2/3}$ times the yield strength in tension. The ratio of shear to tensile yield strength varies widely in anisotropic materials, but is still less than unity. This, coupled with the fact that the elastic limit is always slightly less than the 0.2% yield strength, explains the large differences between the elastic limits in shear and the tensile yield strengths. The variation in elastic limit with shear orientation is reasonable when analyzed on the basis of

---

[6]P. L. Rittenhouse and M. L. Picklesimer, Metallurgy of Zircaloy. Part II. The Effects of Fabrication Variables on the Preferred Orientation and Anisotropy of Strain Behavior, ORNL-2948 (January 1961).

[7]P. L. Rittenhouse and M. L. Picklesimer, The Effect of Preferred Orientation and Stress on the Directional Precipitation of Hydrides in Zircaloy-2, ORNL-TM-844 (June 1964).

[8]D. O. Hobson and M. L. Picklesimer, Fuels and Materials Development Program Quart. Progr. Rept. Mar. 31, 1966, ORNL-TM-1500, pp. 43–47.

[redacted]

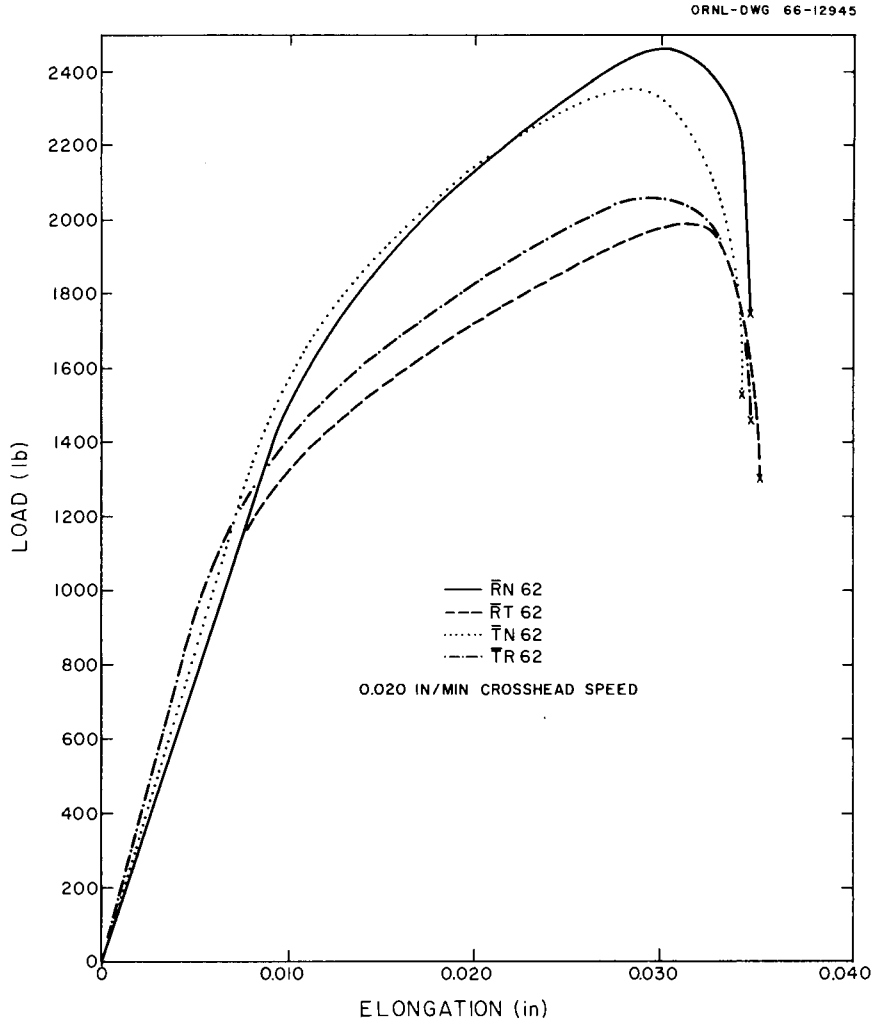

Fig. 6.4. Load-Elongation Curves for Four Shear Orientations of Schedule 62 Zircaloy-2.

Table 6.2. Ultimate and Yield Strengths of Zircaloy-2 in Tension and Shear[a]

Schedule	Ultimate Shear Strength				Ultimate Tensile Strength		Elastic Limit (Shear)				0.2% Tensile Yield Strength	
	R̄N	R̄T	T̄N	T̄R	RD	TD	R̄N	R̄T	T̄N	T̄R	RD	TD
9		65.0		61.8	68.3	67.0	39.7	31.0	44.3	31.4	53.3	55.7
18	70.4	72.4		64.2	77.6	74.9	32.6	34.0	42.9	31.8	54.7	69.4
62	84.3	69.8	77.5	76.0	75.8	74.2	41.8	34.8	38.8	35.4	55.8	63.2

[a]In thousands of pounds per square inch.

[redacted]

texture and biaxial yield locus. There is little merit in discussing the ultimate strengths in terms of failure theory. We can say only that the recorded values do seem reasonable.

Zirconium Single-Crystal Shear Studies

In our continuing effort to analyze the factors leading to texture formation in zirconium and its alloys, we are deforming zirconium single crystals of selected crystallographic orientations. In a prior report,[8] we discussed the deformation systems that might contribute to the formation of the observed textures. A system was postulated that might operate under complex stress situations and would explain the stability of the rolling textures found in zirconium. We have attempted to isolate this system, the $\langle 11\bar{2}3\rangle$ direction on any of the $\{10\bar{1}0\}$, $\{10\bar{1}1\}$, $\{11\bar{2}1\}$, or $\{11\bar{2}2\}$ planes, by proper orientation of the single-crystal specimens in the shear jig. Single-crystal specimens were cut and sheared in the postulated $\{10\bar{1}1\}\langle 11\bar{2}3\rangle$ deformation system and in the $\{10\bar{1}0\}\langle 11\bar{2}0\rangle$, "easy glide," deformation system. Figure 6.5 shows the load-elongation curves for the two systems. The $\langle 11\bar{2}3\rangle$ is certainly not an easy glide direction on the $\{10\bar{1}1\}$ plane. Figure 6.6 illustrates the microstructure ture of one of the shear zones. Even at this low magnification (30×),

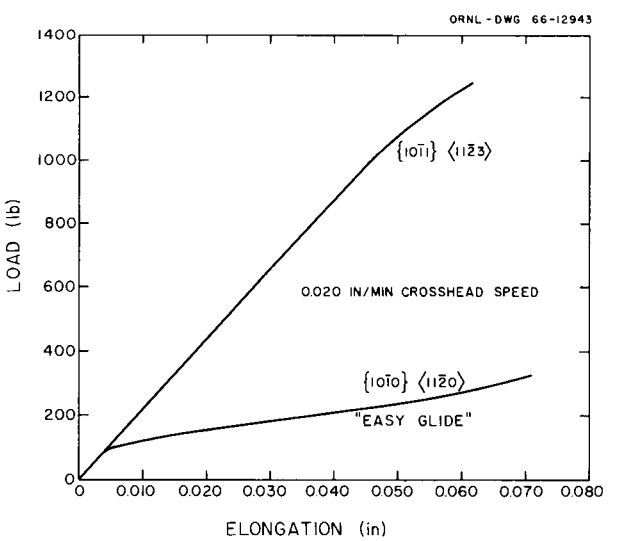

Fig. 6.5. Load-Elongation Curves for Shear on the Systems $\{10\bar{1}1\}\langle 11\bar{2}3\rangle$ and $\{10\bar{1}0\}\langle 11\bar{2}0\rangle$ in Zirconium.

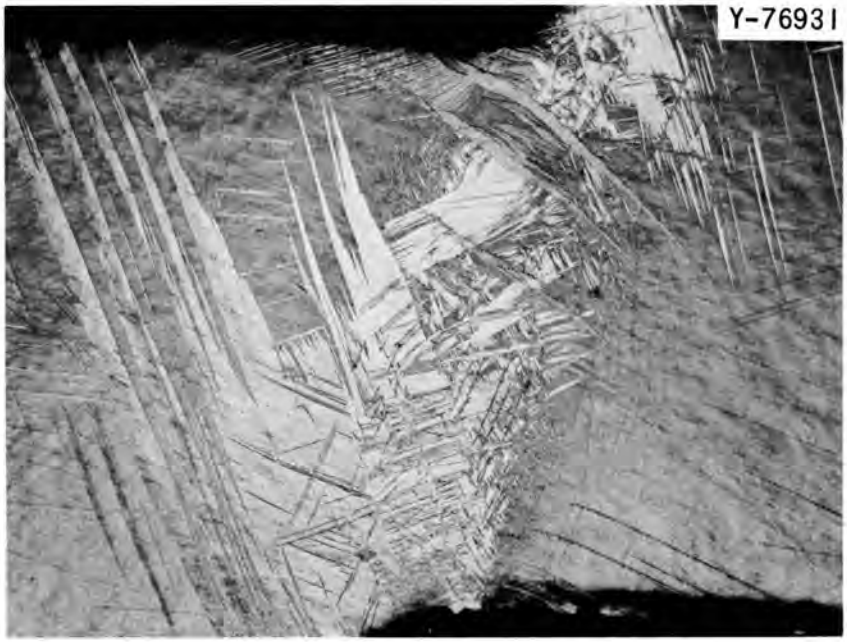

Fig. 6.6. Microstructure of a Shear Zone in a Zirconium Single Crystal Sheared in the System $\{10\bar{1}1\}\langle 11\bar{2}3\rangle$. 30×.

the complexity of twinning is apparent. At higher magnification, third- and fourth-order twinning is seen. There appears to be little, if any, of the expected slip, although accommodation slip is noticeable.

In an effort to suppress twinning and thereby force the material to slip, one specimen was sheared at 200°C. The twins were fewer and more coarse, but were by no means eliminated. A new shear jig is being designed which will allow testing at temperatures up to 500°C. It is entirely possible that $\langle 11\bar{2}3\rangle$ slip occurs only at elevated temperatures under complex stresses.

Optical Properties of Zirconium Alloys

L. T. Larson[9] M. L. Picklesimer

Determination of the optical properties of zirconium and its alloys has been discussed in other reports of this series.[10–12] It has been shown that the apparent angle of rotation, A_r, is a function of wavelength of incident light and of crystallographic orientation and that the measurement of this property allows, for both zirconium[11,13] and Zircaloy-2 (Ref. 12), the determination of the tilt of the basal pole from the normal to the surface to within ±3 deg from a single-surface examination. This has provided the background that has permitted the development of the equipment and technique for determining texture, microtexture, and texture gradients in polycrystalline material by polarized light microscopy.

The indices of refraction and absorption of a metal are related to the conduction electron band and to the chemical composition of the metal. The measured values of A_r for Zircaloy-2 (Ref. 12) can be compared to those for zirconium[11,13] to show that the optical properties of the two are different. These differences indicate that it may be possible to determine the chemical composition at the interface between the metal and the corrosion film by optical techniques. Measurement of A_r and ellipticity does not provide sufficient information to calculate the indices of refraction and reflection. Reflectivities for both the ordinary and extraordinary rays must also be measured. Equipment suitable for these measurements is not available commercially so that the equipment had to be designed and constructed. This equipment is now

---

[9]Consultant, Department of Geology, the University of Tennessee.

[10]L. T. Larson and M. L. Picklesimer, Fuels and Materials Development Program Quart. Progr. Rept. Sept. 30, 1964, ORNL-960, pp. 41–43.

[11]L. T. Larson and M. L. Picklesimer, Fuels and Materials Development Program Quart. Progr. Rept. June 30, 1965, ORNL-TM-1200, pp. 36–39.

[12]L. T. Larson and M. L. Picklesimer, Fuels and Materials Development Program Quart. Progr. Rept. Sept. 30, 1966, ORNL-TM-1700, pp. 45–48.

[13]L. T. Larson and M. L. Picklesimer, "Determination of the Basal Pole Orientation in Zirconium by Polarized Light Microscopy," Trans. Met. Soc. AIME 236, 1104–1106 (August 1966).

available and a study of the variation of optical properties of zirconium alloys as functions of alloying element and content has been initiated. This study is a necessary prerequisite to a study of the partitioning of alloying elements between the oxide and the metal during corrosion.

Reflectivity is considered by several investigators[14,15] to be the most important optical property of a reflecting surface. From the measurement of this property and those mentioned previously, it is possible to calculate the refractive index and absorption coefficient. These values should provide information on the electron band configuration and its change with alloying elements. In addition, as zirconium and its alloys are noncubic, the reflectivity will vary with crystallographic orientation.

Accurate reflectivity measurements are subject to several preparatory instrumental and interpretative problems.[14,16] Based on the results reported by several investigators in the field of ore microscopy,[14,15,17] the requirements for accurate measurements include perfectly polished specimens, accurate specimen leveling and alignment, superior standards of known reflectivity, a stable and intense source of incident light, a mechanically stable and accurately aligned microscope, and a high quality photometric device for readings of reflected light intensity. To satisfy these requirements we have taken the following steps.

Excellent scratch-free polishes of zirconium and Zircaloy-2 have been produced through experimentation with various chemical and electrolytic polishing solutions. The best finishes have been obtained by electrolytic polishing in a methanol–2% perchloric acid solution at –70°C at 30 v direct current.[18] Accurate specimen leveling and alignment have

---

[14]H. Piller and K. V. Gehlen, "On Errors of Reflectivity Measurements and on Calculations of Refractive Index n and Absorption Coefficient k," Am. Mineralogist 49, 867–882 (1964).

[15]S.H.U. Bowie and K. Taylor, "A System of Ore Mineral Identification," Mining Mag. (London) 99, 265 (1958).

[16]E. N. Cameron, Ore Microscopy, Wiley, New York, 1963.

[17]E. N. Cameron, "Optical Symmetry from Reflectivity Measurements," Am. Mineralogist 48, 1070–1079 (1963).

[18]E. N. Hopkins and D. T. Peterson, A Universal Electropolishing Method, ORNL-TM-1761 (1965).

been ensured by the design and construction of a spring-loaded double-opposed screw-tilting stage for flat specimens and a "Universal" stage comprised of five independent adjustable axes plus x-y-z translation for spherical specimens. In the "Universal" stage the inner two rotation axes plus the translations are provided by a Charles Supper eucentric x-ray goniometer. This goniometer permits alignment and centering of the optical axes of the spherical specimen along the rotation axes of the "Universal" stage and allows the specimen to be moved from the microscope stage to x-ray diffraction equipment for precise determination of crystallographic orientation.

Standards selected for reflectivity measurements are in accord with those prepared by the National Physical Laboratory of Great Britain, which has been working on the standardization of reflectivity measurements in conjunction with the International Commission on Ore Microscopy.[19] We have provided polished single crystals of high-purity silicon, germanium, chromium, and aluminum to E. N. Cameron at the University of Wisconsin for calibration with specimens provided him by the National Physical Laboratory.

The microscope used in our reflectivity measurements is a Vickers M73 with a Smith mirror illumination system.[12] The microscope has been modified by the addition of a slotted Wright ocular and an extension in the stand to enable it to accept the "Universal" stage. A motor drive and a positioning sensor have been added to the microscope stage, and we are able to translate stage rotation onto the x axis of an x-y recorder (see Fig. 6.7).

No commercially available illumination and photometer array is sufficiently precise and flexible to provide the required values throughout the visible light spectrum and at the same time ensure stability of the incident light intensity. We have designed and built a dual instrument which makes use of the high intensity light provided by either a Zirconium Arc Lamp or a 100-w Quartz Iodine Lamp. A schematic of this system is shown in Fig. 6.7. The system consists of a reference

[19]E. N. Cameron, University of Wisconsin, private communication.

[redacted]

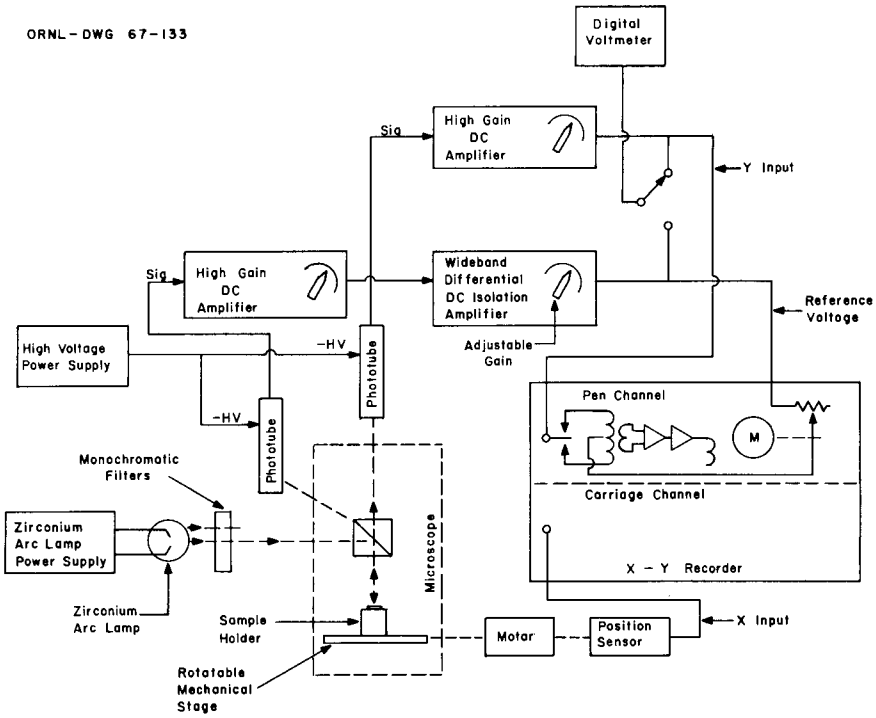

Fig. 6.7. Schematic of Photometer System and Associated Instrumentation.

photometer and a reading photometer plus the necessary power supplies, amplification, and readouts. Both phototubes have been carefully matched as to response in the visible and near-visible ultraviolet regions of the spectrum. The reference phototube is illuminated by "waste" light picked off the reflection mirror in the microscope and piped through a flexible light tube. This photometer circuit provides the bridge voltage for the y axis of the x-y recorder. The signal from the reading phototube, provided by reflection from the specimen, is balanced against the bridge voltage. Any fluctuation in the intensity of light from the illuminator produces a corresponding fluctuation in the bridge voltage. This ensures that the reflectivity measurements are not affected by instabilities in the light source. The light reflected from the specimen is picked up by the reading photometer and translated into y-axis movement on the recorder. By using reference standards of known percentage reflectivity, our measurements can be calibrated in standard reflectivity units.

Preliminary measurements indicate that the system operates properly and calibration with standards is in progress.

[redacted]

[redacted]

Properties of High-Purity Zirconium and Its Alloys

J. C. Wilson

Anisotropy of Oxidation in Zirconium

A single-crystal hemisphere and three plates of high-purity zirconium [$(10\bar{1}5)$, (0001), and $(11\bar{2}0)$ orientations] were oxidized 100 hr in 360°C water. The oxidation pattern, Fig. 6.8, is generally similar to that observed before in air and steam [i.e., the regions of thickest oxide can be described as bands from (0001) to $(11\bar{2}2)$, $(11\bar{2}2)$ to $(31\bar{4}4)$, and from $(31\bar{4}4)$ to $(10\bar{1}0)$], but, in addition, the region around $(11\bar{2}0)$ is also covered with a thick oxide.

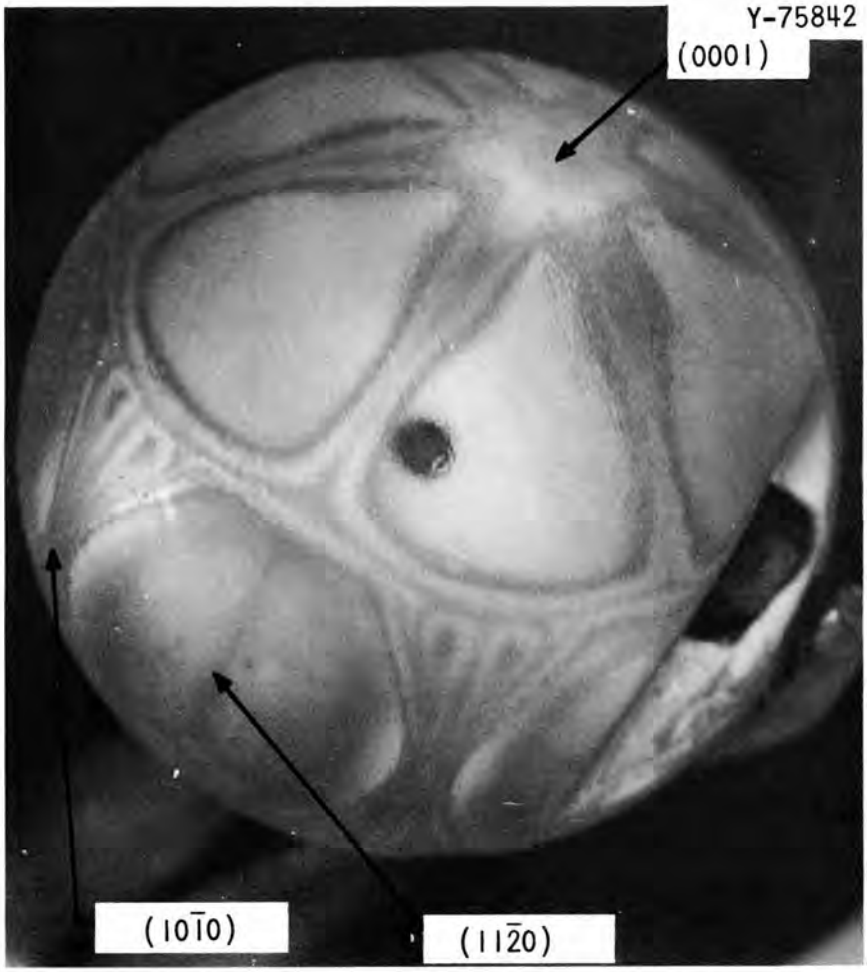

Fig. 6.8. The Oxidation Pattern or Interference Colors on a 1-cm-diam Hemispherical Single Crystal of Zone-Refined Zirconium Oxidized 100 hr in 360°C Deionized Water of pH 6. The pattern is similar to that developed in oxygen at 400°C and steam at 500°C (15 psia) except that the region around the $(11\bar{2}0)$ is thicker.

[redacted]

The oxide thicknesses on (0001), $(10\bar{1}5)$, and $(11\bar{2}0)$, determined in the visible and ultraviolet ranges of the spectrophotometer, were 3200, 1070, and 1720 A, respectively (approx 5, 2, and 3 mg/dm^2). The respective specific weight gains (approximate because of irregular geometry) were 10, 8, and 15 mg/dm^2. Microscopic examination at 1000× showed the reason for at least part of the discrepancy. Localized, accelerated oxidation was visible on all three specimens. Furthermore, micron-size "subgrains" of various hues were visible on the (0001). These samples are now being used for x-ray determination of oxide structure and possibly the epitaxy of the oxide.

The weight gains of high-purity zirconium in 360°C water are made up in large part from the oxide protuberances rather than from the uniform film seen with the eye and the spectrophotometer. The same was found true in 500°C steam.

We earlier determined that there was some small dependence of anodic film thickness on crystallographic orientation.[20] There was also an apparent variation in relative rate (thickness per volt) with voltage, but we could not measure it by visual comparison of colors. Therefore, we have used the spectrophotometer to measure the thickness of anodic films formed from 2 to 126 v in a 1% KOH solution on (0001), $(10\bar{1}0)$, and $(11\bar{2}0)$ planes of zone-refined zirconium. Above about 35 v the anodic oxide is thickest on $(11\bar{2}0)$, but between 10 and 25 v it is thinnest on this same plane. Above 60 v the oxide on the $(10\bar{1}0)$ becomes thicker than on (0001). Although the thickness differences between different planes are small (less than 10% at 40 v), they apparently are real and the results correctly predict the behavior of the previously anodized sphere.

An interesting feature of the wavelength-reflectivity curves from the spectrophotometer is an abrupt change in slope in the region of 225 to 230 mμ on $(10\bar{1}0)$ and $(11\bar{2}0)$ planes, but not on the (0001), for films formed below about 20 v. The reason for this behavior is not known, but

---

[20] J. C. Wilson, Metals and Ceramics Div. Ann. Progr. Rept. June 30, 1966, ORNL-3970, p. 138.

an absorption at 229 mμ has been found in oxides produced thermally on zirconium.[21] Several other irregularities were observed on the single-crystal curves, but not on those for polycrystals.

The diffusion constant for oxygen in zirconium has been determined by others by dissolving anodic films into the metal at elevated temperatures.[22] While there is some criticism of the method, the results have so far agreed with other types of determination. We dissolved 126-v anodic films (approx 3200 A thick) into single-crystal zirconium for 5 hr at 495°C in a vacuum of 10^{-8} torr. The dissolution rates were 2.0 A/min on the (0001), 3.1 A/min on $(10\bar{1}0)$, and 3.0 A/min on $(11\bar{2}0)$. Misch[23] obtained a rate of 2.3 A/min at the same temperature in polycrystalline zirconium. We are continuing this work over a broader range of temperatures and orientations.

Inhibition of Oxidation by Anodic Films

Banter[24] noticed that the dissolution of anodic films into zirconium was inhibited when certain anodizing solutions were used to form the film. He suggested that preanodizing might decrease the oxidation rate at high temperatures where the solution of oxygen into the metal becomes important. He found that a solution developed by Picklesimer[25] (to show color differences due to different phases or compositions) produced a film that slowed the dissolution rate. Banter[26] further showed (by infrared absorption spectrophotometry) that phosphate ions were incorporated in the anodized films formed in this solution.

---

[21] N.J.M. Wilkins, Corrosion Sci. 5, 3 (1965).

[22] G. V. Kidson, Electrochem. Technol. 4, 193 (1966).

[23] R. D. Misch, Acta Met. 5, 179 (1957).

[24] J. C. Banter, Electrochem. Technol. 4, 237 (1966).

[25] M. L. Picklesimer, Anodizing as a Metallographic Technique for Zirconium-Base Alloys, ORNL-2296 (April 26, 1957).

[26] J. C. Banter, Fuels and Materials Development Program Quart. Progr. Rept. Mar. 31, 1966, ORNL-TM-1500, p. 50.

[redacted]

We attempted to test Banter's suggestion by comparing specimens of arc-melted crystal-bar zirconium unanodized, anodized in KOH (aqueous), and anodized in the photphate-containing solution. Unfortunately, this metal had a very high weight gain in 500°C steam, but after 6 hr the specimen anodized in the phosphate-containing solution had a weight gain of only 25 mg/dm^2 as compared to 48 mg/dm^2 for the unanodized specimen and 43 mg/dm^2 for the KOH anodized specimen. The anodized films were about 1 mg/dm^2. White oxides were formed along intermetallic stringers in the rolled strip. The amount of white oxide along the stringers was very much less on the specimen preanodized in the phosphate solution.

Another interesting result of these experiments was that preanodizing the steam oxidized specimens reduced the absorption in the ultraviolet. This suggests that the source of the absorption in thermally formed films may occur only through a very small part of the film thickness.

Effect of Purity on Oxidation

Ten specimens from known locations in three zone-refined bars of zirconium were rolled to sheet and annealed (1 hr at 500°C), then oxidized in 360°C water for 100 hr. Weight gains varied from −4 to 26 mg/dm^2 for the purified material (180 mg/dm^2 for one of the unzoned crystal-bar materials). All specimens were polished in 46% H_2O–46% HNO_3–8% HF solution before oxidation. Microscopic examination revealed that localized, accelerated oxidation had occurred to varying degrees (and with different morphologies) in the different specimens. Weight losses probably resulted from oxide lost during washing and handling. The spectrophotometric thickness measurements gave weight gains between 4 to 5 mg/dm^2 (2800 to 3400 A), but these values represent the thickness of the more or less uniform film of oxide.

There is apparently a distinct effect of purity on oxidation rate. In general, the specimens from near the head of the zone-refined bar, purest except for elements such as oxygen and hafnium which have distribution coefficients greater than unity, appear to show the least oxidation.

[redacted]

Detection of Weld Contamination in Zircaloy-2 by Anodizing

M. L. Picklesimer

The only reliable and accepted method for detecting contamination of Zircaloy-2 welds by air during welding has been that of autoclaving the finished part. The two tests in common use are (1) two weeks in 680°F water and (2) three days in steam at 750°F and 1500 psi. The observation of "white" oxide on or near the weld indicates that contamination has occurred during welding. Both of these tests require autoclaving the entire part and, therefore, rather extensive and expensive facilities. It was thought desirable to attempt to simplify the testing procedure for use in facilities where "hot" fuels are to be reprocessed and new elements manufactured from them.

It has long been known that the color (thickness) of an anodized film formed at a given, constant voltage depended on the composition of the specimen.[25] The technique has been used to locate and evaluate segregation in zirconium, uranium, titanium, and niobium alloys.[25,27] It was believed that the anodizing technique should allow quantitative detection of contamination during welding.

Tungsten-arc fusion passes were made on 1/16 × 3 1/4 × 5 in. sheet Zircaloy-2 specimens in argon atmospheres contaminated with known amounts of air, oxygen, or nitrogen. Samples of the continuously flowing atmosphere were taken at the start and the end of each fusion pass and were analyzed by mass spectroscopy. The analyses are given in Table 6.3.

Preliminary tests indicated that it was not feasible to depend on the color of the anodized film, formed at any voltage between 10 and 500 v, to determine the degree of contamination or the corrosion behavior of the contaminated weld and its associated heat-affected zone. Experiments showed that the contamination could be detected quantitatively by examining the anodized specimen in polarized light at low magnification. Visual comparison in polarized light of the anodized and the control

[27] M. L. Picklesimer, "A Note on Some of the Intermediate Phases in the Nb-Sn System," Appl. Phys. Letters 1(3), 64 (1962).

[redacted]

Table 6.3. Analyses of Welding Atmospheres at Start and Finish of Each Fusion Pass

Specimen Number	Intended Atmosphere	Atmosphere Analysis (ppm)						Argon (%)
		H_2	CH_4	H_2O	N_2+CO	O_2	CO_2	
171	Ar–0.005% air							
	Before	9	5	4	91	26	1	99.987
	After	19	5	6	333	97	6	99.954
172	Ar–0.01% air							
	Before	6	4	19	565	165	4	99.924
	After	9	3	5	119	38	2	99.983
173	Ar–0.02% air							
	Before	7	4	7	2692	102	1	99.719
	After	17	4	9	719	176	7	99.908
174	Ar–0.05% air							
	Before	5	3	5	371	105	4	99.951
	After	9	2	3	343	93	1	99.955
175	Ar–0.1% air							
	Before	15	5	4	856	237	6	99.888
	After	17	5	8	1023	264	10	99.867
176	Ar–0.2% air							
	Before	12	5	7	1344	361	6	99.826
	After	16	5	6	2675	508	11	99.678
177	Ar–0.005% N_2							
	Before[a]	14	8	520	30730	8803	56	95.987
	After	11	2	105	1794	653	8	99.743
178	Ar–0.025% N_2							
	Before	6	2	5	299	8	5	99.967
	After	6	2	6	306	6	4	99.967
179	Ar–0.1% N_2							
	Before	6	2	5	857	12	3	99.911
	After	9	4	6	861	11	4	99.910
180	Ar–0.2% N_2							
	Before	7	2	25	1887	142	6	99.793
	After	9	2	4	1662	19	4	99.830
181	Ar–0.4% N_2							
	Before	7	3	9	3397	170	5	99.641
	After	10	4	6	3020	23	5	99.693
182	Ar–0.8% N_2							
	Before	7	2	5	5525	18	4	99.444
	After	12	2	49	5603	31	5	99.430
183	Ar–2.0% N_2							
	Before	9	5	7	19340	6	6	98.063
	After	10	3	7	18770	11	3	98.120

[redacted]

[redacted]

Table 6.3 (continued)

Specimen Number	Intended Atmosphere	Atmosphere Analysis (ppm)						Argon (%)
		H_2	CH_4	H_2O	N_2+CO	O_2	CO_2	
184	Ar–0.012% O_2							
	Before	7	3	6	56	152	6	99.977
	After	7	2	7	80	178	6	99.972
185	Ar–0.025% O_2							
	Before	6	2	5	46	265	8	99.967
	After	1	3	5	63	238	12	99.968
186	Ar–0.05% O_2							
	Before	8	3	21	285	644	7	99.903
	After	9	3	10	57	503	4	99.941
187	Ar–0.1% O_2							
	Before	7	2	4	57	1041	3	99.889
	After[a]	19	7	225	34380	10440	61	95.486
188	Ar–0.2% O_2							
	Before	11	3	5	110	1824	8	99.804
	After	10	2	20	248	1810	14	99.789

[a]High nitrogen and oxygen probably due to leak in sample bottle as observed in other cases, but no check sample is available on these runs. The specimens do not show that these levels were present during welding.

specimens showed that, under proper anodizing conditions, the anodized specimen could show the presence of a white to gray or brown oxide at the same positions as the steam-corroded control specimen. Two sets of anodizing conditions were found to be acceptable. One was at 300 v direct current in 40 ml glycerin, 120 ml ethanol, 70 ml water, 20 ml lactic acid, 10 ml phosphoric acid, and 4 g of citric acid. Use of this solution gave the best results but the solution "ages" rapidly; after 4 hr, the results are not consistent with those obtained with a freshly mixed solution. Anodizing the specimens at 100 v direct current in a 1 vol % solution of H_3PO_4 in water produced acceptable results. This solution is stable indefinitely but H_3PO_4 should be added periodically to make up for loss of the phosphate ion to the anodic film.[28] Many

[28]J. C. Banter, Fuels and Materials Development Program Quart. Progr. Rept. Sept. 30, 1966, ORNL-TM-1700, pp. 48–52.

[redacted]

other solutions were tried but none gave acceptable results unless elaborate precautions were taken with cleaning and drying.

A photomacrograph of a typical specimen anodized at 100 v direct current in 1% H_3PO_4 and its companion steam-corroded control is shown in Fig. 6.9. Two lighting conditions are shown — oblique unpolarized light in Fig. 6.9a and polarized light with crossed polars in Fig. 6.9b. Photometer traces made on both specimens in polarized light at a microscope magnification of 27.5× are given in Fig. 6.9c.

Anodization at lower voltages did not always show the zones of poor corrosion behavior, and anodization at higher voltages indicated poor corrosion resistance in some zones that had acceptable corrosion resistance by the steam autoclave test. Exploration showed that the anodization voltage was critical to ±10 v.

Examination of all of the specimens of the test series showed that visual examination with a polarized light microscope at low magnification can be used to detect poor corrosion resistance resulting from contamination during welding. The photometer traces show that the technique can be automated for remote inspection. The photometer signal is fed to a system that will reject a part whenever the instantaneous signal or the integrated intensity of the scan is greater than a preset level. The peak marked "dust" on the photometer trace for the control specimen indicates the importance of "clean practice" and suggests that all parts rejected during automated inspection should be examined visually to ensure that the rejection was justified.

Other experiments have shown that the technique can be used for in-field inspection of welds on large parts. A dam is constructed around the weld to contain the solution, a cathode of nickel or stainless steel is inserted, and the direct-current voltage applied. The voltage can be increased slowly (to stay within the amperage limitations of the power supply) to the final value without affecting the validity of the test. After rinsing with water and drying free of stain, the weld and the heat-affected zone can be inspected with a hand-held low-power polarized-light microscope fitted with a battery-powered light source. Extraneous light should be blocked with an opaque, flexible skirt on the microscope.

[redacted]

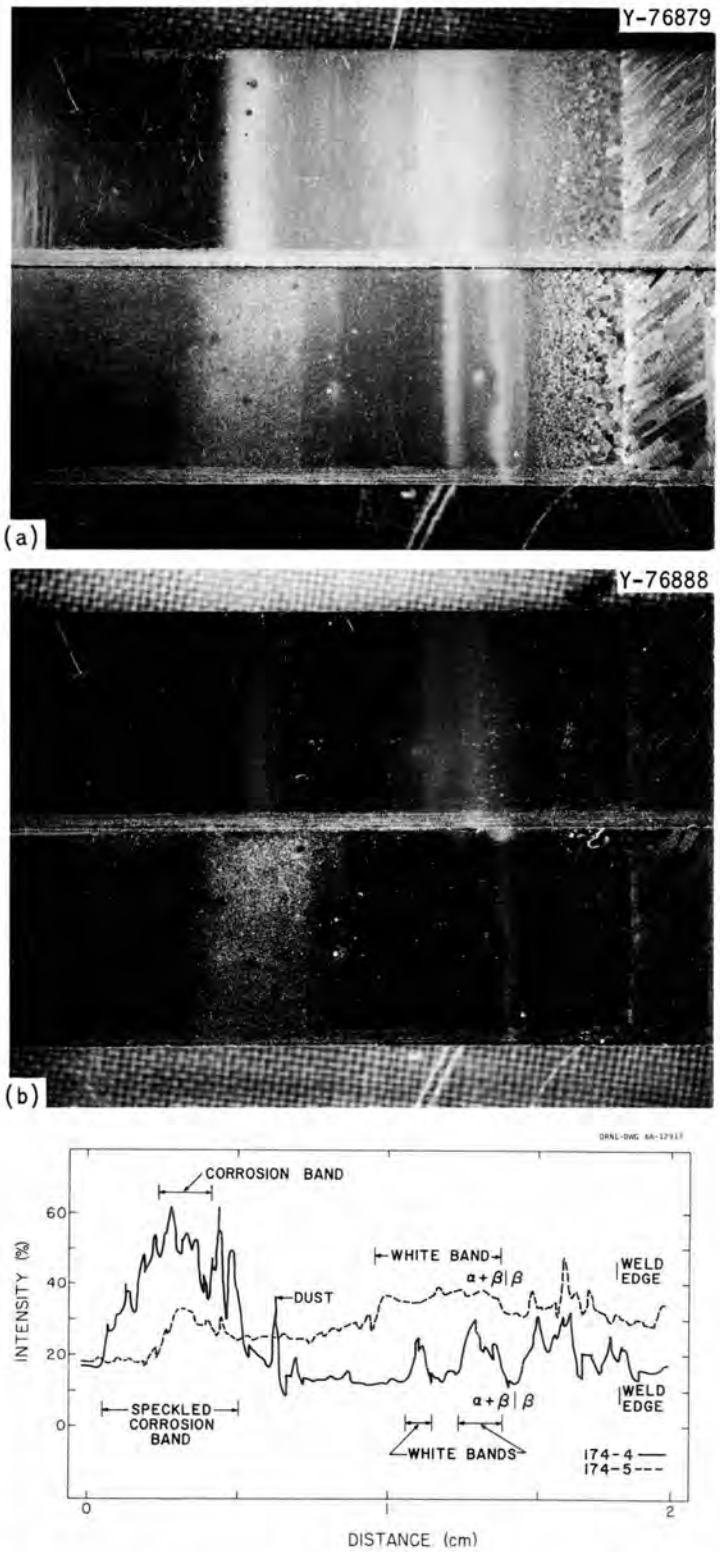

Fig. 6.9. Photomacrographs of a Specimen Anodized at 100 v Direct Current in 1% H_3PO_4 (top) and Its Companion Steam-Corroded Control (bottom) (a) Oblique unpolarized light, 4.5×, and (b) polarized light with crossed polars, 4.5×. (c) Photometer traces made on both specimens in polarized light at a microscope magnification of 27.5×. Reduced 20%.

[redacted]

Photometer traces were made on all of the weld specimens listed in Table 6.3. The specimens were examined visually at the same magnification during the photometer scan by observing through one eyepiece of the binocular head. Notes were made to locate the "corrosion bands" and dust particles. These traces show that no weld was made in an atmosphere sufficiently pure to prevent detection of poor corrosion behavior at some point in the scan on both the anodized specimen and its corroded control. At contamination levels of less than 100 ppm N_2 and 200 ppm O_2, the weld metal and areas in the heat-affected zone which were at a temperature of 950°C or above dissolved the contaminants as rapidly as they were picked up and did not indicate poor corrosion resistance in the corroded control. In these specimens the poor corrosion resistance was observed at regions of the specimen which could not have been at temperatures higher than about 700°C. Such a region is shown in Fig. 6.9b and in Fig. 6.9c by the region labeled "speckled corrosion band".

7. WELDABILITY OF NICKEL-BEARING ALLOYS

G. M. Slaughter

Studies are well under way on the program to determine the effects of minor elements, individually and combined, upon the cracking behavior and mechanical properties of welds in nickel-bearing alloys. Much of the effort in this reporting period, as well as the last, has been aimed at procuring high-purity raw materials and at fabricating special alloys for weldability testing both at Rensselaer Polytechnic Institute under subcontract and at ORNL. These materials procurement and alloy preparation phases of the investigation are relatively time-consuming and involve long lead-times; the welding experiments are proceeding concurrently as specimens become available.

Special Alloy Fabrication

R. E. McDonald W. J. Werner
D. A. Canonico

Table 7.1 gives the chemical compositions of the experimental aluminum- and titanium-containing Incoloy 800 alloys which have been analyzed to date.[1] Excellent quality, reproducibility, and fabricability were obtained for all the alloys with the in-house melting and fabrication processes. These alloys were prepared from high-purity raw materials (99.9% Fe, 99.8% Cr, and 99.9% Ni); the analyses of which are given in Table 7.2.

From a comparison of the compositions of the alloys with the parent melting stock, it is obvious that the contamination that occurred during melting and fabrication is minor. Furthermore, comparisons of carbon, sulfur, and phosphorus contents with those of commercial heats of nickel alloys show that carbon and phosphorus contents are about the same and that sulfur contents are about one-half those of commercial alloys.

[1]D. A. Canonico, R. E. McDonald, and W. J. Werner, Fuels and Materials Development Program Quart. Progr. Rept. Sept. 30, 1966, ORNL-TM-1700, pp. 90–92.

[redacted]

Table 7.1. Chemical Analyses of Raw Materials

Element	Source of Analysis	Impurity Content, wt %		
		C	S	P
Iron	Vendor	0.005	0.004	
	ORNL	0.005	0.004	0.002
Nickel	Vendor	0.01		
	ORNL	0.007	< 0.002	0.0005
Chromium	Vendor	0.014	0.014	0.001
	ORNL	0.004	0.015	0.002

Table 7.2. Chemical Analyses of Special Incoloy 800 Alloys

Alloy Number	Chemical Content,[a] wt %							
	Ni	Cr	Al	Ti	C	S	P	Fe
800-1	32.5	21.0						bal
	(33.43)	(21.65)			(0.007)	(0.003)	(0.005)	(bal)
800-2	32.5	21.0	0.15	0.15				bal
	(33.26)	(21.66)	(b)	(b)	(0.008)	(0.003)	(0.006)	(bal)
800-3	32.5	21.0	0.38	0.38				bal
	(32.78)	(22.18)	(b)	(b)	(b)	(0.003)	(0.007)	(bal)

[a]First entries are the nominal compositions; the ORNL analyses are shown in parentheses.

[b]Analyses in process.

Work also was initiated on the production of a 700-lb high-purity ingot for one portion of the weldability study being carried out at Rensselaer (see following section). The initial intention was to obtain, from a commercial vendor, material melted and fabricated to our specifications and from our melting stock. The reaction to inquiries, however, was disappointing; no bids were received. As a result, the 700 lb of material will be melted at ORNL as seven 100-lb ingots. We will produce these ingots by induction melting and subsequent consumable-arc melting. Furnace modifications for the production of 6-in.-diam ingots are presently under way. Negotiations are also under way with an outside vendor to process the ingots to 1/4-in.-thick plates.

[redacted]

[redacted]

A series of selectively contaminated Inconel 600 alloys is being prepared for weldability evaluations using the hot-ductility test. Table 7.3 shows the nominal compositions of the alloys melted to date; the certified analyses of the melting stock are shown in Table 7.1. Electrodes for vacuum consumable-arc melting the alloys into 3-in.-diam billets were prepared by tungsten-arc melting. Fabrication was accomplished by hot extrusion to bar stock followed by hot swaging to rod. Chemical analyses for actual impurity content are currently under way.

Table 7.3. Composition of Inconel 600 Alloys Prepared for Hot-Ductility Testing

Alloy Number	Composition, wt %							
	Fe	Cr	C	Cu	Mn	Si	S	Ni
600-1	8	15.5						bal
600-2	8	15.5	0.03	0.04	0.20	0.20		bal
600-3	8	15.5	0.03	0.04	0.20	0.20	0.005	bal
600-4	8	15.5	0.03	0.04	0.20	0.20	0.010	bal
600-5	8	15.5	0.03	0.04	0.20	0.20	0.015	bal
600-12	8	15.5	0.03	0.04	0.40	0.20	0.010	bal
600-13	8	15.5	0.03	0.04	0.60	0.20	0.010	bal
600-14	8	15.5	0.03	0.04	0.80	0.20	0.010	bal

Weldability Studies

VARESTRAINT Testing Performed Under Subcontract at Rensselaer Polytechnic Institute (W. F. Savage, C. D. Lundin)[2]

Rensselaer Polytechnic Institute is conducting weldability tests using their VARESTRAINT testing apparatus. This equipment and test were discussed in the last progress report.[3] During the past quarter, testing

[2]Department of Materials Engineering, Rensselaer Polytechnic Institute, Troy, N. Y. Subcontract is funded jointly with BONUS Core II Superheater Research and Development.

[3]W. F. Savage and C. D. Lundin, Fuels and Materials Development Program Quart. Progr. Rept. Sept. 30, 1966, ORNL-TM-1700, pp. 92–97.

[redacted]

has been completed on the first three experimental heats of Incoloy 800 (800-1, -2, and -3). The nominal and actual compositions of this series of alloys are given in Table 7.1. The welding parameters that were used were also described in the previous report.[3]

The data obtained on these three heats of Incoloy 800 are shown in Fig. 7.1. The total crack length plotted on the ordinate represents the cracks found on a polished surface oriented parallel to and 0.010 in. below the as-welded surface of the specimens. A representative crack is shown in Fig. 7.2.

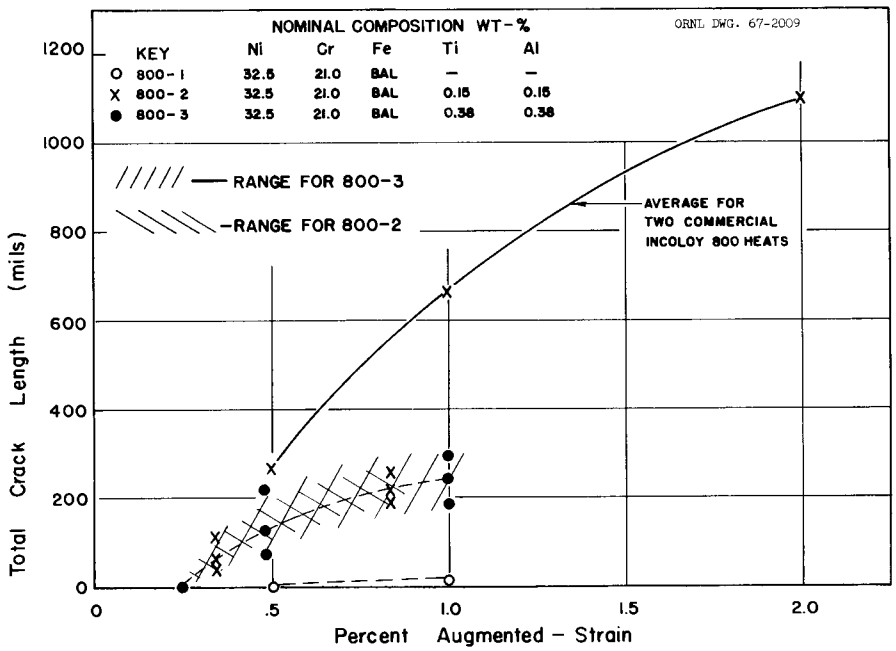

Fig. 7.1. VARESTRAINT Results for the First Three Experimental Heats of Incoloy 800 Composition. The results of two commercial heats have been included for comparison.

The VARESTRAINT results obtained from the three experimental heats illustrate vividly the deleterious effects of minor additions of titanium and aluminum on weldability. The threshold strain for the ternary iron-nickel-chromium alloy was 0.5%. The presence of 0.15% Ti and 0.15% Al decreased this value to 0.25%. In addition, at 1% augmented strain, the total crack length was increased, on the average, thirteenfold (250 vs 19 mils) over that observed in the simple ternary alloy. The difference

[redacted]

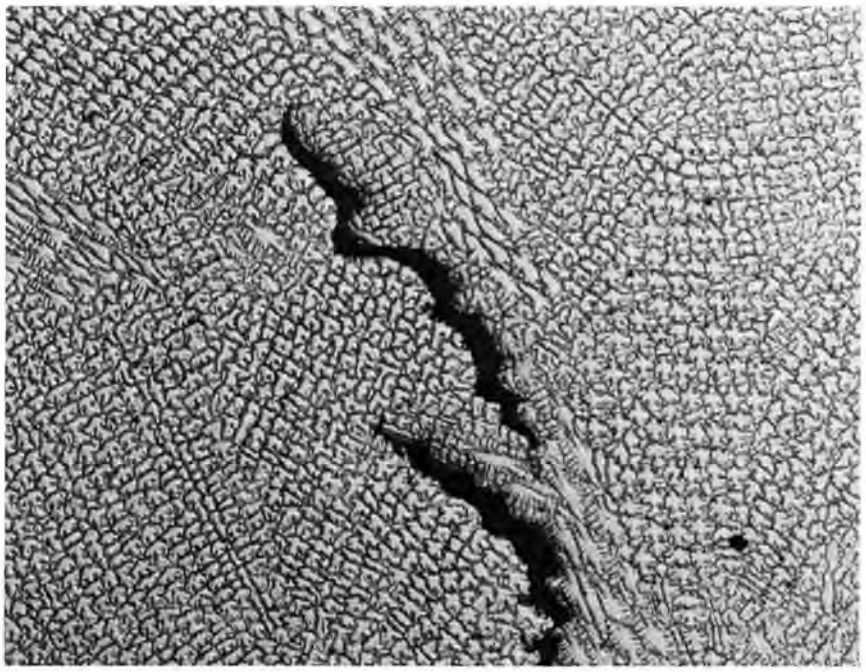

Fig. 7.2. Crack at Center of Fusion Zone in Incoloy 800 VARESTRAINT Test. Etchant: 10% oxalic acid—electrolytic. 100×. (Rensselaer Polytechnic Institute photomicrograph.)

between the 0.15% Ti–0.15% Al alloy and the 0.38% Ti–0.38% Al alloy is not as sharply delineated. However, there is a greater spread in the results obtained for the more highly alloyed composition.

For comparative purposes, the VARESTRAINT results obtained from two commercial heats of Incoloy 800 reported last quarter[3] have been included in Fig. 7.1. It is evident that the amounts of the various other minor elements (such as C, Mn, Si, S, P, etc.) normally found in commercial heats of Incoloy 800, but which are either eliminated or minimized in our special heats, have a profound effect on the crack sensitivity. While the presence of titanium and aluminum has undoubtedly been responsible for a considerable portion of the aggravated cracking in the commercial heats, the presence of the other elements caused an even larger percentage increase in the total crack length. This work is being continued and the remainder of the aluminum- and titanium-bearing compositions discussed last quarter currently are being prepared for testing.

[redacted]

[redacted]

The data reported to date were all obtained using the same welding parameters. It is highly probable that variations in welding conditions and processes will also influence the cracking behavior of these nickel-bearing alloys and, to further pursue this, we have supplied RPI with additional specimen blanks of the Inconel 600 and Hastelloy X heats tested previously. These specimens will be tested at one level of augmented strain. In addition, we are supplying a 2-in.-thick plate of Inconel 600, 12 by 24 in., which will, in turn, be sliced into 1/2-in.-thick blanks 2 in. wide by 12 in. long. The 2-in.-thick plate will provide an abundant supply of specimens, all chemically and mechanically identical, for an even more detailed determination of the effects of wide variations in welding parameters on weld cracking propensities.

As one means of minimizing the cost and time delays in preparing relatively large amounts of special alloys, Rensselaer has devised the modified VARESTRAINT test specimen shown in Fig. 7.3. The body of the specimen is composed of a commercial heat of material, while the "shim insert" is composed of the base composition and varying amounts of minor

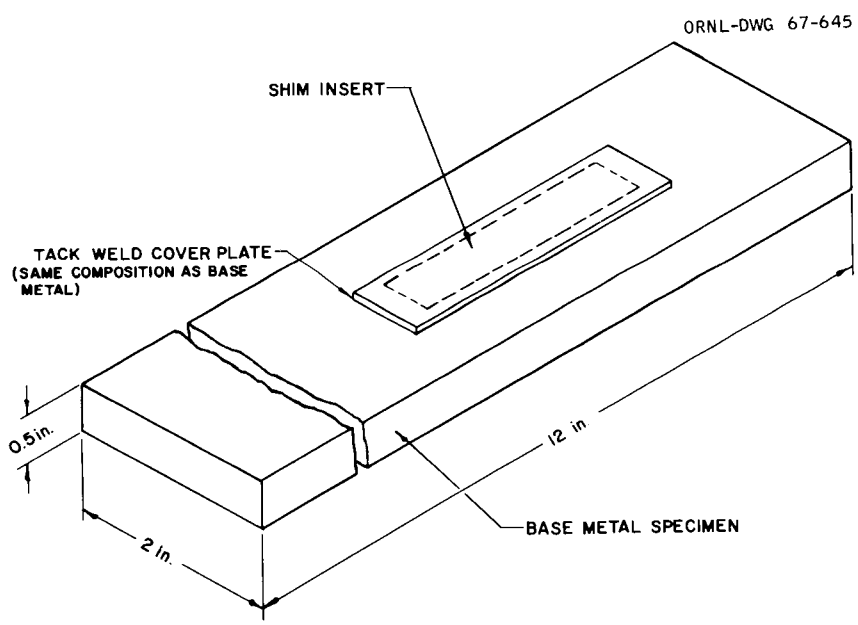

Fig. 7.3. Modified VARESTRAINT Test Specimen.

[redacted]

elements. As the welding arc passes over the insert, it is melted and fused into the body of the specimen. Thus, by a factorial experiment, the individual and combined effects of several elements at various levels of contamination can hopefully be determined. The procurement of a large quantity of material for preparing the specimen blanks has been discussed in "Special Alloy Fabrication," p. 80, this report.

Hot-Ductility Testing (D. A. Canonico, W. J. Werner)

The hot-ductility test using the Duffer's Gleeble was briefly described in the last quarterly report.[4] The first alloys to be tested are of the Incoloy 800 type; these eight special compositions (Incoloy 800-1 to -8) were listed in the last progress report.[5] Materials for these experiments have been melted and swaged, and the rod-type specimens are currently being machined. Testing of the second group of alloys (Inconel 600 type) will provide information concerning the effects of variations in the sulfur, phosphorus, and manganese contents on the weldability of nickel-chromium-iron alloys. Table 7.3 (p. 82, this report) lists the compositions of the alloys currently being prepared for these tests.

Influence of Flaws on Properties of Nickel-Bearing Alloys (D. A. Canonico, R. W. Swindeman)

A study was initiated to determine the influence of occasional minute flaws, such as microfissures or microporosity, upon the low-cycle fatigue properties of welds in nickel-bearing alloys.[6] During this reporting period, fatigue specimens were prepared from type 304 stainless steel plate and several were annealed at either 2050 or 2250°F. In an effort to produce internal flaws, some of these specimens will be

---

[4]D. A. Canonico and W. J. Werner, Fuels and Materials Development Program Quart. Progr. Rept. Sept. 30, 1966, ORNL-TM-1700, pp 97 and 99.

[5]D. A. Canonico, R. E. McDonald, and W. J. Werner, Ibid., p. 91.

[6]D. A. Canonico and R. W. Swindeman, Ibid., pp. 99–101.

plastically strained and cycled until flaws can be detected by nondestructive testing methods. When flaws have developed, their size and location will be determined. The specimens will then be retested to failure at a lower plastic strain level. The results of these studies will be compared to "defect-free" specimens tested only at the lower plastic strain levels. It is hoped that, by cyclic straining at the higher strain levels, the flaw sizes that develop can be controlled and that their influence on fatigue life can be determined.

All-weld-metal type 308 stainless steel fatigue specimens are also being machined. The specimens were prepared from weld metal that has been deposited under three controlled energy inputs, 10,000, 20,000, and 40,000 joules/in. It has been established that the higher heat inputs produce a coarser weld-metal structure, and it is likely that the time necessary to develop flaws and the size of the flaws may be related to the weld-metal microstructure.

[redacted]

[redacted]

[redacted]

PART II.

REACTOR CHEMISTRY DIVISION

[redacted]

[redacted]

[redacted]

8. FISSION-GAS RELEASE AND PHYSICAL PROPERTIES OF FUEL MATERIALS DURING IRRADIATION

R. M. Carroll R. B. Perez[1]
J. G. Morgan O. Sisman

A hollow-cylinder specimen of single-crystal UO_2 is being irradiated for the purpose of measuring thermal conductivity and fission-gas release during irradiation. In these experiments the specimen is oscillated sinusoidally in the reactor so as to oscillate the neutron flux and thus oscillate the fission rate in the specimen in a sinusoidal manner. The specimen temperature, measured by axial thermocouples, will also oscillate in response to the changing fission power. The base specimen temperature can be controlled by air cooling the outside of the specimen capsule.

Fission-Gas Release

To aid in the formation of an effective model for fission-gas release from fuels, a literature survey[2] was made of recent publications that relate to the behavior of fission gas in fuel materials. The survey both confirmed and extended our defect-trap model over a wide range of fuel materials.

The literature review showed that a rather consistent pattern is emerging for the migration and release of noble gas from solids. Isolated gas atoms move comparatively swiftly by an interstitial process until trapped on a defect in the structure of the solid. The gas atom stays trapped for a length of time that depends mainly on the size of the defect, the temperature, and the irradiation level (for fuels). The defect also has a certain mobility depending upon it size, the material, the temperature, and the irradiation level. At temperatures below the grain growth region, the fission gas will collect in existing

[1]Consultant from the University of Florida.

[2]R. M. Carroll, "Fission-Gas Behavior in Fuel Materials," Nucl. Safety 8(4), (in press).

[3]R. M. Carroll and O. Sisman, "Fission-Gas Release During Fissioning in UO_2," Nucl. Appl. 2(2), 142–150 (April 1966).

defects and also in irradiation-produced small bubbles or clusters which will be uniformly distributed through the fuel. The fission gas that escapes from the fuel will originate very near the surface.

A review of our older data showed that the characteristics of fission-gas release conform to our specific defect-trap model for fission-gas release[3] and also to a general pattern of behavior of noble gas in solids. Single atoms join to form clusters, and clusters exist for a longer time than the point defects — their lifetime depending on their size. Thus, the clusters are more effective traps than the point defects. Actually, the probability of trapping a gas atom is greater if point defects are dispersed through the fuel, but the gas atom can also escape rather easily from the point-defect trap. The net result is that when point defects begin to cluster, the amount of gas escaping from the fuel will be decreased.

The clustering effect is shown in Fig. 8.1 where gas release from single-crystal UO_2 is compared to that from fine-grain UO_2. At temperatures up to about 600°C, knockout release predominated and the gas release showed little temperature dependence. The rougher surfaced

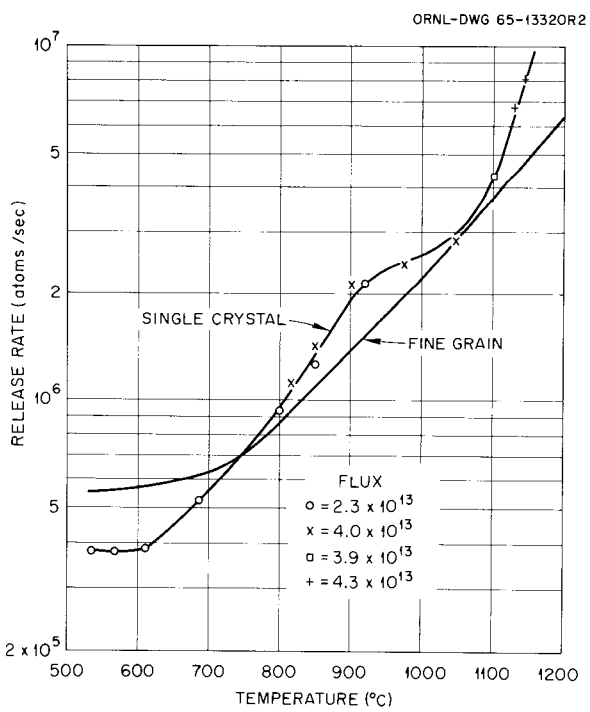

Fig. 8.1. Release Rate of ^{88}Kr from Fine-Grain and Single-Crystal UO_2.

polycrystalline specimen showed greater knockout release (both specimens were the same size). At temperatures above 700°C, the gas release was from point-defect traps for both specimens. At 950 to 1050°C, the point defects were mobile enough to form clusters, increase the trapping efficiency, and thus cause a step in the curve for the single-crystal specimen. The point defects were trapped by grain boundaries in the fine grain specimen before they could cluster, and therefore the step was absent. At higher temperatures, the clusters in the single-crystal specimen could migrate, and once again the release rate had an exponential temperature dependence, but different from that where release was primarily from point defects.

The above effects are more clearly seen in Fig. 8.2 where the data of Fig. 8.1 are plotted with the recoil release subtracted. The single crystal released more gas than the fine-grain specimen even though it had a smaller surface area (the single crystal had a polished surface).

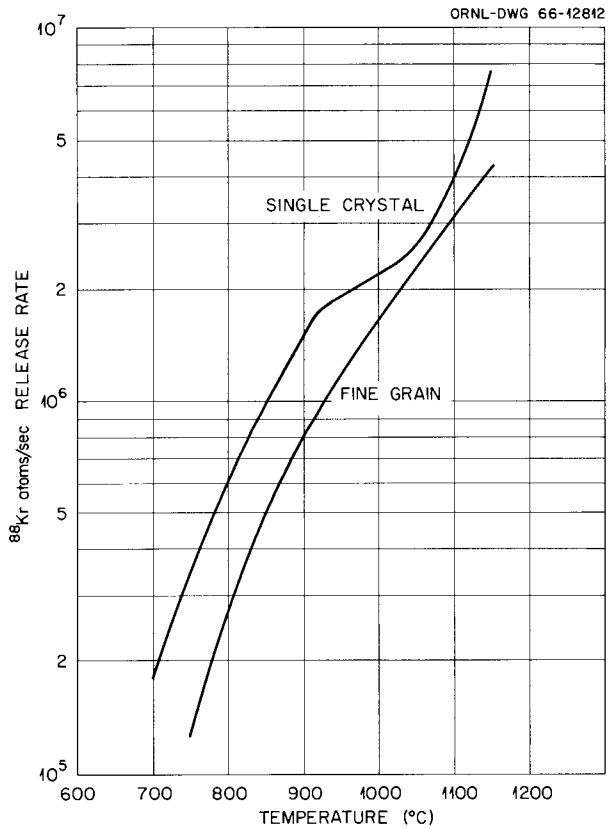

Fig. 8.2. Temperature-Dependent (Recoil Subtracted) ^{88}Kr Release from UO_2 Polished Single-Crystal and Fine-Grain Specimens of the Same Size.

This illustrates the overall trapping effect of the grain boundaries. The temperature-dependent gas release was the same for both specimens and presumably therefore was by the same process. The clustering of point defects had a drastic effect on the fission-gas release from the single-crystal specimens, and at higher temperatures the gas release no longer had the same temperature dependence. Therefore, the gas release at temperatures above 1100°C was by a different process than for lower temperatures.

The clusters are more effective in trapping gas; but, when they can migrate to the surface, they are more effective in delivering gas to be released. The gas release from the single crystal becomes much greater than from the fine-grain specimen at temperatures above 1100°C because of the cluster mobility. The grain boundaries of the fine-grain specimen anchor the clusters, preventing their movement. Thus the temperature dependence of the gas release from the fine-grain specimen remains constant, indicating that the point defects are still the primary source of fission-gas release.

Thermal Conductivity of UO_2 During Irradiation

A large mass of data obtained during flux and temperature oscillations is being analyzed.[4] This consists of computer Fourier analysis of the raw data obtained on punch tape during oscillations. The first harmonic of the amplitudes and of the wave angle so obtained are hand plotted versus the oscillation frequency. A plot such as Fig. 8.3 is obtained by this operation.

The transfer function of the thermocouple itself distorts the frequency-amplitude plots, especially at the high frequencies.[5] The transfer function of the thermocouple has been determined in bench test experiments, where the thermocouple was suddenly moved from one temperature to another and the emf response to the step change of temperature

---

[4]R. M. Carroll, J. G. Morgan, and O. Sisman, Fuels and Materials Development Program Quart. Progr. Rept. Mar. 31, 1966, ORNL-TM-1500, pp. 65–68.

[5]R. M. Carroll, J. G. Morgan, R. B. Perez, and O. Sisman, Fuels and Materials Development Program Quart. Progr. Rept. June 30, 1966, ORNL-TM-1570, pp. 85–95.

[redacted]

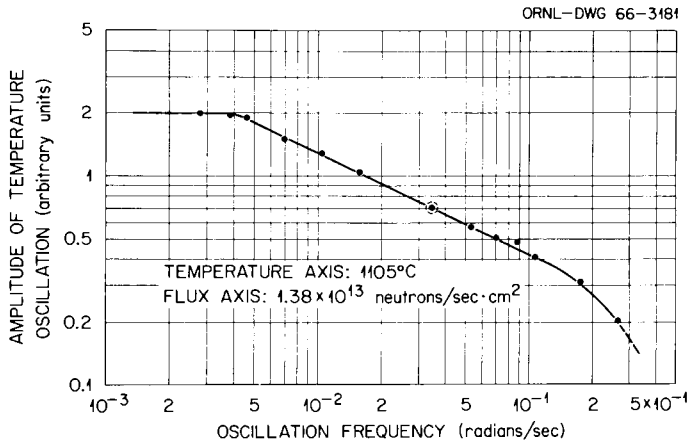

Fig. 8.3. Uranium Dioxide Single-Crystal Temperature Response to Oscillating Fission Rate.

was measured.[4] A graphical correction is made to the plots of amplitude and phase shift versus frequency and a new plot is obtained, such as Fig. 8.4.

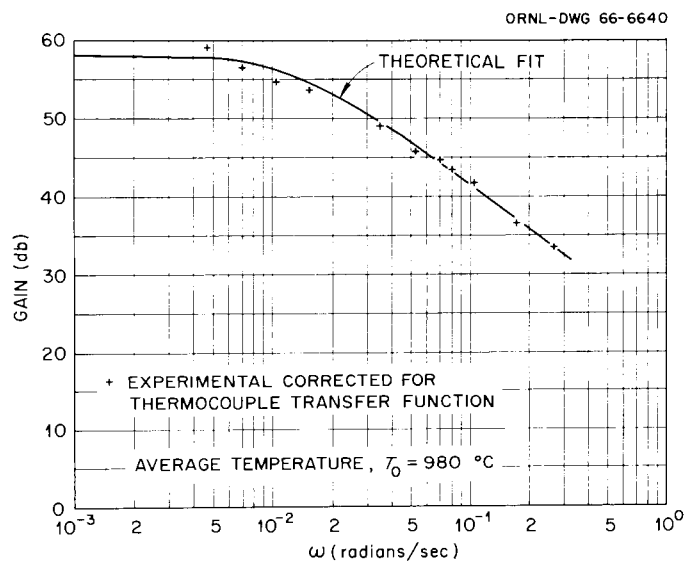

Fig. 8.4. Thermal Conductivity Transfer Function; Amplitude.

The plots of corrected amplitudes and phase shifts are used to obtain values for the complex equations that yield the thermal diffusivity values.[5] Hand computation of these equations proved both useful and costly; useful to obtain an understanding of how the complex equations operated, but wasteful because the hand computations were very time

[redacted]

consuming. Our present procedure is as follows. We examine the first computer processing of the data (Fig. 8.3), correct obvious errors, correct for thermocouple transfer functions (Fig. 8.4), then send the tabulated data back to the computer for the solution of the complex equations. The values of the equations are again plotted and checked for computer errors; and, with a few simple additional calculations, the thermal diffusivity values are obtained.

The in-reactor apparatus is being altered to allow transient testing in addition to the oscillating method. In the transient test, the specimen is moved suddenly from one steady-state flux level to another. The response of the specimen temperature to this step change of fission rate can be analyzed in terms of a series of amplitudes and frequencies. That is, one step change contains all frequencies, and these can be determined by mathematical analysis. This method has already been used to measure thermocouple transfer functions,[6] and we have shown that the transient method yields the same results as the oscillation method.

The great advantage of transient testing is the shorter time required to obtain data. Using the oscillating technique, we sometimes need as much as 20 hr to obtain data over a wide range of oscillation frequencies. Also, during this time the reactor must operate smoothly, and a setback or scram can ruin the entire run. The transient test can be accomplished in about 15 min. Moreover, the transient test will yield very high frequency values, whereas we are mechanically limited to oscillation periods of not less than 24 sec with our oscillation equipment.

To perform the transient test, we have added a small fast-acting positioning cylinder which rides piggyback on the main positioning cylinder. The main cylinder is used to locate the fuel specimen at a specific flux level. The small cylinder is then used to make a rapid step change of position. The usual step is about 1 in. of movement, which requires about 1.5 sec to accomplish.

---

[6] Ibid., Sept. 30, 1966, ORNL-TM-1700, pp. 105–111.

[redacted]

Previous reports in this series are:

ORNL-TM-920	Period Ending June 30, 1964
ORNL-TM-960	Period Ending September 30, 1964
ORNL-TM-1000	Period Ending December 31, 1964
ORNL-TM-1100	Period Ending March 31, 1965
ORNL-TM-1200	Period Ending June 30, 1965
ORNL-TM-1270	Period Ending September 30, 1965
ORNL-TM-1400	Period Ending December 31, 1965
ORNL-TM-1500	Period Ending March 31, 1966
ORNL-TM-1570	Period Ending June 30, 1966
ORNL-TM-1700	Period Ending September 30, 1966

[redacted]

[redacted]

[redacted]

[redacted]

INTERNAL DISTRIBUTION

1–3. Central Research Library
4–5. ORNL – Y-12 Technical Library
Document Reference Section
6–15. Laboratory Records Department
16. Laboratory Records, ORNL R.C.
17. ORNL Patent Office
18. G. M. Adamson, Jr.
19. J. H. Barrett
20. S. E. Beall
21. R. J. Beaver
22. M. Bender
23. R. G. Berggren
24. J. O. Betterton, Jr.
25. D. S. Billington
26. A. L. Boch
27. B. S. Borie
28. G. E. Boyd
29. W. H. Bridges
30. R. B. Briggs
31. W. E. Brundage
32. D. A. Canonico
33. R. M. Carroll
34. J. V. Cathcart
35. G. W. Clark
36. K. V. Cook
37. G. L. Copeland
38. J. H. Crawford
39. F. L. Culler
40. J. E. Cunningham
41. J. H. DeVan
42. C. V. Dodd
43. K. Farrell
44. J. I. Federer
45. B. E. Foster
46. A. P. Fraas
47. E. A. Franco-Ferreira
48. J. H Frye, Jr.
49. R. J. Gray
50. W. R. Grimes
51. H. D. Guberman
52. J. P. Hammond
53. D. G. Harman
54. W. O. Harms
55. R. L. Heestand
56–58. M. R. Hill
59. N. E. Hinkle
60. D. O. Hobson
61. H. W. Hoffman
62. W. R. Huntley
63. H. Inouye
64. T. N. Jones
65. G. W. Keilholtz
66. B. C. Kelley
67. J. A. Lane
68. C. F. Leitten, Jr.
69. A. P. Litman
70. A. L. Lotts
71. R. N. Lyon
72. H. G. MacPherson
73. R. E. MacPherson
74. M. M. Martin
75. W. R. Martin
76. R. W. McClung
77. H. E. McCoy, Jr.
78. H. C. McCurdy
79. R. E. McDonald
80. D. L. McElroy
81. C. J. McHargue
82. F. R. McQuilkin
83. A. J. Miller
84. E. C. Miller
85. J. G. Morgan
86. F. H. Neill
87. S. M. Ohr
88. P. Patriarca
89. A. M. Perry
90. S. Peterson
91. M. L. Picklesimer
92. R. E. Reed
93. P. L. Rittenhouse
94. W. C. Robinson
95. M. W. Rosenthal
96. G. Samuels
97. A. W. Savolainen
98. J. L. Scott
99. O. Sisman
100. G. M. Slaughter
101. N. K. Smith
102. S. D. Snyder
103. I. Spiewak
104. J. T. Stanley
105. W. J. Stelzman
106. J. O. Stiegler
107. D. B. Trauger

[redacted]

[redacted]

108. R. P. Tucker
109. J. T. Venard
110. G. M. Watson
111. A. M. Weinberg
112. J. R. Weir, Jr.
113. W. J. Werner
114. G. D. Whitman
115. J. M. Williams
116. R. O. Williams
117. J. C. Wilson
118. F. W. Young, Jr.
119. C. S. Yust

EXTERNAL DISTRIBUTION

120–123. F. W. Albaugh, Battelle, PNL
124. R. J. Allio, Westinghouse Atomic Power Division
125. R. D. Baker, Los Alamos Scientific Laboratory
126. C. Baroch, Babcock and Wilcox
127. L. Brewer, University of California, Berkeley
128. V. P. Calkins, GE, NMPO
129. W. Cashin, Knolls Atomic Power Laboratory
130. S. Christopher, Combustion Engineering, Inc.
131. D. B. Coburn, General Atomic
132. D. F. Cope, RDT, OSR, AEC, Oak Ridge National Laboratory
133. G. K. Dicker, Division of Reactor Development and Technology, AEC, Washington
134. D. E. Erb, Division of Reactor Development and Technology, AEC, Washington
135. E. A. Evans, GE, Vallecitos
136. W. C. Francis, Idaho Nuclear Corporation
137. A. J. Goodjohn, General Atomic
138. R. G. Grove, Mound Laboratory
139. D. H. Gurinsky, BNL
140. A. N. Holden, GE, APED
141–143. J. S. Kane, Lawrence Radiation Laboratory, Livermore
144. H. Kato, U.S. Department of the Interior, Bureau of Mines
145. E. A. Kintner, Fuel Fabrication Branch, AEC, Washington
146. J. H. Kittel, ANL
147. E. J. Kreih, Westinghouse, Bettis Atomic Power Laboratory
148. W. J. Larkin, AEC, Oak Ridge Operations
149. W. L. Larsen, Iowa State University, Ames Laboratory
150. J. J. Lombardo, NASA, Lewis Research Center
151. J. H. MacMillan, Babcock and Wilcox Company
152. R. Mayfield, ANL
153. M. McGurty, GE, NMPO
154. M. Nevitt, ANL
155. R. E. Pahler, Division of Reactor Development and Technology, AEC, Washington
156. S. Paprocki, BMI
157. D. Ragone, General Atomic
158. B. Rubin, Lawrence Radiation Laboratory, Livermore
159. F. C. Schwenk, Division of Reactor Development and Technology, AEC, Washington
160–162. J. M. Simmons, Division of Reactor Development and Technology, AEC, Washington

[redacted]

[redacted]

163. L. E. Steele, Naval Research Laboratory
164. R. H. Steele, Division of Reactor Development and Technology, AEC, Washington
165. W. F. Sheely, Division of Research, AEC, Washington
166. A. Strasser, United Nuclear Corporation
167. A. Taboada, Division of Reactor Development and Technology, AEC, Washington
168. A. Van Echo, Division of Reactor Development and Technology, AEC, Washington
169. R. Van Tyne, Illinois Institute of Technology Research Institute
170. C. E. Weber, Atomics International
171. J. F. Weissenberger, RDT, OSR, GE, NMPO
172. G. W. Wensch, Division of Reactor Development and Technology, AEC, Washington
173. E. A. Wright, AEC, Washington
174. Division of Research and Development, AEC, Oak Ridge Operations
175–189. Division of Technical Information Extension

[redacted]